The Role of Hypothalamic Astrocytes in the Neural Circuit Controlling Reproduction

by

Chrystian David Phillips

A dissertation submitted in partial fulfillment
of the requirements for the degree of
Doctor of Philosophy
(Molecular and Integrative Physiology)
in the University of Michigan
2026

Doctoral Committee:

Professor Suzanne M. Moenter, Chair
Assistant Professor Christian Burgess
Professor Gabriel Corfas
Professor Carol Elias
Professor Michael A. Sutton

Chrystian David Phillips

chrystip@umich.edu

OCRID iD: 0000-0002-3869-7582

© Chrystian David Phillips 2026

Acknowledgements

I wish to thank my previous scientific mentors for encouraging me to continue my academic pursuits. To Dr. Jimo Borjigin, for providing me with my first laboratory experience. To Dr. Linda Samuelson, for first introducing me to the mouse model and its various genetic tools, as well as encouraging me to continue my career in research. To Dr. Peng Li, whose expertise in neuroscientific techniques, dedication to training, steadfast adherence to scientific rigor, and humility has made me a considerably better scientist.

I wish to thank members of my lab. To Elizabeth Wagenmaker and Laura Burger, for diligently keeping the lab running, as well as providing valuable assistance in techniques including molecular biology and *in vivo* reproductive assays. To Rudi Starrett, Jenn Jaime, Amanda Gibson, and Xi Chen, for assisting me in electrophysiological techniques. To Tony DeFazio, who provided crucial programming tools and other rig-related advice. To Maneet Angra, for being a great undergraduate student.

I wish to thank the members of my dissertation committee, who have always been a wealth of knowledge and expertise that I could tap into when experiments needed troubleshooting or data needed reinterpretation.

To the members of Michigan Games & Cards, who have saddled me with some of the greatest board gaming experiences and memories I have ever had.

I owe a great deal of gratitude to my two younger siblings, Connor and Victoria, for being awesome quirky siblings.

I would not be here without my mother, Kim. We've gone through a lot together in this world. Even when things get seemingly insurmountable, you have always been there for me. I am honored to call you not only my mother, but also my best friend.

Finally, my deepest gratitude to my mentor, Dr. Sue Moenter. Your mentoring has been nothing but sublime. It is from your tireless mentoring that I am now so much more confident at grantsmanship, designing experiments, and engaging in scientific communication.

Table of Contents

Acknowledgements ..... **ii**

List of Tables ..... **vi**

List of Figures ..... **x**

Abstract ..... **xii**

Chapter 1: Introduction **1**

A Brief History of the Field of Reproductive Neuroendocrinology 1

Gonadotropin-releasing hormone (GnRH): The Central Gatekeeper of the HPG Axis 5

Utilizing Mice as an Experimental Model for Reproduction 9

Kisspeptin as a Critical Upstream Factor of GnRH Neuron Function 11

Overview of Glia 15

Mechanisms of Glial Activation and Gliotransmission 17

Glial Regulation of Reproductive Function 21

Dissertation Preview 28

Chapter 2: Sex and Time of Day Alter the Interactions Between Hypothalamic Glia and the Neural Circuits Controlling Reproduction **30**

Abstract 30

Introduction 31

Materials & Methods 32

Results 40

Discussion 58

Chapter 3: Investigation of the Endogenous Activators of Preoptic Area Astrocyte in Reproductive Function **77**

Introduction 77

Materials & Methods 79

Results 86

Discussion 94

Chapter 4: Conclusion 102

Introduction 102

Astrocyte Regulation of the HPG Axis is Modified by Sex-Dependent Factors and the Heterogeneous Regulatory Capacity of Different Astrocyte Populations 102

Diurnal Factors Appear to Influence Gliotransmission Action on GnRH Neurons 110

Purines, but not Glutamate or Endocannabinoid Signaling, Activate POA Astrocytes, Though Underlying Ca^{2+} Signaling is not Necessarily Important for Female Reproduction 111

EP2 Signaling as a Contributing Mechanism behind Female Reproductive Maturation 113

Summary 117

Bibliography 120

List of Tables

Table 2.1: Mouse strains used. 33

Table 2.2: Viruses used. 34

Table 2.3: Antibodies used. 36

Table 2.4: Statistical parameters from three-way mixed model ANOVA assessing the effect of sex/cycle stage and AAV on ΔF/F0 during 200 nM CNO treatment from AM | POA mouse brain slices 64

Table 2.5: Statistical parameters from three-way mixed model ANOVA assessing the effect of sex/cycle stage and AAV on ΔF/F0 during 200 nM CNO treatment from PM | POA mouse brain slices 64

Table 2.6: Statistical parameters from three-way mixed model ANOVA assessing the effect of sex/cycle stage and AAV on ΔF/F0 during 200 nM CNO treatment from AM | ARC mouse brain slices 65

Table 2.7: Statistical parameters from three-way mixed model ANOVA assessing the effect of sex/cycle stage and AAV on ΔF/F0 during 200 nM CNO treatment from PM | ARC mouse brain slices 65

Table 2.8: Statistical parameters from three-way mixed model ANOVA assessing the effect of sex/cycle stage and AAV on GnRH neuron response to 200 nM CNO treatment from AM | POA mouse brain slices 66

Table 2.9: Statistical parameters from three-way mixed model ANOVA assessing the effect of sex/cycle stage and AAV on GnRH neuron response to 200 nM CNO treatment from PM | POA mouse brain slices 66

Table 2.10: Statistical parameters from three-way mixed model ANOVA assessing the effect of sex/cycle stage and AAV on KNDy neuron response to 200 nM CNO treatment from AM | ARC mouse brain slices 67

Table 2.11: Statistical parameters from three-way mixed model ANOVA assessing the effect of sex/cycle stage and AAV on KNDy neuron response to 200 nM CNO treatment from PM | ARC mouse brain slices 67

Table 2.12: Statistical parameters from three-way mixed model ANOVA assessing the effect of sex/cycle stage and AAV on LH levels during 0.3 mg/kg CNO treatment from AM | POA mice 68

Table 2.13: Statistical parameters from three-way mixed model ANOVA assessing the effect of sex/cycle stage and AAV on LH levels during 0.3 mg/kg CNO treatment from PM | POA mice 68

Table 2.14: Statistical parameters from three-way mixed model ANOVA assessing the effect of sex/cycle stage and AAV on LH levels during 0.3 mg/kg CNO treatment from AM | POA mice 69

Table 2.15: Statistical parameters from three-way mixed model ANOVA assessing the effect of sex/cycle stage and AAV on LH levels during 0.3 mg/kg CNO treatment from PM | POA mice 69

Table 2.16: Statistical parameters from three-way mixed model ANOVA assessing the effect of sex/cycle stage and AAV on LH levels during 0.3 mg/kg CNO treatment from AM | ARC mice 70

Table 2.17: Statistical parameters from three-way mixed model ANOVA assessing the effect of sex/cycle stage and AAV on LH levels during 0.3 mg/kg CNO treatment from PM | ARC mice 70

Table 2.18: Statistical parameters from three-way mixed model ANOVA assessing the effect of sex/cycle stage and AAV on LH levels during 0.3 mg/kg CNO treatment from AM | ARC mice 71

Table 2.19: Statistical parameters from three-way mixed model ANOVA assessing the effect of sex/cycle stage and AAV on LH levels during 0.3 mg/kg CNO treatment from PM | ARC mice 71

Table 2.20: Statistical parameters assessing the viral ablation efficiency of KNDy neuron in male mice 72

Table 2.21: Statistical parameters from two-way mixed model ANOVA assessing the effect of KNDy neuron ablation on LH levels during 0.3 mg/kg CNO treatment from AM | ARC male mice 72

Table 2.22: Statistical parameters from two-way mixed model ANOVA assessing the effect of KNDy neuron ablation on LH levels during 0.3 mg/kg CNO treatment from PM | ARC male mice 72

Table 2.23: Statistical parameters from two-way mixed model ANOVA assessing the effect of KNDy neuron ablation on LH levels during 0.3 mg/kg CNO treatment from AM | ARC male mice 73

Table 2.24: Statistical parameters from two-way mixed model ANOVA assessing the effect of KNDy neuron ablation on LH levels during 0.3 mg/kg CNO treatment from PM | ARC male mice 73

Table 2.25: Statistical parameters from three-way mixed model ANOVA assessing the effect of sex and antagonists to receptors EP1 and EP2 on GnRH neuron firing during 200 nM dmPGE2 treatment from AM | POA mice..... 73

Table 2.26: Statistical parameters from one-way repeated measures ANOVA assessing the effect of 1 μM dmPGE2 treatment on GnRH neuron firing from AM | POA diestrous female mice..... 74

Table 2.27: Statistical parameters from three-way mixed model ANOVA assessing the effect of sex and antagonists to receptors EP1 and EP2 on GnRH neuron firing during 200 nM dmPGE2 treatment from PM | POA mice 74

Table 2.28: Statistical parameters from two-way mixed model ANOVA assessing the effect of sex on KNDy neuron firing during 200 nM dmPGE2 treatment from AM | ARC mice..... 74

Table 2.29: Statistical parameters from two-way mixed model ANOVA assessing the effect of sex on KNDy neuron firing during 1 μM dmPGE2 treatment from AM | ARC mice..... 75

Table 2.30: Statistical parameters from two-way mixed model ANOVA assessing the effect of sex on KNDy neuron firing during 200 nM dmPGE2 treatment from PM | ARC mice..... 75

Table 2.31: Statistical parameters from two-way mixed model ANOVA assessing the effect of sex on KNDy neuron firing during 1 μM dmPGE2 treatment from PM | ARC mice..... 75

Table 2.32: Statistical parameters from three-way mixed model ANOVA assessing the effect of sex and antagonists to receptors EP1 and EP2 on GnRH neuron firing during 200 nM CNO treatment from AM | POA mice 76

Table 2.33: Statistical parameters from three-way mixed model ANOVA assessing the effect of sex and antagonists to receptors EP1 and EP2 on GnRH neuron firing during 200 nM CNO treatment from PM | POA mice..... 76

Table 3.1: Mouse strain used..... 79

Table 3.2: Viruses used. 80

Table 3.3: Antibodies used..... 81

Table 3.4: Specificity of *P2ry1* sgRNAs and off-targeting predictions. 83

Table 3.5: Primer probes used for qPCR. 85

Table 3.6: Statistical parameters from two-way mixed model ANOVA assessing the effect of CHPG on $[Ca^{2+}]_i$ in *ex vivo* POA astrocytes 99

Table 3.7: Statistical parameters from two-way mixed model ANOVA assessing the effect of ACPD on $[Ca^{2+}]_i$ in *ex vivo* POA astrocytes 99

Table 3.8: Statistical parameters from two-way mixed model ANOVA assessing the effect of WIN 55,212-2 on $[Ca^{2+}]_i$ in *ex vivo* POA astrocytes 99

Table 3.9: Statistical parameters from two-way mixed model ANOVA assessing the effect of ATP on $[Ca^{2+}]_i$ in *ex vivo* POA astrocytes 99

Table 3.10: Statistical parameters from three-way mixed model ANOVA assessing the effect of ADP and the P_2Y_1 antagonist MRS2179 on $[Ca^{2+}]_i$ in *ex vivo* POA astrocytes 100

Table 3.11: Statistical parameters from two-way mixed model ANOVA assessing the effect of AAV-GFAP-hPMCA2w/b on basal F_0 levels in *ex vivo* POA astrocytes..... 100

Table 3.12: Statistical parameters from three-way mixed model ANOVA assessing the effect of AAV-GFAP-hPMCA2w/b on ADP-induced elevations in $[Ca^{2+}]_i$ in *ex vivo* POA astrocytes 101

Table 3.13: Statistical parameters from χ^2 test assessing the effect of AAV-GFAP-hPMCA2w/b on female mouse estrous cycle staging post-operatively 101

Table 3.14: Statistical parameters from two-way mixed model ANOVA assessing the effect of AAV-GFAP-hPMCA2w/b on frequency of entry into proestrus 101

Table 4.1: Statistical parameters assessing the effect of EP2 knockout in GnRH-expressing cells on puberty onset in males 118

Table 4.2: Statistical parameters assessing the effect of EP2 knockout in GnRH-expressing cells on puberty onset in females 118

Table 4.3: Statistical parameters assessing the effect of EP2 knockout in GnRH-expressing cells on body mass at puberty onset in males..... 118

Table 4.4: Statistical parameters assessing the effect of EP2 knockout in GnRH-expressing cells on body mass at puberty onset in females..... 118

Table 4.5: Statistical parameters assessing the effect of EP2 knockout in GnRH-expressing cells on testis-to-body mass ratio 118

Table 4.6: Statistical parameters assessing the effect of EP2 knockout in GnRH-expressing cells on uterine implantation sites 119

List of Figures

Figure 1.1: Schematics of the HPG axis and the female central reproductive neural circuit. 7

Figure 2.1: AAV5 constructs bearing glial fibrillary acidic protein (GFAP) promoter-driven genes effectively target cells with glial morphology and astrocytic markers in the hypothalamus. 41

Figure 2.2: Activating Gq singaling in GFAP-expressing cells in the POA increases $[Ca^{2+}]_i$ regardless of sex, cycle stage, or time of day. 43

Figure 2.3: Activating Gq singaling in GFAP-expressing cells in the ARC increases $[Ca^{2+}]_i$ regardless of sex, cycle stage, or time of day. 45

Figure 2.4: Activating Gq signaling in GFAP-expressing cells in the POA increases GnRH neuron firing regardless of sex, cycle stage, and time of day. 47

Figure 2.5: Activating Gq signaling in GFAP-expressing cells in the ARC does not alter KNDy neuron firing regardless of sex, cycle stage, and time of day. 49

Figure 2.6: Activating Gq signaling in GFAP-expressing cells in the POA increases circulating LH levels more in males than diestrous females. 51

Figure 2.7: Activating Gq signaling in GFAP-expressing cells in the ARC increases circulating LH levels in males, but not diestrous females. 52

Figure 2.8: Viral knockdown of KNDy neurons in males does not abolish the increase in circulating LH levels induced by activating Gq signaling in GFAP-expressing cells in the ARC. 54

Figure 2.9: GnRH neurons from females are less sensitive to dmPGE2 than males. .. 56

Figure 2.10: dmPGE2 does not alter KNDy neuron firing regardless of sex, time of day, or dose of drug. 57

Figure 2.11: EP1 and EP2 antagonists blunt CNO-induced increases in GnRH neuron firing during the AM regardless of sex, but not in the PM. 58

Figure 3.1: mGluR and CB1 agonists fail to induce Ca^{2+} signaling in POA astrocytes. 87

Figure 3.2: Purines ATP and ADP increase $[Ca^{2+}]_i$ in astrocytes, with the latter partially being mediated via P_2Y_1. 89

Figure 3.3: *In vitro* validation of *P2ry1* single guide RNAs..... 90

Figure 3.4: Reducing Ca^{2+} signaling in POA astrocytes with hPMCA2w/b. 91

Figure 3.5: Attenuation of $[Ca^{2+}]_i$ in POA astrocytes fails to alter reproductive cyclicity in females..... 94

Figure 4.1: Working model of astrocyte contribution to the central reproductive neural circuit in male and diestrous female mice..... 104

Figure 4.2: Preliminary data showing EP2 knockout in GnRH-expressing cells delaying female puberty but not disrupting long-term reproductive function. 115

Abstract

Gonadotropin-releasing hormone (GnRH) neurons in the medial preoptic area (POA) and hypothalamus produce the final central output controlling fertility. A prominent regulator of GnRH neuron function is an afferent network of cells including kisspeptin-, neurokinin-B-, and dynorphin-expressing (KNDy) neurons in the arcuate nucleus (ARC) and glia. Glia, particularly astrocytes, contribute to GnRH neuron regulation via morphological plasticity and the release of chemical messengers in a process called gliotransmission. The gliotransmitter prostaglandin E_2 (PGE2) is a potent activator of GnRH neurons. Disruption of astrocytic erbB receptor signaling – which activates PGE2 synthesis – decreases the release of GnRH and downstream luteinizing hormone (LH). PGE2 signaling disruption has also been implicated in altering reproductive hallmarks, particularly female puberty onset. Despite this, the factors that contribute to astrocyte regulation of the GnRH neuronal network, such as sex, time of day, and the brain region where these relevant astrocytes reside, are incompletely understood. Moreover, the mechanisms of endogenous hypothalamic astrocyte activation, and whether these mechanisms contribute to a variety of *in vivo* reproductive parameters, remain to be investigated. This dissertation attempts to elucidate these knowledge gaps using the mouse model.

We first targeted glial-fibrillary-acidic-protein-(GFAP-)driven expression of the hM3Dq designer receptor exclusively activated by designer drug (DREADD) and the calcium indicator GCaMP6f to astrocytes in the POA and ARC via stereotaxic injections of adeno-associated viruses (AAV). DREADD activation via clozapine N-oxide (CNO) is sufficient to stimulate Ca^{2+} signaling – a hallmark of astrocyte activation – *ex vivo* in astrocytes regardless of sex, time of day, or brain region. Extracellular recordings show GnRH neuron firing rate increasing following CNO treatment, but KNDy neurons were unresponsive to CNO in both sexes and regardless of time of day. Pretreatment with antagonists to PGE2 receptor 1 and 2 (EP1 and EP2) partially blocks CNO-induced

GnRH neuron firing in the morning, but this effect is absent in the afternoon. GnRH neurons from males were more responsive than females to treatment with the stable PGE2 analog dimethyl PGE2. To assess the effect of astrocyte activation on the reproductive neuroendocrine axis, *in vivo* LH release was measured in DREADD-expressing mice. CNO treatment induces greater and more rapid secretion of LH in male mice compared to females in a KNDy-neuron-independent manner. To investigate the endogenous mechanisms of POA astrocyte activation, we next performed *ex vivo* Ca^{2+} imaging to assess the effectiveness of candidate astrocytic activators. Agonists to metabotropic glutamatergic and endocannabinoid receptors do not induce Ca^{2+} signaling, while the purines ATP and ADP were successful. Purinergic signaling is mediated, in part, through the receptor subtype P_2Y_1. While a CRISPR-Cas9 approach to knock down the P_2Y_1 gene *P2ry1* is in development, we utilized the modified Ca^{2+} pump hPMCA2w/b to constitutively reduce astrocytic Ca^{2+} levels. Although validated *in vitro*, hPMCA2w/b does not disrupt long-term female reproductive cycles *in vivo*.

Together, the work in this dissertation furthers our understanding of the extent to which hypothalamic astrocytes regulate the neuronal elements of the GnRH neuron network. These data also establish candidate endogenous mechanisms of astrocyte activation, as well as preliminary results pertaining to the necessity of astrocytic Ca^{2+} signaling in murine adult reproduction.

Chapter 1: Introduction

A Brief History of the Field of Reproductive Neuroendocrinology

The field of neuroendocrinology weds aspects of the nervous system and the endocrine system to describe how hormone-secreting neurons contribute to physiology. The road to our modern understanding of how neuroendocrine mechanisms underlie reproduction stretches back millennia. One of the earliest and most prominent theories that attempted to describe the etiology of human health and disease was the 5th century BCE treatise *The Nature of Man* in the Hippocratic Corpus[1], which was further refined in the 2nd century CE by Grecco-Roman physician Claudius Galen into the humoural theory[2,3]. The theory explained that various organs excreted four types of juices or "humours". A balance of these humours results in good health, while an imbalanced humoural mixture, or dyscrasia, resulted in disease[1,2,4]. Notably, blood was one of the humours, justifying treatment of ailments by bloodletting to remove the proposed abnormal or excessive humours[4]. This theory was a crude explanation for the maintenance of human health. The philosophical underpinnings relied on contemporary ideas - particularly during Galen's time - revolving around mixing the classical elemental qualities of hot, cold, dry, and wet (or fire, earth, air, and water), as well as the influence of astrology[1,4]. Importantly, two concepts of humoral theory would become the prescient foundations to current understandings of endocrinology. First, specific organs, or glands, secrete compounds that are released into the blood. This was further refined by French physician Théophile de Bordeu in 1775 when he posited that secreted compound, or "emanations", from the testes and ovaries entered the blood vessels to influence secondary sex characteristics[5–7]. This hypothesis pioneered the concept of "internal secretions"[7], a term later coined by French physiologist Claude Bernard[6,8], who particularizes the humours as chemical messengers in the body. Second, if the homeostatic levels of these humours or internal secretions were disrupted, then health would be compromised.

The physiological role of the nervous system, and particularly the brain, was also debated for millennia. Numerous civilizations have conveyed their understanding of the brain as an essential organ for life via medical records of traumatic head injuries[9]. Some of these injuries were man-made through the practice of trepanation, which involved deliberately boring holes into the skull. This has been speculated to have been conducted to treat headaches and convulsions, though other explanations were more superstitious; it is possible trepanation was considered a way to allow evil spirits to exit the body[9]. Aristotle adhered to a model in which the brain serves as a conduit of heat from the heart, similar to a radiator[9,10]. Other works like those from Greek anatomists Herophilus and Erasistratus, followers of the Hippocratic Corpus, provided an understanding of brain structures including the cerebellum, cerebrum, and ventricles as being responsible for sensory and motor function[9,11]. Ventricular localization of intellect was a model adopted by numerous philosophers, spanning from Galen's followers to René Descartes[9]. It proposed that ventricular secretions, or "nerve fluids", were circulated through hollow nerves to convey neural information. Thomas Willis' book *Cerebri Anatome* would be a milestone in neuroanatomy as it established the concept that different brain tissues delegated specific neurological processes[12]. For example, the cortex was posited to be the seat of cognitive function, while other structures like the pons and cerebellum controlled the autonomic nervous system.

Around the time of Théophile de Bordeu's observations, groundwork was being laid to determine which regions of the brain were executive control centers of certain physiological behaviors. This was done by isolating or ablating parts of the brain *in vivo* while monitoring physiological parameters to detect any changes due to the intervention. The first widely accepted experiment employing this principle was the discovery of the central respiratory control center in the medulla oblongata of rabbits by Julien Jean César Legallois in 1806[9]. Further, the concept of nerve fluid was also gradually superseded during the 18th century by the hypothesis that electricity was the mediator of neurological function. This was serendipitously discovered by anatomist Luigi Galvani while dissecting a frog in 1786[9]. Galvani's observation of electrical stimulation, but not mechanical stimulation, being sufficient to induce muscle contractions in dissected frogs heralded the concept of "animal electricity". This electric

mode of communication was thus assumed to underpin the brain's direct coordination of the body's organs.

The fields investigating internal secretions and animal electricity would finally intersect with the pivotal 1849 gonadal transplantation study by Arnold Berthold[6,7,13]. In it, Berthold severed the nerve connections between the testes and the body of chickens while maintaining the vasculature between the two systems. These birds continued to exhibit masculine secondary sex characteristics. Moreover, transplanting mature testes to the abdomens of castrated chickens recapitulated masculine behavior, thus demonstrating that internal secretions from the gonads control secondary sexual development, and not direct innervation of the gonads by the brain. Charles-Édouard Brown-Séquard's controversial 1889 rejuvenation experiment, wherein he self-injected testicular extracts from dogs and claimed to have experienced improved vigor, strength, and pleasure, further demonstrated the downstream effects of these internal secretions on various organs, which likely included the brain[6,7,14].

By the turn of the century, definitive material evidence of internal secretions was presented by William Bayliss and Ernest Starling in their work observing pancreatic juices[15]. Further discussions of this work between Starling and biologist Sir William Bate Hardy resulted in the adoption of the term *hormone* (from Greek *hormon*, or "that which sets in motion") as successor to internal secretions[6]. This new term would describe hormones as chemical messengers that travel through the blood stream from an organ of origin to a target organ to induce a change in state. With support behind the hormonal theory, work began during the interwar years to isolate and purify the sex hormones. In a span of just seven years from 1929 and 1935, estrogens, progesterone, and androgens were successfully identified[16–18], though it would take decades more to elucidate the mechanisms behind gonadal hormone signaling to the brain.

One element that emerged as a critical component in the communication between the gonads and the brain was the pituitary gland. Evidence for the importance of the pituitary in gonadal function came from experiments adopting the ablation and replacement therapy strategy utilized by Berthold. In 1910, surgeon John Homans and

colleagues performed partial canine hypophysectomies to determine whether this gland was required for the maintenance of life[19]. They observed that ablation of the pituitary resulted in gonadal atrophy in adult dogs, as well as persistence of “sexual infantilism” in adolescent pups. Similarly, partial decerebration experiments in female rabbits by researchers Aurther R. Fee and Alan S. Parkes successfully prevented coitus-stimulated ovulation so long as the pituitary was removed[20]. When testing for sufficiency of the pituitary in reproductive function, endocrinologist Philip E. Smith demonstrated that daily injections of exogenous pituitary extracts dramatically improved gonadal status with a 10- to 20-fold increase in gonadal mass as well as recapitulated sexual function in immature hypophysectomized rodents[21,22]. Importantly, the anterior pituitary was identified as a site of production of at least one gonadotrophic hormone by Smith and endocrinologist Earl T. Engle in 1927[23,24]; a second adenohypophyseal hormone would be discovered four years later[25]. These findings, thus, led many researchers to consider the pituitary as the primary regulatory gland of reproductive function.

However, it would be shown in further studies that the pituitary was, itself, under tight regulation from inputs originating in the brain. After confirming the findings by Homans, physician Bernhard Aschner hypothesize that the pituitary likely is dependent upon higher brain structures[26]. This gave credence to earlier observations by physician Jean-Baptiste Marc Bourgery who, in 1845, first observed nerve fibers passing through the pituitary[27], though the extent of innervation was incompletely understood at the time. Indeed, several studies that utilized silver impregnation to visualize nerve fibers would claim to observe the existence of these fibers in the anterior pituitaries of dogs, cats, rabbits, and rats[28–32]. Yet, it would later be shown that this method of staining also labeled reticular fibers, which were confused with nervous tissue[33]. The question regarding how these two structures communicate would be answered in 1930 when physician Gregor Popa and neuroanatomist Una Fielding discovered a vascular link between the hypothalamus and the anterior pituitary[34]. The work by anatomists George Wislocki and Lester King in 1936 demonstrated that the flow of blood primarily descends from the hypothalamus to the anterior pituitary[35]. Thus, this vascular link between these two structures supported a humoral mode of communication originating at hypothalamic centers[36].

Questions rose as to the nature of this hormonal control over the anterior pituitary. While transplantation of immature gonads to distant sites on a mature animals can successfully recapitulate the former's reproductive capacity[37], immature pituitary transplants must be grafted at or near the sella turcica[38], indicating that the humoral mechanism of pituitary activation is not systemic but local. A 1936 study by physiologist Francis Marshall and pharmacologist Ernest B. Verney showed that the passing of electrical current through the whole brain of anesthetized rabbits induces ovulation[39]. This study was refined a year later by neuroendocrinologist Geoffrey W. Harris when successful electrical stimulation was localized to the tuber cinereum, which contains the median eminence of the hypothalamus[40]. Improvements in microscopy supported this by revealing the presence of hypothalamic neuronal terminals located in the median eminence next to the fenestrated portal blood vessels[41]. This points to a neurosecretory hormone released from the median eminence that travels down the portal blood vasculature to the anterior pituitary. Together with the discovery of secretory neurons residing in the hypothalamus[42], these studies were critical in establishing the hypothalamus as the upstream regulator of the pituitary, though the precise identity of these hypothalamic neurotransmitters was still lacking. Harris' famous 1955 monograph synthesized these data to build the most comprehensive model of reproductive neuroendocrinology[43], one that is governed by the hypothalamic-pituitary-gonadal (HPG) axis.

Gonadotropin-releasing hormone (GnRH): The Central Gatekeeper of the HPG Axis

The HPG axis is the core regulator of reproduction in vertebrates. Though all elements of the axis are critical for maintaining fertility, the hypothalamus is notable for being the primary central regulator. By the 1950s and '60s, *in vivo* bioassays and purification methods were refined enough to detect and isolate hypothalamic chemical messengers capable of regulating the anterior pituitary, though these methods were still crude to the point of requiring the harvesting of hundreds of thousands of ovine and porcine hypothalami. The first of these hypothalamic hormones to be isolated and molecularly characterized was thyroid-releasing hormone (TRH)[44,45]. The discovery of TRH was

independently made in 1969 by former colleagues and bitter rivals Andrew Schally and Roger Guilleman.

Their rivalry would continue into their next effort, which was to isolate the hypothalamic releasing factor, or factors, that regulated reproduction. Multiple hypothalamic hormones were suspected because of the earlier discovery and isolation of two pituitary hormones that independently regulated ovulation and follicular development: interstitial-cell-stimulating hormone (later called luteinizing hormone [LH]) and follicle-stimulating hormone (FSH), respectively[46–48]. Though some studies claimed the existence of two separate regulators of LH and FSH[49], further investigation showed that there was likely only one hypothalamic messenger regulating both pituitary hormones, which was subsequentially named luteinizing-hormone-releasing hormone (LHRH)[50,51]. The sequencing of the decapeptide LHRH, now known as GnRH, was achieved in 1972 independently by Schally and Guillemin. This discovery resulted in the two being awarded the 1977 Nobel Prize in Physiology and Medicine along with Rosalyn Yalow, who codeveloped the radioimmunoassay technique used to measure hormone concentrations.

Using immunocytochemical and fluorescent antibody techniques, the neurons responsible for secreting GnRH were found to populate various regions of the hypothalamus and other forebrain regions like the medial preoptic area (POA)[52,53]. The majority of GnRH neurons project their axons to the median eminence and the organum vasculosum of the lamina terminalis (OVLT) of the hypothalamus, while a lesser number of projections terminate in other brain regions like the stria terminalis and the subfornical organ[54]. GnRH that is secreted in the median eminence is transported via the hypothalamo-hypophyseal portal capillaries to the anterior pituitary. Gonadotropes in the anterior pituitary are stimulated by GnRH, which induces the synthesis and release of LH and FSH[50,55–58]. The gonadotropins LH and FSH are released and travel through the systemic circulation until they ultimately bind to their respective receptors in the gonads to induce gametogenesis and steroidogenesis. The synthesized sex steroids, which include testosterone, progesterone, and estradiol, are carried systemically to regulate other elements of the HPG axis through feedback loops.

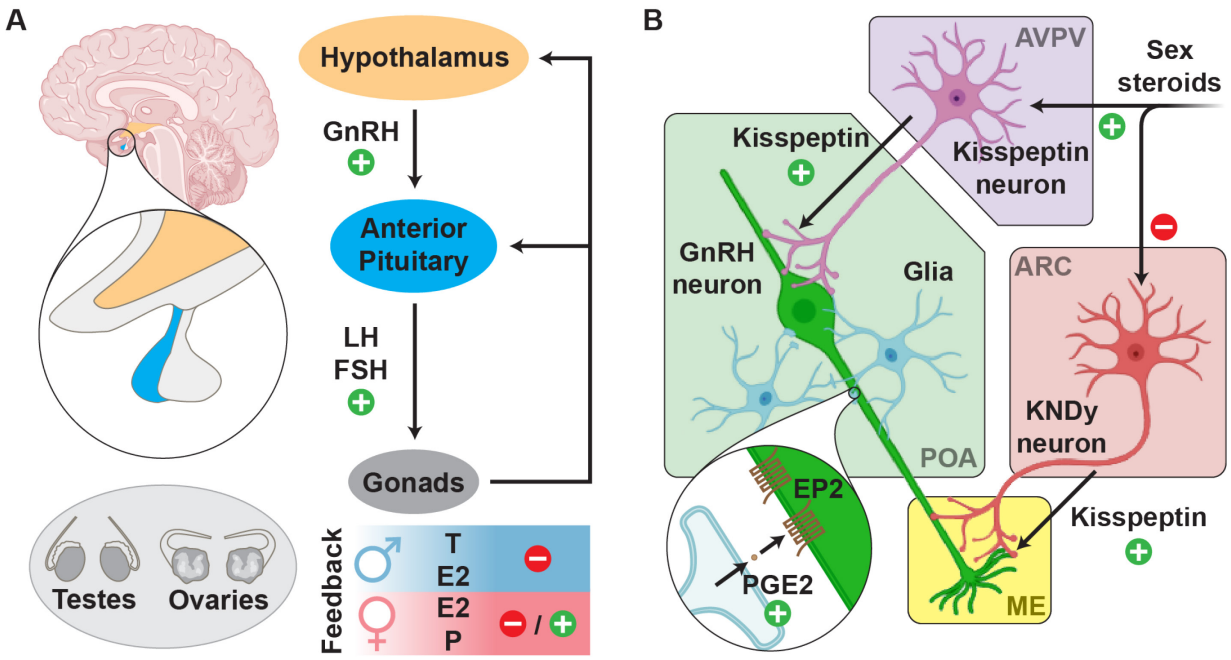


Figure 1.1: Schematics of the HPG axis and the female central reproductive neural circuit. **A,** Hypothalamic gonadotropin-releasing hormone (GnRH) stimulates the anterior pituitary, which further releases luteinizing and follicle-stimulating hormones (LH and FSH, respectively). These gonadotropin hormones induce, among other outputs, gonadal steroidogenesis, which feedback to the hypothalamus and pituitary in a sex-dependent manner. T, testosterone; E2, estradiol; P, progesterone. **B,** Within the hypothalamus, negative sex steroid feedback is relayed to GnRH neurons via arcuate (ARC) kisspeptin-, neurokinin-B-, dynorphin-expressing (KNDy) neurons, while positive sex steroid feedback is relayed by anteroventral periventricular (AVPV) kisspeptin neurons. Preoptic (POA) glia, particularly astrocytes, release the gliotransmitter prostaglandin E_2 (PGE2), which stimulates GnRH neurons by activating prostaglandin E_2 receptor 2 (EP2).

Homeostatic mechanisms that utilize feedback loops aim to have a system operated at a desired range of functions. The two main types of feedback loops are negative and positive. In a negative feedback loop, the output of the system hovers around a stable equilibrium. The underlying process requires an inhibitory branch to keep the output within a narrow operating range. Otherwise, the output could deviate to extreme levels and, in a physiological context, risk injury or death. It is thus unsurprising that most homeostatic mechanisms utilize negative feedback (e.g., body temperature, blood glucose levels, blood oxygen content). A positive feedback loop, in contrast, is inherently unstable and aims to amplify an output. This self-reinforcing process requires an excitatory branch to increase the output to higher levels. Although this would

theoretically risk a run-away effect, the output tends to halt or eventually ramp down when any one of the previous steps in the loop is interrupted. Though rarer than its counterpart, positive feedback is critical for behaviors that require a strengthening of their output over time (e.g., labor contractions, ejaculation).

The HPG axis is among only a few physiological regulators that utilizes both negative and positive feedback loops. One of the clearest manifestations of these feedback loops can be seen from the different patterns of GnRH secretion. Within a decade of the successful isolation of GnRH, studies began utilizing rhesus monkeys to test the importance of GnRH release patterns on reproduction[59,60]. These studies performed radioablation on the hypothalamus to destroy, among other cells, GnRH neurons. This dramatically decreased circulating LH and FSH levels. Importantly, when GnRH was continuously infused in these monkeys, LH and FSH remained low. Prior work showed that LH release exhibited a pulsatile release pattern in humans, monkeys, and sheep[61–63], so there was a likelihood that GnRH also followed a similar pattern. When GnRH was instead infused in a pulsatile fashion in monkeys, LH and FSH levels were restored to typical levels[59,60]. Further studies showed that the ratio of LH-to-FSH secreted changes with the frequency of GnRH administration[60]; higher GnRH pulse frequencies favored greater release of LH, while a lower GnRH pulse frequency favored greater release of FSH. These differential effects of GnRH administration patterns on LH and FSH secretion form the basis of female reproductive cyclicity.

Most mammals have either a menstrual or estrous cycle consisting of a follicular and a luteal phase. The start of the follicular phase follows the loss of progesterone negative feedback (if pregnancy was not achieved) of the previous luteal phase[64]; this causes the GnRH pulse frequency to slowly increase from relatively low levels. Tangentially, males solely exhibit negative feedback, which is mediated by a combination of estradiol and testosterone[65,66]. In the early follicular phase in females, the initially low GnRH pulse frequency promotes more FSH release compared to LH[60]. This prepares the maturation of several ovarian follicles[67]. The maturing follicles increase production of sex steroids like estradiol[68]. As the follicular phase progresses, the GnRH pulse frequency increases with rising estradiol levels[69], foreshadowing an eventual shift from negative to positive

steroid feedback. Higher frequency GnRH release suppresses FSH and results in higher frequency LH release, which drives more steroidogenesis. The increasing estradiol levels eventually reach a critical point in the late follicular phase where the transition from negative to positive feedback finally occurs. Here, the pulsatile GnRH release pattern transitions into a “surge” of persistent GnRH release[70]. LH release mimics this surge in response, and this then induces ovulation[70,71]. With the release of the oocyte, the follicular cells form the corpus luteum which secretes progesterone[72]. Progesterone prepares the uterus for blastocyst implantation by increasing endometrium differentiation and vascularization[73]. The corpus luteum is maintained for about two weeks. Embryonic signals such as interferon-τ in ruminants and chorionic gonadotropin in humans and other primates are required to prevent prostaglandin $F_{2\alpha}$ ($PGF_{2\alpha}$)-mediated luteolysis[74–76]. If pregnancy is not achieved, progesterone levels fall with the regression of the corpus luteum. Progesterone engages in negative feedback with the HPG axis, so its loss results in gradually increasing GnRH pulse frequency between the luteal phase and the next follicular phase.

Utilizing Mice as an Experimental Model for Reproduction

Rodents, such as mice, are particularly useful for studying the physiology of reproduction. One of the main reasons is that the estrous cycles of mice are characterized very well and exhibit similar sequences of hormonal events, particularly leading up to ovulation, compared to humans, although there are key differences. The rodent estrous cycle has four phases (diestrus, proestrus, estrus, and metestrus), and a single cycle typically lasts for 4 to 5 days. Progression through the estrous cycle can be monitored via vaginal lavage and cytology, which is relatively non-invasive. Ovulation in mice is preceded by a rise in estradiol that begins during diestrus and peaks on the morning of proestrus to ultimately cause a switch from negative to positive feedback during the late afternoon of proestrus. A similar rise in estradiol occurs during the mid-late follicular phase in humans, which leads to the LH surge in the late follicular phase. The LH surge in rodents is regulated by the onset of daylight and is initiated before the start of the active period (i.e., darkness in nocturnal rodents) during proestrus. While timing of ovulation is not as tight in humans, there is evidence of diurnal regulation as a

higher proportion of ovulation occurs near the onset of activity[77]. Unlike other mammals, rodents do not have a full luteal phase due to the corpus luteum being functionally short-lived[78,79]. These caveats must be considered when interpreting the mechanisms behind rodent reproductive physiology compared to human reproduction.

An advantage of mice in reproductive research is the availability of genetic tools. The GnRH-GFP mouse line, for example, has been essential in identifying GnRH neurons by expressing green fluorescent protein, or GFP, in a promoter-driven manner. Other genetic tools include the Cre/lox recombination system, wherein Cre recombinase recognizes pairs of loxP sequences flanking a gene or other genetic material of interest, and successful recombination results in expression or deletion of the flanked DNA[80]. Temporal and regional regulation of transgene expression can be achieved using the Cre/lox system. For example, chemogenetics utilizes the expression of designer receptors exclusively activated by designer drugs (DREADDs), which are modified G-protein-coupled receptors (GPCRs), in cells[81]. DREADDs can be activated with administration of a synthetic ligand like clozapine N-oxide (CNO), which induces a signaling cascade in the cell dependent upon the type of DREADD.

The cellular outputs induced by methods like chemogenetics manifest in numerous ways, which can be measured using various techniques. An electrophysiological technique relevant to this body of work is targeted extracellular recordings, which measure the action potential frequency of neurons. An electrode is placed in the extracellular fluid near the neuronal membrane *ex vivo* or *in vitro* to measure action currents (a proxy for action potentials). This technique is useful primarily due to it being relatively non-invasive at the cellular level, as the cytosol of the neurons is not disturbed. Calcium imaging is another relevant technique that monitors changes in intracellular calcium levels ($[Ca^{2+}]$)[82]. This is achieved in a cell-specific manner by expressing a genetically encoded calcium indicator such as GCaMP under a specific promoter. Calcium influx is a key step in neurotransmitter release. However, it is noteworthy that not all action potentials are accompanied by calcium events, and vice versa. Although useful in drawing associations between the manipulation of a cell type

and a specific behavior, these techniques likely do not exactly phenocopy the output seen under physiological conditions.

Kisspeptin as a Critical Upstream Factor of GnRH Neuron Function

Estradiol regulation of both of negative and positive feedback modes converge on estradiol receptor, subtype α (ERα). This is apparent in ERα knockout mice, in which the loss of estradiol action via ERα resulted in higher LH levels in models that are used to test negative feedback, as well as the absence of the LH surge and ovulation[83–86]. Despite the importance of ERα in GnRH and LH release, it is not expressed at detectable levels in GnRH neurons[87]. This lack of ERα expression has led to extensive work since the 1990s in determining which estradiol-sensitive afferents to GnRH neurons were responsible for mediating the effects of estradiol on GnRH release patterns.

In 1996, a study investigating melanoma metastasis discovered a candidate metastasis-suppressing gene on chromosome 6. The gene was aptly named *Kiss1* due to the discovery being made in Hershey, PA. The product of *Kiss1*, named metastin[88], was soon found to be a peptide that binds to a GPCR called GPR54, now known as KISS1R[89]. In 2003, loss-of-function mutations in GPR54 were discovered in humans, and these mutations resulted in hypogonadotropic hypogonadism. The hypogonadotropic hypogonadism phenotype would subsequently be recapitulated in mice with the GnRH-neuron-specific *Kiss1r* knockout model[90,91]. This established the necessity of metastin, now known as kisspeptin, in reproduction.

In the brain, neurons expressing kisspeptin are primarily located in the arcuate nucleus (ARC) and anteroventral periventricular nucleus (AVPV), with smaller populations found in the amygdala and bed nucleus of the stria terminalis (BNST). Anatomical studies soon revealed that kisspeptin neurons from the two hypothalamic regions send their projections to GnRH neurons[92–94]. ARC kisspeptin neuron projections synapse onto GnRH neuron soma and terminals in sheep and primates. In rodents, however, ARC projections exclusively localize at the GnRH neuron terminals. AVPV kisspeptin neuron projections synapse onto GnRH neuron soma and terminals across species. Moreover,

GnRH neurons are a critical site of kisspeptin action, with over 90% of these neurons expressing KISS1R[95–98]. Injections of kisspeptin stimulate rapid LH release in rats, sheep, monkeys, and humans[99–102]. Unlike GnRH neurons, kisspeptin neurons highly express ERα, ERβ, progesterone, and androgen receptors[103–105]. Studies that knocked down ERα expression in mouse kisspeptin-expressing cells reported a failure of those mice to achieve proper estrous cyclicity and to have disrupted LH release responses[106].

Another distinguishing factor between ARC and AVPV kisspeptin neuron populations is the differential effect of estradiol on these neurons, which was first observed by Robert Steiner in 2005[107]. They compared *Kiss1* mRNA expression between mice from the following groups: diestrus, ovariectomized (OVX), and OVX with estradiol supplementation (OVX+E). *Kiss1* expression in the ARC was lower in diestrus than OVX, but suppressed to diestrous levels by estradiol in OVX+E mice. Conversely, the AVPV *Kiss1* expression was lower in OVX than diestrous mice, but restored to diestrous levels by estradiol. This suggested that the ARC kisspeptin neurons relay negative steroid feedback to modulate GnRH pulse frequency, while AVPV neurons relayed positive feedback to drive the GnRH/LH surge. These results confirmed earlier ablation experiments aimed at altering LH pulses and surges in a region-specific manner; ablations generally localized to the suprachiasmatic nucleus, POA, and, incidentally, the AVPV blocked LH surges, but pulses remained[108]. Ablations of the medial basal hypothalamus (which includes the ARC and median eminence), however, did not interfere with ovulation, but LH secretion patterns during the reproductive cycles were compromised[109,110].

The association between the AVPV region and the GnRH/LH surge had been known well before the importance of kisspeptin on reproductive function was made. The AVPV exhibits stark sexual dimorphisms, being considerably larger in females than in males. This was shown in rodents to be the result of defeminization of the male AVPV during the transient perinatal testosterone surge[111]. When aromatase, which synthesizes estradiol from testosterone, was inhibited in males, both AVPV *Kiss1* expression and LH surges were recapitulated. This is because estradiol is responsible for masculinization of the brain, which normally does not occur in females due to the sequestering of the

steroid to the peripheral circulation by α-fetoprotein. Similarly, neonatally androgenized females lost the capacity to generate LH surges. Moreover, correlations between AVPV neuronal activity and LH surges have been established. cFos, a marker for neuronal activity, is expressed in AVPV neurons in both proestrous and OVX+E mice and the POA kisspeptin neurons in ewes and monkeys[112–115]. Unusually, the males of some species of Old World primates, such as Japanese macaques, can undergo estradiol-induced LH surges during which an increased number of POA kisspeptin neurons express cFos[114]. Thus, the AVPV and the increased activity of these kisspeptin neurons is a key factor in the LH surge across species and, to a limited extent, across sex.

As was the case with the AVPV and the GnRH/LH surge, there was an implied link between ARC kisspeptin neurons and GnRH/LH pulses before the discovery of kisspeptin. In addition to the aforementioned lesion studies, evidence suggested that the timing of LH pulses correlated with increased spiking in neuronal multiple-unit activity (MUA) recordings of the medial basal hypothalamus[116]. More recent approaches of measuring ARC kisspeptin neuron activity involve targeted expression of the calcium indicator GCaMP6 followed by observation of changes in fluorescence via fiber photometry[117]. In 24-hour recordings of male mice, bulk fluorescent signals from ARC kisspeptin neurons correlated with pulsatile LH release. This has led many researchers to claim that the ARC kisspeptin population dictates this frequency, with some dubbing it the “pulse generator.” Studies have further shown that the activation of ARC kisspeptin neurons *in vivo* resulted in robust LH release in rodents[118]. These optogenetic studies utilized adeno-associated viruses (AAVs) that expressed channelrhodopsin selectively in ARC kisspeptin neurons. Synchronized optogenetic activation of these neurons induced a pulse-like release of LH.

ARC kisspeptin neurons, in addition to secreting kisspeptin, coexpress the peptides neurokinin B (NKB) and dynorphin (Dyn). These ARC neurons expressing kisspeptin, NKB, and Dyn are collectively referred to as KNDy neurons. The effect of NKB and Dyn appear to oppose each other; intracerebroventricular injections of NKB increases MUA activity and LH pulse frequency in goats. Injections of Dyn, however, decreases MUA activity and LH pulse frequency[119]. Further, injections of a Dyn-specific kappa opioid

receptor (KOR) antagonist recapitulated MUA activity. These KNDy neurons are posited to form a network where NKB and Dyn act as the accelerator and brake, respectively, of synchronized network activity to drive the GnRH/LH pulses. This is supported by observations of NKB receptor, NK3R, and, to a lesser extent, KOR expression amongst KNDy neurons[120,121]. Together, this suggests KNDy neurons form a network among themselves with coordinated firing, likely orchestrated by NKB and Dyn, contributing to the GnRH/LH pulse frequency.

The unique activity patterns of both AVPV kisspeptin and KNDy neurons are modulated by estradiol. Early studies addressing the importance of estradiol action on these kisspeptin circuits were done utilizing mouse models for the knockout of ERα across all kisspeptin cells (KERKO)[106,122–124]. KEKRO mice exhibit signs of reproductive dysfunction including disrupted reproductive cycles and delayed vaginal opening during puberty. Moreover, these mice had elevated LH levels, KNDy neuron firing rates were higher compared to controls, and estradiol-induced LH surges were not observed. This shows the importance of kisspeptin-specific ERα expression in reproduction, but there are caveats to this model. ERα is knocked out the moment *Kiss1* is expressed by any cell, so developmental changes may occur which could confound these findings. In addition, deletion of ERα occurs in both ARC and AVPV kisspeptin populations, so it is impossible to distinguish which population is responsible for each individual reproductive outcome.

To temporally and spatially control the expression, or lack thereof, of ERα, a CRISPR-Cas9 approach was used[125]. In this mouse model, Cas9 was expressed specifically in kisspeptin neurons, and sgRNAs designed to target the ERα gene *Esr1* were packaged into an AAV and injected into either the ARC or AVPV. Although the number of cells expressing ERα was only partially reduced by the sgRNAs, reproductive function was disrupted in stereotyped ways. ARC-targeted mice had disrupted estrous cycles and the LH response to GnRH and kisspeptin administration was attenuated. In contrast, AVPV-targeted mice did not exhibit disrupted cyclicity, but proestrous and estradiol-induced LH surges were blunted. Thus, these data point to the importance of estradiol feedback

modulating AVPV kisspeptin and KNDy neuron populations differentially to regulate reproductive function.

Overview of Glia

The history of glial research stretches back as far as research into their neuronal counterparts[126]. The distinction between gray matter and white matter was likely first made by anatomist Andreae Vesalii from his dissection of human cadavers in the 16th century. Advances in rudimentary light microscopy over the next few centuries would help with the distinction between these cell types. By 1824, two main types of tissue were described in the central nervous system, later referred to as neurons and glia. In the 1850s, physician Rudolf Virchow introduced the term “neuroglia” (or from German “Nervenkitt”, which means adhesive nerve cement) to describe the apparently homogeneous connective substance between nerve fibers[127,128]. Numerous neuroanatomists would go on to characterize the structure of glia through the latter half of the 19th century. The first detailed images of glial cells came from pioneering neuroscientist Camillo Golgi in the 1870s, who utilized a histological silver staining procedure known as the “black reaction” (now known as Golgi staining) to visualize both glia and neurons[129]. Golgi distinguished between neurons and glia by identifying cells lacking an axon. There was confusion whether neurons and glia formed cell-type-specific continuous anastomosing networks, similar to capillaries, or whether the cells were individual units with extended processes. Fellow neuroscientist Santiago Ramón y Cajal would improve the Golgi staining technique and distinguished neurons and glia as entities in their own right[130,131]. Ramón y Cajal’s development of gold and mercury chloride-sublimate staining was found to label glial fibrillary acidic protein (GFAP), a protein with expression highly specific to astrocytes[131,132]. With improved visualization of astrocytes, Ramón y Cajal observed that these astrocytic networks were contiguous rather than continuous. This, along with Ramón y Cajal’s improved staining methods for axons[130], established the neuron doctrine, coined by Heinrich von Waldeyer-Hartz in 1891, wherein neurons (and glia) were discrete entities that communicated through chemical signaling at junctions between nerve terminals, later called synapses[133].

These histological studies by Golgi and Ramón y Cajal ultimately culminate in them being awarded the 1906 Nobel Prize in Physiology and Medicine.

As the dawn of the 20th century approached, advances in histology facilitated the morphological and purported functional characterization of glia. Ramón y Cajal and contemporaries classified glia into protoplasmic and fibrous forms, suggesting region- and function-specific roles[134,135]. Importantly, the first major protoplasmic glial subtype was coined by Mihály Lenhossék in 1895 who distinguished a subset of glia with a unique star-like morphology; hence, the term "astrocyte" (from the Greek astron for 'star') was established[136]. Early functional hypotheses primarily regarded astrocytes as passive elements, providing nutritive and structural support for neurons and maintaining extracellular ion homeostasis; Golgi's observations revealed that astrocytic endfeet adhere to nearby blood vessels, suggesting a metabolic supporting role for astrocytes[137]. Though early assessment of glia was largely restricted to their morphological characteristics, much was still ascertained. Changes in glial morphology were identified in a variety of neuropathologies including gliosis in the cortex of epileptic patients and hypertrophy of astrocytes in the brains of alcoholics[135,138]. Ramón y Cajal hypothesized that the plasticity seen in axons and dendrites were likely mimicked by astrocytic endfeet. The movement of endfeet would regulate the level of vasodilation and vasoconstriction, which would manifest in behavioral changes such as in sleep-wake cycles[139]. The morphological plasticity of astrocytes, thus, raised many hypotheses beyond that of a structural framework.

The next 50 years marked a paradigm shift in astrocyte research, as more sophisticated techniques could better address the physiological roles of glia in the CNS. In 1907, psychiatrist Ernesto Lugaro posited that glial appositions to neurons could potentially take in locally released neurotransmitters[140,141]. With the advent of the electron microscope, astrocytic membranes were eventually identified surrounding synapses, which directly positions them to participate in neurotransmission[142,143]. This idea of astrocytes being intimately involved with the pre-and postsynaptic elements underlying the communication between neurons has culminated into a model known as the tripartite synapse[144]. Neurotransmitters released into the synaptic cleft must be cleared

from the region to reduce postsynaptic receptor desensitization, which is required to maintain proper synaptic transmission. For example, astrocytes express high levels of glutamate membrane transporters, which use the ion gradients of Na^+ and K^+ to uptake neurotransmitter into the astrocyte and thus contribute to reducing postsynaptic glutamate responses[145,146]. Likewise, the expression of astrocytic K^+ channels and Na^+-K^+ ATPases permit the uptake of extracellular K^+, which reduces the possibility of postsynaptic depolarization[147,148]. The clearance of the synaptic space of chemical messengers is a role that elevates astrocytes to a more active agent directly involved in neuronal function.

However, it was unknown if astrocytes themselves meaningfully responded to these neurotransmitters. Unlike neurons, glia do not have axons, and experimentally-induced depolarization of astrocytes does not lead to action potentials[149]. Moreover, the membrane potential of astrocytes only changes slightly following stimulation by upstream neuronal activity. The lack of electrical activity made it difficult to further assess the physiological role of these cells because there was no experimental method to investigate them for the next 40 years.

Mechanisms of Glial Activation and Gliotransmission

In 1990, the research group under Stephen Smith reported a finding regarding cultured hippocampal astrocytes and their ability to respond to extracellular signals[150]. These cultured hippocampal astrocytes expressed a variety of glutamate receptors that, when activated with exogenous glutamate, induced either increases or oscillations in cytoplasmic Ca^{2+} levels ($[Ca^{2+}]_i$). The detection of these changes in $[Ca^{2+}]_i$ was made possible by loading these astrocytes with the Ca^{2+} indicator dye fluo-3. Moreover, these Ca^{2+} signals appeared to travel in waves between adjacent astrocytes, which suggested that an astrocytic network was capable of propagating signals over relatively long distances. These results would soon be replicated in brain slices and *in vivo*[151,152]. Later studies would confirm that glutamate released from neurons was capable of inducing these $[Ca^{2+}]_i$ elevations, and the mechanism of this astrocytic Ca^{2+} signaling was due to the activation of metabotropic glutamate receptors (mGluRs)[151].

Since then, astrocytic Ca^{2+} signaling events have also been observed to be evoked by other neurotransmitters acting on different GPCRs including the receptors for, but not limited to, ATP, GABA, endocannabinoids, norepinephrine, dopamine, and acetylcholine[153]. G proteins can be classified into four subtypes (G_s, G_q, $G_{i/o}$, and $G_{12/13}$), and their effect of cellular activity varies depending on the subtype. Canonically, G_q and $G_{i/o}$ proteins have an excitatory and inhibitory effect, respectively, on neurons. In astrocytes, evidence suggests that there is little distinction between G_q- and $G_{i/o}$-mediated Ca^{2+} signaling. Stimulation of astrocytic $GABA_B$ receptors or the DREADD hM4Di, both of which utilize $G_{i/o}$ proteins, in mouse hippocampal brain slices increases astrocytic $[Ca^{2+}]_i$[154]. These G_i-induced Ca^{2+} signaling events mimicked those observed when activating muscarinic acetylcholine receptors and the DREADD hM3Dq, both of which utilize G_q proteins. In addition, astrocytes exhibit spontaneous Ca^{2+} fluctuations[155]. Both evoked and spontaneous changes in astrocytic $[Ca^{2+}]_i$ are primarily the product of activation of the phospholipase C (PLC)/inositol 1,4,5-triphoshate (IP3) pathway[156]. This pathway ultimately leads to IP3 receptor activation on the endoplasmic reticulum and subsequent release of Ca^{2+} stores within the endoplasmic reticulum into the cytosol. Interestingly, the Ca^{2+} fluctuations within an astrocyte endfeet are not necessarily temporally correlated with the Ca^{2+} events at the soma, suggesting a level of independent functionality in the endfeet[157,158]. Moreover, given the variable distance of these endfeet from the endoplasmic reticulum, evidence suggests that Ca^{2+} stores in these distal regions arise from different organelles; other pathways including Ca^{2+} release from mitochondria or the activation of local TRPC1 channels appear to play a role[159,160]. Regardless, GPCR activation is widely regarded as the typical mode of inducing changes in $[Ca^{2+}]_i$ at the level of both the soma and endfeet of astrocytes. Together, these discoveries spurred investigation into the functional consequences of these changes in astrocytic $[Ca^{2+}]_i$.

The functional breakthroughs would emerge contemporaneously with Smith's discovery, as glia were found to contain, synthesize, and secrete numerous neuroactive chemicals. Compounds including eicosanoids (e.g., prostaglandins), cytokines (e.g., tumor necrosis factors α [TNGα]), neurotrophins, steroids, purines (e.g., ATP), neuropeptides, and even canonical neurotransmitters like glutamate and GABA were found to be present in glia in

cell cultures, *in vivo*, and *ex vivo*[161,162]. By 1992, over twenty of these substances were observed in glia[161]. The discovery that some transmitters were synthesized and released by glia clashed with the long-standing dogma in the field, which posited glia as either a passive element or, at best, a supportive network of cells behind neural function. However, the work by the research group under neuroscientist Philip G. Haydon in 1994 would finally link glial secretion of neuroactive substances with GPCR-induced Ca^{2+} signaling[163]. Initially, Haydon's team observed the release of glutamate from neocortical astrocyte cultures using high performance liquid chromatography (HPLC). While monitoring astrocytic $[Ca^{2+}]_i$, cultures were treated with bradykinin which elevated mean $[Ca^{2+}]_i$ over 5-fold and induced glutamate release. $[Ca^{2+}]_i$ in neocortical neurons were insensitive to bradykinin, indicating the action of the drug was directed specifically at astrocytes. Moreover, co-cultures of both cell types showed that increases in astrocytic $[Ca^{2+}]_i$ subsequentially increased neuronal $[Ca^{2+}]_i$, and this effect in the neurons was blocked by NMDA receptor antagonists. Later work by the lab would show that mechanical or electrical stimulation of astrocytes in mixed cultures induced increases in $[Ca^{2+}]_i$, which induced both glutamate-dependent slow inward currents (SICs) and miniature postsynaptic currents (mPCSs) via NMDA receptors in patched adjacent neurons[164,165]. These data show that astrocytes respond to external signals with the induction of Ca^{2+} signaling, which can manifest in the release of its own chemical messengers that can act on nearby cells like neurons.

It is now known that GPCR-mediated Ca^{2+} signals in astrocytes have the potential to induce the release of chemical messengers. Borrowing from the superficial similarities to neurotransmission, physiologist Paola Bezzi and neuropharmacologist Andrea Volterra coined the term "gliotransmission" in 2001 to describe this method of glial communication[166]. The mechanisms behind gliotransmission are diverse, but some are shared with neurotransmission[167–170]. For context, the primary mechanisms of neurotransmission include neurotransmitters being packaged into vesicles at presynaptic terminals and subsequentially released via regulated exocytosis following local increases in $[Ca^{2+}]_i$[171]. Although there is some discrepancy in the field[172–174], numerous research groups have shown in astrocyte cultures the presence of small clusters of glutamatergic vesicles[175]. The vesicular glutamate transporters (VGLUT1,

VGLUT2, and VGLUT3) have been shown to colocalized with astrocytic markers, and mRNA expression of VGLUTs is also shown in astrocytes isolated from mouse brains[176–181]. Likewise, the vesicular transporter for ATP (VNUT) and D-serine have also been shown to be expressed in astrocyte cultures, and the secretion of these gliotransmitters, like glutamate, have been linked to Ca^{2+} signaling[182–186]. While there is some evidence for the expression of the vesicular GABA transporter VIAAT, it is not clear if astrocytes use this cellular machinery for GABA exocytosis[187].

Interestingly, astrocytes also utilize several non-exocytotic mechanisms to release gliotransmitters, and the links between these mechanisms and Ca^{2+} signaling vary[167,169]. A prominent method of transferring gliotransmitters out of astrocytes is through plasma membrane channels. Gap junction hemichannels such as connexin can route gliotransmitters like glutamate and ATP out of astrocytes independent of changes in astrocytic $[Ca^{2+}]_i$[188–190]. The activation of the ionotropic purinergic receptor $P2X_7$ is also capable of Ca^{2+}-signaling-independent opening, which permits the movement of glutamate, ATP, and possibly D-serine out of astrocytes *in vitro* and *in situ*[191–194]. Although GABA-regulated exocytosis is unknown, the reversed uptake of GABA through the transporter GAT-1 has been observed in astrocyte cultures from rats[195]. When mimicking pathological conditions such as those during a stroke, researchers have also observed that astrocytes, when induced to swell, will release glutamate and GABA through volume-regulated anion channels[196]. Bestrophin-1, one of these anion channels, has been shown to not only be sensitive to Ca^{2+} signaling, but it can also be permissive to tonic release of these gliotransmitters even in the absence of Ca^{2+} fluctuations[197–199].

Gliotransmitters sufficiently small or lipophilic can be secreted by astrocytes via diffusion through the plasma membrane, while larger ones require transporters to cross the cell membrane. For example, the metabolites of arachidonic acid, a core component of cell membranes, are prominent examples of gliotransmitters that utilize transporters such as prostaglandin transporter (PTG)[200–204]. Following a mGluR-mediated rise in $[Ca^{2+}]_i$, PLC and phospholipase A_2 (PLA_2) become activated, which increases the synthesis of arachidonic acid. This, in turn, activates cyclooxygenases (COXs) 1 and 2, which

synthesizes eicosanoids including the vasoconstrictor thromboxane and various vasodilative prostaglandins. As was observed by Ramón y Cajal a century earlier, astrocytes are poised to regulate cerebral blood flow via the regulation of vessel diameters, thus providing neurons with indirect metabolic support. It is postulated that prostaglandin E_2 (PGE2) is, in part, an active regulator of this vascular action by astrocytes[205–207]. PGE2 signaling action is ultimately mediated via a family of four GPCRs, EP1-EP4[208]. As will be discussed in the next section, the roles of hypothalamic astrocytes and their gliotransmitter PGE2 will not only be viewed as key regulators behind neuronal energy homeostasis, but also within the neuronal circuit underlying reproduction.

Glial Regulation of Reproductive Function

Similar to the role of KNDy and AVPV kisspeptin neurons, accumulating evidence has indicated that glial cells, particularly astrocytes and tanycytes, contribute to GnRH neuron functions via gliotransmission of, in part, prostaglandins. In particular, PGE2 has been known to play a role in the central control of reproduction for at least 50 years, although the source and mechanism of this action was initially unclear. In the 1970s, research teams under neuroendocrinologists Samuel McCann and John Porter observed that intracerebroventricular and hypophyseal injections of PGE2 in rats induced stark increases in LH, FSH, and prolactin[209,210]; LHRH (GnRH) also increased 2- to 3-fold in pituitary stalk blood[209]. McCann's team, spearheaded by neuroendocrinologist Sergio Ojeda, would further investigate the location of PGE2 action within the brain, particularly if this action was directed at the underlying reproductive neural circuit. In one study, rats had cannulas implanted in various hypothalamic locations, and PGE2 was delivered to these regions followed by bioassays for LH release[211]. Cannulas implanted near the ventromedial hypothalamus or caudal to the ARC had little effect on LH levels, but dorsal ARC and, more potently, POA implants strongly raised LH levels. Other studies have utilized indomethacin, a COX inhibitor, to disrupt PGE2 synthesis and alter downstream LH secretion. Indomethacin delivered via intraventricular injections or hypothalamic implantations in rats decreases LH levels[212]. *In vitro* release of LHRH from dissected rat median

eminence tissue is also sensitive to indomethacin; catecholamine-induced LHRH release was blocked by application of indomethacin, and spontaneous LRHR release was attenuated[213].

Indomethacin belongs to the family of antipyretic and analgesic drugs called nonsteroidal anti-inflammatory drugs (NSAIDs), and a side effect of these drugs includes disruption in follicular function[214]. Since the 1970s, NSAIDs such as aspirin have been known to disrupt ovulation in various species including rats, mice, rabbits, rhesus monkeys, pigs, and goldfish[215–220]. Given that ovulation itself is essentially an acute inflammatory reaction, and the canonical role of prostaglandins is inducing inflammation, it followed that prostaglandins played a considerable role at the follicular level[221]. Clinical data have mirrored the results from these animal studies, as females undergoing NSAID therapy often display recurrent and reversible luteinized unruptured follicles (LUTs), one marker for infertility[222]. The endometrium is another source of prostaglandins like PGE2, which drive uterine contractions[223]. Although counter to ovarian function, NSAIDs are also used to treat menstrual headaches and dysmenorrhea[224,225]. Despite these effects on the uterus and ovaries, it was still unclear to what extent NSAIDs alter other elements of the HPG axis in a physiological context.

The effect of PGE2 on GnRH and LH secretion would influence efforts to determine to what extent this interaction manifests in a physiological setting. Early evidence of this interaction would arise from the relationship between PGE2 synthesis and pubertal onset. Ojeda and pharmacologist William Campbell measured the levels of thromboxane and various prostaglandins, including PEG2, in rats on the day of first proestrus before and during the LH surge[226]. Among the eicosanoids measured, only PGE2 exhibited increased synthesis during the LH surge compared to before. This increased synthesis correlated with the increasing uterine masses of the rats, so the researchers determined whether estradiol was a contributing factor in PGE2 synthesis by injecting juvenile rats with estradiol. Once more, PGE2 synthesis increased in the absence of any change in synthesis of the other eicosanoids. Further investigations showed that PGE2-induced LHRH release was blunted in juvenile OVX rats, while OVX+E rats exhibited recapitulated PGE2-induced LHRH release similar to levels seen

in ovary-intact adult rats[227]. Correlating with these findings is a study by Ojeda investigating the effects of reduced bioavailability of arachidonic acid precursors on reproductive development[228]. Here, rats that were provided with a diet that was deficient in essential fatty acids experienced both belayed pubertal onset and first ovulation. This was due, in part, to reduced PGE2 synthesis, as norepinephrine-induced PGE2 secretion from the median eminence was lower compared to non-dieted rats.

Between the 1970s and ‘90s, researchers investigating PGE2 action within the context of reproduction operated under the assumption that PGE2 was synthesized primarily by afferent neurons or by GnRH neurons themselves, and that PGE2 functioned as an intracellular messenger[213,229–231]. However, it would be revealed that these notions were incomplete. Astrocytes emerged as another source of prostaglandin synthesis, including in the hypothalamus[232–235]. In addition, eicosanoids were discovered to bind to a family of GPCRs, and both GnRH neurons in rats and immortalized GnRH neuron GT1-1 cultures expressed EP1 mRNA *in situ* and *in vitro*, respectively[236,237]. Finally, it was observed that noradrenergic neurons do not synapse onto LRHR neurons directly, indicating that norepinephrine-induced LHRH secretion likely required an intermediate cell type conveying PGE2[238,239]. These data would lead Ojeda and colleagues to the hypothesize that hypothalamic astrocytes synthesize PGE2, which then acts on GnRH neurons or their afferents to induce GnRH release[237].

One of the earliest mechanisms by which hypothalamic astrocytes could be stimulated to release PGE2 was via activation of growth-factor-dependent signaling pathways. Ojeda and colleagues first investigated the role of the epidermal growth factor (EGF) homolog transforming growth factor α (TGFα) in reproduction, as earlier reports indicated a role of EGF ligands in LHRH release[240,241]. TGFα was sufficient to induce both LHRH and PGE2 release in microdissected median eminence tissue from rats, and blockading the EGF receptor (EGFR, or erbB1) eliminated TGFα-induced LHRH and PGE2 release. These findings comport with studies observing erbB receptor expression in glia including hypothalamic astrocytes, and a lack of expression in neurons including GnRH neurons in rats and humans[242–245]. In addition, it is observed that EGF signaling via the cognate erbB receptor family is necessary for timely pubertal onset in rats[246–249].

In one study, neuregulin, an EGF-like signaling molecule, was observed to signal via erbB2-erbB4 heterodimers expressed by hypothalamic astrocytes primary cell cultures, which subsequentially induced PGE2 release[250]. Moreover, *in vivo* disruption of erbB2 via intraventricular injection of erbB2-targeted oligodeoxynucleotide resulted in delayed puberty onset in rats.

As was the case with PGE2 synthesis, hypothalamic erbB mRNA expression was also observed to be upregulated by estradiol levels *in vitro* and at the peripubertal stage of development[247,250,251]. Moreover, this estradiol-induced change in hypothalamic expression appears region specific, as cerebellar and cortical expression of erbB and their ligands did not change[247,250,251]. erbB expression also increases throughout juvenile development in a gonad-independent manner. Early in postnatal development, a transient period of sexually dimorphic increase in LH, FSH, and sex steroids levels occurs in a process called “minipuberty”. This event is critical for ensuring proper maturation of germ cells, growth during infancy, and neurobehavioral development in mammals including humans and mice[252,253]. In a transgenic mouse model with a dominant negative erbB4 receptor under control of a GFAP promoter (GFAP-DN-erbB4), FSH levels become blunted during minipuberty. The infantile FSH surge is a critical step in the development of ovarian follicles before puberty, so it is likely that the blunted FSH was a contributing factor behind the delayed sexual maturation observed in these GFAP-DN-erbB4 females.

erbB signaling has also been shown to alter the morphology of hypothalamic and, to a lesser extent, cerebral astrocytes *in vitro*[245]. This supplements several studies showing that glial coverage of reproductive neuronal circuit elements is dynamic. Early studies investigating the role of gonadal steroids on gonadotropin secretion found that rising estradiol levels in the ARC induced synaptic remodeling[254–256]. Similarly, estradiol was found to redistribute astrocytic processes in brain regions including the ARC[254,257]. The relationship between glia and synaptic plasticity comports with imaging data showing how astrocytes are critical in the development, maintenance, and pruning of synapses across the CNS[258]. This interaction between astrocytes and synapses also applies to reproductive circuits in the POA; GnRH neurons in OVX rhesus monkeys were

observed to have glial appositions across a majority of GnRH neuronal membranes, and this also resulted in reduced neuronal innervation[259]. In OVX+E monkeys, however, the amount of glial ensheathment of GnRH neuron somas fell and innervation rose. The remodeling of the GnRH neuron dendritic tree due to glial ensheathment is also found in seasonal breeders like ewes and birds[260–262]. This dynamic level of glial contact with GnRH neurons is thus a mechanism that modifies the neuronal and glial inputs, potentially altering pulse frequency.

Interestingly, PGE2 can mimic the effects of estradiol-induced increases in spine density and innervation in the POA of rodents *in vivo* and *in vitro*[263]. The administration of indomethacin blocks these estradiol-induced effects, indicating estradiol is likely to act upstream of PGE2 synthesis. Whether astrocytes express sex steroid receptors to drive these morphological changes via PGE2, however, is debated[264]. There is evidence of direct estradiol action on astrocytes *in vitro*[265–268]. For example, the findings by neuroendocrinologist Paul Micevych and colleagues showed that estradiol acts on cultured hypothalamic astrocytes to induce progesterone synthesis, which is an important pre-LH surge step[268,269]. However, *in vivo* evidence of estradiol receptor expression in astrocytes is still lacking[264]. Regardless, this indicates that mechanisms of PGE2 and estradiol signaling are intertwined at the level of glial plasticity.

The relationship between glial morphology and levels of sex steroids is also sexually dimorphic[270]. The POA, and particularly the AVPV, are regions of the brain with extensive sexual dimorphism in the neuropil[271–273]. The levels of estradiol and testosterone during development are critical in determining cell fates and reproductive capacity later in adulthood. Early postnatal exposure to androgens in female rats permanently induces anovulatory sterility as well as masculinized sexual behavior as seen in males[274,275]. It is possible for glia to contribute to these phenotypic differences, as astrocyte morphology is also sexually differentiated in a sex-steroid-dependent manner. GFAP-expressing cells in the POA of neonatal male rats are longer and possess more primary processes compared to females[276]. Female rat pups that received PGE2 administration later experienced masculinization of their mating behavior as adults[277]. In addition, the POA of these females during adulthood exhibited

upregulation of COX-2 mRNA expression and increased synaptic density similar to control males. Thus, the morphological differences in astrocytes being sexually dimorphic are likely a consequence of the downstream effects of estradiol-induced PGE2 signaling on masculinization of the underlying reproductive circuit.

Similar to astrocytic morphological plasticity, tanycytes undergo estradiol-dependent morphological rearrangement in females, which may be important in regulating the amount of GnRH secretion from GnRH neuron terminals[278]. Tanycytes are embedded along the wall of the 3rd ventricle including the median eminence where they form an array of tight junction not dissimilar to the blood-brain barrier[279]. Their proximity to the portal blood vessels makes them keenly situated to interact with descending GnRH neuron axon terminals[280]. During low levels of estradiol such as in diestrous or gonadectomized mice, GnRH neuron terminals are almost entirely engulfed by tanycyte endfeet, stymying the access of GnRH to the portal blood vasculature[281]. Conversely, increasing estradiol levels seen during the pre-ovulatory phase of the day of proestrus cause tanycyte endfeet to retreat from GnRH neuron terminals. This permits the effective diffusion of GnRH. Although astrocytes and tanycytes utilize similar molecular pathways including PGE2 synthesis and neuregulin-erbB4 signaling, other mechanisms used by tanycytes include signaling via nitric oxide (NO) and semaphorin, which are stimulated by increasing estradiol levels[282–284]. NO release promotes tanycyte endfeet retraction, while the semaphorin SEMA3A binds to NRP1 receptors on GnRH neurons to promote axonal outgrowth towards to pericapillary space. Overall, these data show that tanycytes work in tandem with astrocytes to regulate the reproductive circuit.

The estradiol-mediated changes in glial morphology, and the level of ensheathment of GnRH neurons, introduces a time-of-day factor during proestrus in rodents. In young female rats, the surface area of GFAP-expressing cells in the POA undergoes diurnal changes on proestrus, where morning surface area is greater than that in the afternoon[285]. The reduced afternoon glial coverage likely permits greater excitatory afferent signaling to GnRH neurons immediately before the preovulatory LH surge. Reduced diurnal glial plasticity is also observed in the POA of middle-aged rats, which would alter the cyclic neurotransmitter inputs on the afternoon of proestrus. This may

explain the notable changes in the LH surge between young and adult rats, where the surge becomes more delayed and the amount of LH released decreases with aging[286]. In addition, the characteristics of diurnal glial plasticity are themselves heterogeneous across the hypothalamus. While POA glia increase the level of synaptic spine density in the presence of rising estradiol levels, ARC glia have the opposite effect[270]. Thus, it is important to consider the impact of diurnal factors when investigating how each glial population in the hypothalamus contributes to the reproductive circuit in rodents.

Although the role of PGE2 in GnRH and LH release was described nearly 50 years ago, its effect on GnRH neuronal activity was not reported until the last decade. In 2011, neuroendocrinologist Vincent Prevot and colleagues conducted *ex vivo* patch-clamp recordings on GnRH neurons from adult GnRH-GFP mice[287]. Treatment of these POA brain slices with PGE2 induced robust and reversible GnRH neuron depolarization in a majority of these neurons regardless of sex and cycle stage. PGE2 acts directly on GnRH neurons, as the presence of tetrodotoxin (TTX) and blockers for the receptors of fast-synaptic transmission still induced depolarization. In line with this, the EP2 agonist butaprost, but not EP1 or EP3 agonists, mimicked the PGE2 effects. Blocking the synthesis of endogenous PGE2 in acute POA slices by using indomethacin leads to a dramatic suppression of spontaneous action potential firing in GnRH neurons. Inhibition of astrocytic metabolism with the glial toxin fluoroacetate mimicked the inhibitory effect of indomethacin on GnRH neuronal activity. Similarly, *ex vivo* recordings of GnRH neurons from GFAP-DN-erbB4 mice showed reduced excitability, while exogenous PGE2 administration recapitulated GnRH depolarization. These data indicate that astrocytes are the main source of PGE2 in the POA, and that endogenous PGE2 production is required for normal GnRH neuronal activity.

To measure the direct communication between POA astrocytes and GnRH neurons, a recent study utilized DREADDs to artificially activate astrocytes to elicit downstream neuronal responses[288]. DREADD expression in astrocytes was spatially and temporally controlled using AAVs with GFAP promoters, wherein these AAVs were intracerebrally injected into the POA or ARC regions on mice. When targeted extracellular recordings of GnRH neurons were performed in acutely prepared POA slices with DREADD-

expressing astrocytes, CNO increased GnRH neuron firing in male mice. In contrast, recordings of ARC KNDy neurons did not show a respond to CNO treatment in males, which indicates that KNDy neurons - purported to be the pulse generator of GnRH neurons - likely do not relay astrocyte signaling within the context of reproduction. This stimulation of GnRH neurons by POA astrocytes was also shown to be, in part, mediated by PGE2, as blockage of the EP1 and EP2 receptors with pretreatment of their antagonists attenuated CNO-induced GnRH neuron firing. Finally, *in vivo* assays of LH levels in mice injected with DREADD-expressing AAVs indicated that CNO increased LH levels in POA-targeted males. As with the targeted extracellular recordings, LH levels did not change in ARC-targeted males after being administered CNO. Contemporaneous studies in females were inconclusive because these experiments were conducted much longer after viral injection, and the time of day of these experiments differed to that conducted in males. Further work is needed to delineate the sex differences in astrocytic regulation of GnRH neurons.

Dissertation Preview

The cumulative work of this dissertation aims to better understand the role of hypothalamic astrocytes in reproduction, and what endogenous mechanisms underly the communication between these astrocytes and the central reproductive neural circuit, particularly GnRH and KNDy neurons. This glial-neuronal communication was assessed while considering the influences of both sexual differentiation and time-of-day-dependent factors. Regarding the former, it was necessary to investigate the neuronal elements most analogous between females and males. Thus, our focus was also extended to KNDy neurons, but not AVPV kisspeptin neurons, due to the former neurons being responsible for the negative steroid feedback in males and diestrous females and fewer AVPV kisspeptin neurons in male rodents.

Chapter 2 details to what extent hypothalamic astrocyte chemogenetic activation and downstream GnRH and KNDy neuron responses are modified by the sex of the mouse and the time of day of the experiments. Chapter 3 will focus on the endogenous mechanisms that underlie hypothalamic astrocyte activation. Candidate mechanisms of

activation are screened for using *ex vivo* calcium imaging of hypothalamic astrocytes expressing GCaMP6f. Ongoing experiments utilizing CRISPR/Cas9 then assess if knockdown of a candidate receptor of these endogenous signaling pathways compromises reproductive function *in vivo.* Tangentially, pilot studies aimed at attenuating Ca^{2+} signaling in astrocytes using viral expression of a Ca^{2+} ATPase are also discussed. Chapter 4 summarizes these findings to advance our understanding of the extent of astrocyte-GnRH neuron communication and the mechanisms driving this crosstalk. In addition, future directions and ongoing experiments will be addressed, particularly a study that is investigating the *in vivo* consequences of PGE2 signaling disruption at the level of EP2 receptor expression in GnRH neurons using a conditional *Ptger2* knockout mouse model.

Chapter 2: Sex and Time of Day Alter the Interactions Between Hypothalamic Glia and the Neural Circuits Controlling Reproduction[1]

Abstract

An upstream network, including glia and arcuate nucleus (ARC) kisspeptin neurons, controls hormone secretion from preoptic area (POA) gonadotropin-releasing hormone (GnRH) neurons, which form the final common pathway for the central control of fertility. In males, chemogenetic activation of Gq-mediated signaling in POA glia activated GnRH neurons and downstream luteinizing hormone (LH) release, while chemogenetic activation of ARC glia had no effect on ARC kisspeptin neurons. We characterized sex differences and time-of-day effects in these critical circuits to understand their effects on reproduction. Chemogenetic activation of glial fibrillary acidic protein (GFAP)-expressing cells increased intracellular calcium concentrations regardless of sex, brain region, or time of day. Activation of POA glia or treatment with the gliotransmitter analog dimethyl prostaglandin E_2 (dmPGE2) increased GnRH neuron firing rate, and these responses were dependent upon sex and time of day. In contrast, ARC kisspeptin neuron firing rate was unresponsive to ARC glia activation or dmPGE2 regardless of sex or time of day. POA glial activation increased LH levels in males and females but the response in males was more rapid. ARC glia activation had no effect on LH in females and the response in males was delayed compared to POA glia activation. A similar LH response persisted after ARC kisspeptin neuron ablation, suggesting it is not mediated by those neurons. GnRH neurons rather than arcuate kisspeptin neurons are thus the main target of glial regulation of reproductive neuroendocrine output and this regulation is dependent on sex and time of day.

[1] Phillips CD, DeFazio RA, Moenter SM. Sex and time of day alter the interactions between hypothalamic glia and the neural circuits controlling reproduction. *Endocrinology*. 2025;166:bqaf057. DOI: 10.1210/endocr/bqaf057

Introduction

The hypothalamic-pituitary-gonadal axis forms the core of reproductive regulation. Underlying the hypothalamic component is the gonadotropin-releasing hormone (GnRH) network, which consists of the GnRH neurons and inputs to these cells from different cell types. Episodic GnRH release is the final hypothalamic output to the anterior pituitary in both sexes and changes in this episodic release drive reproductive cycles in females[289,290]. GnRH stimulates the synthesis and release of the gonadotropins luteinizing hormone (LH) and follicle-stimulating hormone (FSH) in a frequency-dependent manner[60,291]. LH and FSH activate gametogenesis and gonadal steroidogenesis, the latter being critical for feedback regulation of GnRH release[292].

Many factors regulating fertility, including steroid feedback, are primarily relayed to GnRH neurons via neurons and/or glia sensitive to those cues[293]. A major neuronal contributor is the population of hypothalamic arcuate (ARC) kisspeptin neurons expressing sex steroid receptors[107,294] and the neuropeptides neurokinin B and dynorphin (KNDy neurons)[121,295–297]. KNDy neurons have been postulated to be involved in generating episodic GnRH release. The application of their peptides, particularly kisspeptin, contribute to the regulation of GnRH neuron activity and LH release[95,98,118,298–300]. Glial cells, particularly astrocytes, are integral non-neuronal elements regulating reproduction[243,301–303]. In addition to their roles in central nervous system maintenance, astrocytes interact with neurons through at least two mechanisms: direct coverage and gliotransmission. Regarding the latter, signaling molecules secreted by astrocytes via gliotransmission can regulate GnRH neuron function. Prostaglandin E_2 (PGE2), likely glia-derived, is a potent activator of GnRH neurons[287,288]. Disrupting astrocytic erbB receptor signaling (an important activator of PGE2 synthesis) and dietary deficiency of essential fatty acids, including the PGE2 precursor arachidonic acid, decreases GnRH/LH release and disrupts sexual maturation in females[228,243,246,250]. Gliotransmission and astrocyte plasticity are postulated to be caused, at least in part, by an increase of intracellular calcium levels ($[Ca^{2+}]_i$) in astrocytes through activation of Gq-coupled GPCRs[304,305]. Chemogenetic activation of Gq signaling in preoptic (POA) astrocytes proximal to GnRH neurons in male mice

increased the firing rates of these cells in a manner at least in part dependent on PGE2 receptors, and induced LH release[288]. Interestingly, when ARC astrocytes are similarly chemogenetically activated, KNDy neuron firing rates and LH levels were unchanged in males[288].

The above findings point to the critical role of glia in regulation of the GnRH network in a region-specific manner. It remains unknown, however, if or how several fundamental aspects that are crucial to the central regulation of reproduction are mediated by glia. Here, we test the working model that hypothalamic astrocyte regulation of GnRH and KNDy neuron activity and LH release are dependent upon sex, cycle stage, and time of day.

Materials & Methods

All reagents were purchased from Sigma-Aldrich (St. Louis, MO) unless noted otherwise.

Animals. Mouse strains are listed in Table 2.1. Mice expressing green fluorescent protein (GFP) under the control of the *Gnrh1* promotor (B6;CBA-Tg[Gnrh1-EGFP]51Sumo/J, "GnRH-GFP" mice, 033639)[306] and *Tac2*-enhanced GFP BAC transgenic mice (STOCK Tg[Tac2-EGFP]HF381Gsat/Mmucd, "Tac2-GFP" mice, 015495-UCD) were obtained from The Jackson Laboratory and The Mutant Mouse Resource & Research Centers, respectively; these mice were propagated in our colony to identify GnRH and KNDy neurons, respectively, for electrophysiological experiments. *Tac2* encodes neurokinin B, which is coexpressed with kisspeptin and dynorphin in most KNDy neurons[307]. C57BL/6J mice were obtained from The Jackson Laboratory (000664) and propagated in our colony for Ca^{2+} imaging experiments. Mice expressing Cre recombinase under control of the *Tac2* promoter ("Tac2-Cre" mice) have been described[122], and were crossed with Tac2-GFP mice and propagated in our colony for KNDy neuron ablation experiments. Mice were maintained under a 14-hour light, 10-hour dark photoperiod (lights on at 0300 h) with *ad libitum* access to Teklad 2916 chow (Envigo; Madison, WI) and water. Adult mice aged 2 to 6 months were used for stereotaxic injections. In females, estrous cycle stage was determined by vaginal lavage

and confirmed by uterine mass (< 80 mg for diestrus, and > 100 mg for proestrus)[308]. Animals were randomized among experimental groups. The Institutional Animal Care and Use Committee at the University of Michigan approved all procedures.

Table 2.1: Mouse strains used.

Strain name	Shorthand	Reference	Supplier	Catalog number	RRID
C57BL/6J	Wild Type	[309]	The Jackson Laboratory	000664	IMSR_JAX:000664
B6;CBA-Tg(Gnrh1-EGFP)51Sumo/J	GnRH-GFP	[306]	The Jackson Laboratory	033639	IMSR_JAX:033639
STOCK Tg(Tac2-EGFP)HF381Gsat/Mmucd	Tac2-GFP	[307]	MMRRC	015495-UCD	MMRRC_015495-UCD
$Tac2^{tm1.1(cre)Mgmj}$	Tac2-Cre	[122]	Martin Myers, University of Michigan	N.A.	N.A.

Stereotaxic injections. Adeno-associated viruses (AAVs) are listed in Table 2.2. Mice were anesthetized with isoflurane (30 s at 5% for induction, and 1.5% for maintenance) and given carprofen (5 mg/kg, sc) before surgery and 24 hours post-surgery for analgesia. Anesthetized mice were placed in a stereotaxic instrument (Model 942, David Kopf Instruments) with body temperature maintained at 36°C using a feedback-controlled heating pad (TCAT-2LV Controller, Physitemp Instruments). AAV5 containing a payload of the mCherry-fused designer receptor exclusively activated by designer drug (DREADD) hM3Dq under the control of the GFAP promoter (“AAV-GFAP-hM3Dq”, Addgene 50478) or a GFAP-driven control AAV5 (“AAV-GFAP-mCherry”, Addgene 58989) was injected into the POA of GnRH-GFP or the ARC of Tac2-GFP mice. AAV5 encoding GFAP-driven GCaMP6f (“AAV-GFAP-GCaMP6f”, Addgene 52925) was mixed with either AAV-GFAP-hM3Dq or AAV-GFAP-mCherry in a 1:1 ratio and injected into either the POA or ARC of C57BL/6J mice. AAV5 encoding a floxed caspase-3 (“AAV-flex-taCasp3”, Addgene 45580) was mixed with either AAV-GFAP-hM3Dq or AAV-GFAP-mCherry in a 1:1 ratio and injected into the ARC of Tac2-Cre::Tac2-GFP males. AAVs

were bilaterally injected into the POA (1.2 mm anterior to bregma; 0.2 mm from the midline; 5 mm ventral from the skull surface at bregma) or ARC (1.3 mm posterior to bregma; 0.2 mm from the midline; 5.95 mm ventral from the skull surface at bregma). In situations in which multiple viruses were needed for a single study, 100 nL of each AAV were mixed together and the total volume (up to 200 nL) injected into the POA or ARC at a rate of 50 nL/min. Mice were monitored until fully recovered from anesthesia. Surgical sites were monitored daily for 10 days for signs of infection or dehiscence. Viral transduction proceeded for 3-6 weeks before experiments were conducted.

Table 2.2: Viruses used.

AAV	Shorthand	Reference	Supplier	Catalog number	RRID
pAAV-GFAP-hM3D(Gq)-mCherry	AAV-GFAP-hM3Dq	[288]	Addgene	50478-AAV5	Addgene_50478
pZac2.1 gfaABC1D-cyto-GCaMP6f	AAV-GFAP-GCaMP6f	[310]	Addgene	52925-AAV5	Addgene_52925
pAAV-GFAP104-mCherry	AAV-GFAP-mCherry	[311]	Addgene	58909-AAV5	Addgene_58909
pAAV-flex-taCasp3-TEVp	AAV-flex-taCasp3	[312]	Addgene	45580-AAV5	Addgene_45580

Immunofluorescence. Antibodies are listed in Table 2.3. Mice were deeply anesthetized with isoflurane and transcardially perfused for 2-5 min with 10-20 mL filtered 0.9% NaCl followed by 20 mL 10% neutral-buffered formalin for 5 min. Brains were placed into the same fixative overnight at 4°C. Brains were then transferred to a 30% sucrose solution for at least two days for cryoprotection. Four series of 40-µm sections were cut on a cryostat (CM30505 S, Leica) and stored at -20°C in antifreeze solution (25% ethylene glycol and 25% glycerol in PBS). Before labeling, sections were washed once with PBS containing 0.1% TritonX-100 (PBST), then treated with 0.1% $NaBH_4$ in PBST for 10 min to reduce background autofluorescence. Sections were washed with PBST (3 times, 5 min each) and then placed in blocking solution (PBST containing 10% normal goat

serum; Jackson ImmunoResearch) for 1 h at room temperature. Sections were incubated in primary antibodies diluted in blocking solution for 48 h at 4°C. Sections were washed in PBST (3 times, 5 min each) and then incubated in Alexa-conjugated secondary antibodies for 1.5 h at room temperature (Molecular Probes and Jackson ImmunoResearch). Sections were washed in PBS (3 times, 5 min each) and then mounted on Superfrost Plus slides (Thermo Fisher Scientific) with ProLong Gold antifade reagent containing DAPI (Invitrogen) and coverslipped (VWR International). Images were collected on a Nikon Eclipse TE200 (lower magnification) or on a Nikon A1 confocal microscope (colocalization studies). The number of mCherry-only, GCaMP6f-only, mCherry/S100β, GCaMP6f/S100β, mCherry/NeuN, and GCaMP6f/NeuN coexpressing cells were counted from pictures (signal observed by eye, 5 fields/mouse in the infected region).

Table 2.3: Antibodies used.

Antibody	Species	Working dilution	Reference	Supplier	Catalog number	RRID
Anti-S100β	Rabbit	1:500	[313]	GeneTex	GTX129573	AB_2886037
Anti-mCherry	Rat	1:3,000	[314]	Thermo Fisher Scientific	M11217	AB_2536611
Anti-NeuN	Rabbit	1:3,000	[315]	Abcam	ab177487	AB_2532109
Anti-GFP	Chicken	1:1,000	[316]	Abcam	ab13970	AB_300798
Anti-bovine LHβ subunit	Mouse	1:1,000	[317]	Janet Roser, UC Davis	518B7	AB_2665514
AFP240580 Rb	Rabbit	1:10,000	[317]	National Hormone and Peptide Program	rLH	AB_2665533
Anti-rabbit, horseradish peroxidase	Goat	1:2,000	[317]	Dako-Cytomation	D048701-2	AB_2617144
Anti-rabbit, Alexa Fluor 488	Goat	1:500	-	Thermo Fisher Scientific	A-11008	AB_143165
Anti-chicken, Alexa Fluor 488	Goat	1:500	-	Thermo Fisher Scientific	A-11039	AB_142924
Anti-rat, Alexa Fluor 594	Goat	1:500	-	Thermo Fisher Scientific	A-11007	AB_141374
Anti-rabbit, Alexa Fluor 647	Goat	1:500	-	Thermo Fisher Scientific	A-21244	AB_2535812

Tail tip blood sampling. To examine the effect of DREADD activation on LH levels, GnRH-GFP and Tac2-GFP mice were acclimated to daily handling and mock blood

collection for at least three weeks following stereotaxic injections. During experimentation, the tip of the tail was nicked and 6 µL of blood was collected and mixed immediately with 54 µL of assay buffer (PBS, 0.05% Tween, and 0.2% BSA). Mice were sampled every 10 min for 2 h (0800 - 1000 h or 1500 - 1700 h for the AM and PM groups, respectively); IP injections of 0.9% saline (volume matched to CNO) and 0.3 mg/kg CNO were given at the 30-min and 1-h marks, respectively. Blood samples diluted with assay buffer were kept on ice until the end of sampling, and were then stored at -20°C.

LH assay. LH assays were conducted at the Ligand Assay and Analysis Core of the University of Virginia Center for Research and Reproduction[317]. The capture monoclonal antibody (anti-bovine LHß subunit, 518B7) is provided by Janet Roser, University of California, Davis. The detection polyclonal antibody (rabbit LH antiserum, AFP240580Rb) is provided by the National Hormone and Peptide Program (NHPP). Horseradish peroxidase-conjugated polyclonal antibody (goat anti-rabbit, D048701-2) is purchased from DakoCytomation (Glostrup, Denmark). Mouse LH reference prep (AFP5306A; NHPP) is used as the assay standard. The limit of quantitation (functional sensitivity) was 0.016 ng/mL, defined as the lowest concentration that demonstrates accuracy within 20% of expected values. Intraassay coefficient of variation (%CV) determined from serial dilutions of a defined sample pool was 2.2%. Interassay %CVs for the same pools were 7.3% (low QC, 0.13 ng/mL), 5.0% (medium QC, 0.8 ng/mL), and 6.5% (high QC, 2.3 ng/mL).

Brain slice preparation. All solutions were bubbled with 95% O_2 and 5% CO_2 to maintain pH and oxygenation for at least 15 min before use and throughout electrophysiological and Ca^{2+} imaging experiments[318]. Brains were rapidly removed (0900 - 1000 h or 1500 - 1600 h for the AM and PM groups, respectively) and placed in ice-cold sucrose saline solution containing the following (in mM): 250 sucrose, 3.5 KCl, 26 $NaHCO_3$, 10 D-glucose, 1.25 Na_2HPO_4, 1.2 $MgSO_4$, and 3.8 $MgCl_2$[318]. Coronal brain slices (300 µM) were cut with a VT1200S (Leica Biosystems). Slices were incubated for 30 min at room temperature (21-23°C) in 50% sucrose saline and 50% artificial cerebrospinal fluid (ACSF, pH 7.4) containing the following (in mM): 135 NaCl, 3.5 KCl, 26 $NaHCO_3$, 10 D-

glucose, 1.25 Na_2HPO_4, 1.2 $MgSO_4$, and 2.5 $CaCl_2$. Slices were then transferred to 100% ACSF and held at room temperature for at least 30 min before recording. Individual slices were transferred to a recording chamber mounted on an Olympus BX51WI upright fluorescent microscope (Evident). Perfusion of ACSF was maintained at a rate of 3 mL/min with a MINIPULS 3 peristaltic pump (Gilson) and heated by an in-line heater (Warner Instruments) to 29-32°C. Slices were used within 6 h of preparation. No differences in results associated with time after brain slice preparation were observed.

Electrophysiological recordings. Targeted single-unit extracellular recordings were used to characterize neuronal firing rates as they minimally disrupt the intrinsic properties of the neuron[318,319]. GFP-positive cells were targeted for recording in the POA or ARC of slices from GnRH-GFP or Tac2-GFP mice, respectively. Cells inside the mCherry signal were considered within the infected area and used for recordings. Recording pipettes (2-4 MΩ) were pulled from borosilicate glass (Schott no. 8250, World Precision Instruments) with a P-97 puller (Sutter Instrument). Pipettes were filled with HEPES-buffered solution containing the following (in mM): 150 NaCl, 10 HEPES, 10 D-glucose, 2.5 $CaCl_2$, 1.3 $MgCl_2$, and 3.5 KCl (pH = 7.4). Low-resistance seals (6-20 MΩ) were formed between the pipette and neuron. The pipette potential was held at 0 mV in voltage-clamp mode. Recordings were acquired at 10 kHz and filtered at 5 kHz using one channel of an EPC10 dual patch-clamp amplifier controlled with PatchMaster software (HEKA Elektronic). Following a 2-10-min stabilization period, recordings consisted of a 5-min baseline period, a 6-min bath-applied treatment period, and a 9-min wash period that was extended if needed to observe neuron firing rates returning towards baseline firing rates. If action currents were not observed near the end of a recording session, then 20 mM KCl or either 100 nM kisspeptin (GnRH-GFP recording) or 100 nM senktide (Tac2-GFP recording) was bath-applied; neurons that were unresponsive to these control stimuli were excluded from analysis. A minimum of three mice were studied per group with the exception of two mice in the proestrous AM | POA control virus group (Figure 2.4). Up to three recordings were conducted per mouse.

Ca^{2+} imaging. Ca^{2+} imaging was used to characterize the effect of activating the DREADD hM3Dq on $[Ca^{2+}]_i$ in GFAP-expressing cells. GCaMP6f-expressing cells in

either the POA or ARC were imaged under a 20x objective with an ORCA-FLASH4.0 V3 CMOS camera (Hamamatsu). Imaging was acquired at 500 ms intervals with 50 ms exposure times using Olympus cellSense software (Evident). Following a 5-min stabilization period, imaging sessions consisted of a 5-min baseline period, a 6-min bath applied treatment period, and a 9-min wash. Regions of interest (ROIs) were selected based on signal fluctuations that were identified before treatment. Each ROI is assumed to represent the soma or processes of a GFAP-expressing cell.

Analysis and statistics. Action current event detection was completed using Igor Pro 8 (Sutter Instruments) using custom routines (https://gitlab.com/um-mip/coding-project.git), and all events were manually confirmed. Short breaks in the recording (< 2 s) were introduced to monitor the seal resistance; these breaks were excluded when calculating mean firing rates. Mean firing rates were calculated for the last 2 min of baseline, minutes 2-4 of treatment, and the last 2 min of wash. In experiments in which vehicle pretreatment was done, no differences were observed between the firing rates during that phase and baseline firing rates, thus the presentation of this data is simplified by omitting baseline firing in graphs; this did not alter statistical outcomes.

The algorithm used to calculate Ca^{2+} signals ($\Delta F/F_0$) was derived from prior research analyzing Ca^{2+} signals[320]. This algorithm was coded into Igor Pro 8. In brief, mean fluorescence $F(t)$ of an ROI was calculated for each time point t. The time-dependent baseline $F_0(t)$ for that ROI was then calculated; $F_0(t)$ was defined as the minimum value of the smoothed $F(t)$ during a user-defined time window of duration τ (500 s) extending from $t - \tau$ to t. The relative change of fluorescent signal between $F(t)$ and $F_0(t)$ was calculated and filtered to yield $\Delta F/F_0$. To quantify the effect of treatment on Ca^{2+} signaling, the area under the curve (AUC) from each ROI's $\Delta F/F_0$ curve was calculated. The AUCs obtained from 10 to 27 independent ROIs (23.3 ± 0.6) were averaged to yield the average AUC of the slice. Up to three slices were used per mouse, and a minimum of three mice were studied per group. AUC values were calculated for the last 2 min of baseline, minutes 2-4 of treatment, and the last 2 min of wash.

Statistical analyses were conducted with Prism 10 (GraphPad, Version 10.4.1 [627]) and SPSS (IBM, Version 29.0.0.0 [241]). Distribution of data was checked with Shapiro-Wilk; most experiments included one or more groups that were not normally distributed. ANOVA was conducted to evaluate the main effects and interactions of sex, cycle stage, and/or time of day. Bonferroni correction for multiple comparisons was used as this test is sufficiently robust for non-normally distributed data[321]. The level accepted as significant was set to $p < 0.05$. Statistics tests for each experiment are specified in the figure legends.

Results

AAV5 delivery of glial fibrillary acidic protein (GFAP) promoter-driven constructs targets glial cells. To characterize the effect of chemogenetic activation of glial cells on reproduction, we used AAV5s bearing constructs driven by the GFAP promoter. GFAP is a commonly used marker for glial cells, and is expressed not only in the brain but across the body[322]. We thus manipulated glia in specific regions by performing stereotaxic viral injections. Viral payloads included the following: a control mCherry reporter (AAV-GFAP-mCherry), the mCherry-tagged designer receptor exclusively activated by designer drug (DREADD) hM3Dq (AAV-GFAP-hM3Dq) that activates Gq-coupled signaling upon exposure to the DREADD ligand clozapine N-oxide (CNO), and/or the calcium indicator GCaMP6f (AAV-GFAP-GCaMP6f). All mouse strains are listed in Table 2.1, and all viruses in Table 2.2. Mice received bilateral injections of AAVs into the POA containing GnRH neurons or the ARC containing KNDy neurons. To characterize the cell types expressing the AAVs, we performed dual immunofluorescence of either mCherry (Figure 2.1A) or GCaMP6f (Figure 2.1B) with the astrocytic cytoplasmic marker S100β or the neuronal marker NeuN. Over 90% of cells expressing the control virus, hM3Dq, or GCaMP6f also expressed S100β regardless of the brain region (Figure 2.1C). In contrast, less than 8% of cells expressing any AAV were also positive for NeuN regardless of the brain region (Figure 2.1C). This confirms the efficacy of AAV payload expression in predominantly glial cells. To increase rigor, we also visually examined brain slices during recordings for mCherry-expressing cells exhibiting neuronal morphology; data gathered from brain slices

containing such cells were excluded. Notably, mCherry co-expression was not observed in any GnRH-GFP or Tac2-GFP cells.

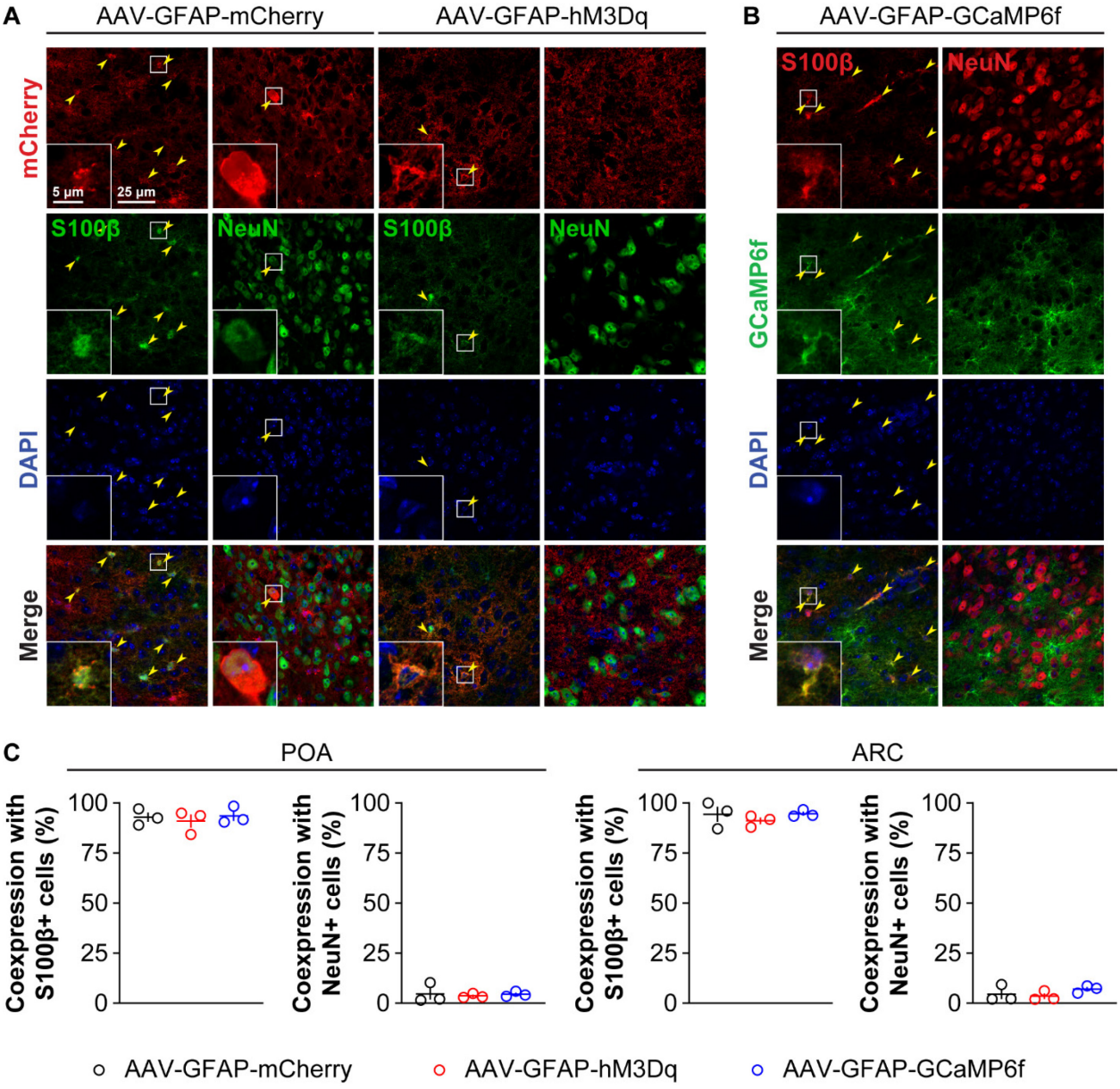


Figure 2.1: AAV5 constructs bearing glial fibrillary acidic protein (GFAP) promoter-driven genes effectively target cells with glial morphology and astrocytic markers in the hypothalamus. **A and B,** Representative dual immunofluorescent images of mCherry+ (A) and GCaMP6f+ (B) cells stained with either S100β or NeuN to show colocalization of the two signals. Yellow arrowheads point to instances of colocalization. Areas in the small white boxes are magnified and displayed in the larger white boxes. **C,** Quanitification of infected cells expressing either S100β or NeuN in the POA and ARC (n = 3 mice per group, 5 fields per mouse).

Activation of Gq signaling in GFAP-expressing cells in the POA and ARC increases $[Ca^{2+}]_i$ levels regardless of sex, time of day, or cycle stage. Having verified successful targeting of the AAVs, we set up comparisons to address our working model. To examine sex differences, males and females were studied. In females, cycle stages characteristic of steroid negative feedback (diestrus) and positive feedback (proestrus) were examined. Time of day is an important variable regulating ovulation in females, with the preovulatory GnRH/LH surge occurring in the late afternoon, thus morning (AM) and late afternoon (PM) conditions were compared; mice were studied or brain slices prepared in these timeframes.

First, we investigated if $[Ca^{2+}]_i$ was augmented in GFAP-expressing cells by activating DREADDs with CNO, and if any increase was dependent upon sex, time of day, or cycle stage. Spontaneous $[Ca^{2+}]_i$ changes were observed before CNO treatment in all brain slices recorded. To assess the response to CNO treatment, the area under the curve (AUC) was calculated from $\Delta F/F_0$ traces as a proxy for elevations in $[Ca^{2+}]_i$ (Figure 2.2A and B). In POA slices from mice coinjected with AAV-GFAP-GCaMP6f and the control AAV-GFAP-mCherry, AUC was not altered by bath application of CNO in the AM or PM (Figure 2.2C and D, respectively; Figure 2.2 statistical parameters in Tables 2.4 and 2.5) regardless of sex or cycle stage. In contrast, POA slices from mice that received co-injections of AAV-GFAP-GCaMP6f and AAV-GFAP-hM3Dq showed clear increases in $\Delta F/F_0$ that were reflected in increased AUC during CNO treatment in the AM (Figure 2.2C) and PM (Figure 2.2D) regardless of sex or cycle stage. In the afternoon, the CNO-induced increase in AUC in slices from male DREADD mice was greater than that in diestrous and proestrous females (Figure 2.2D).

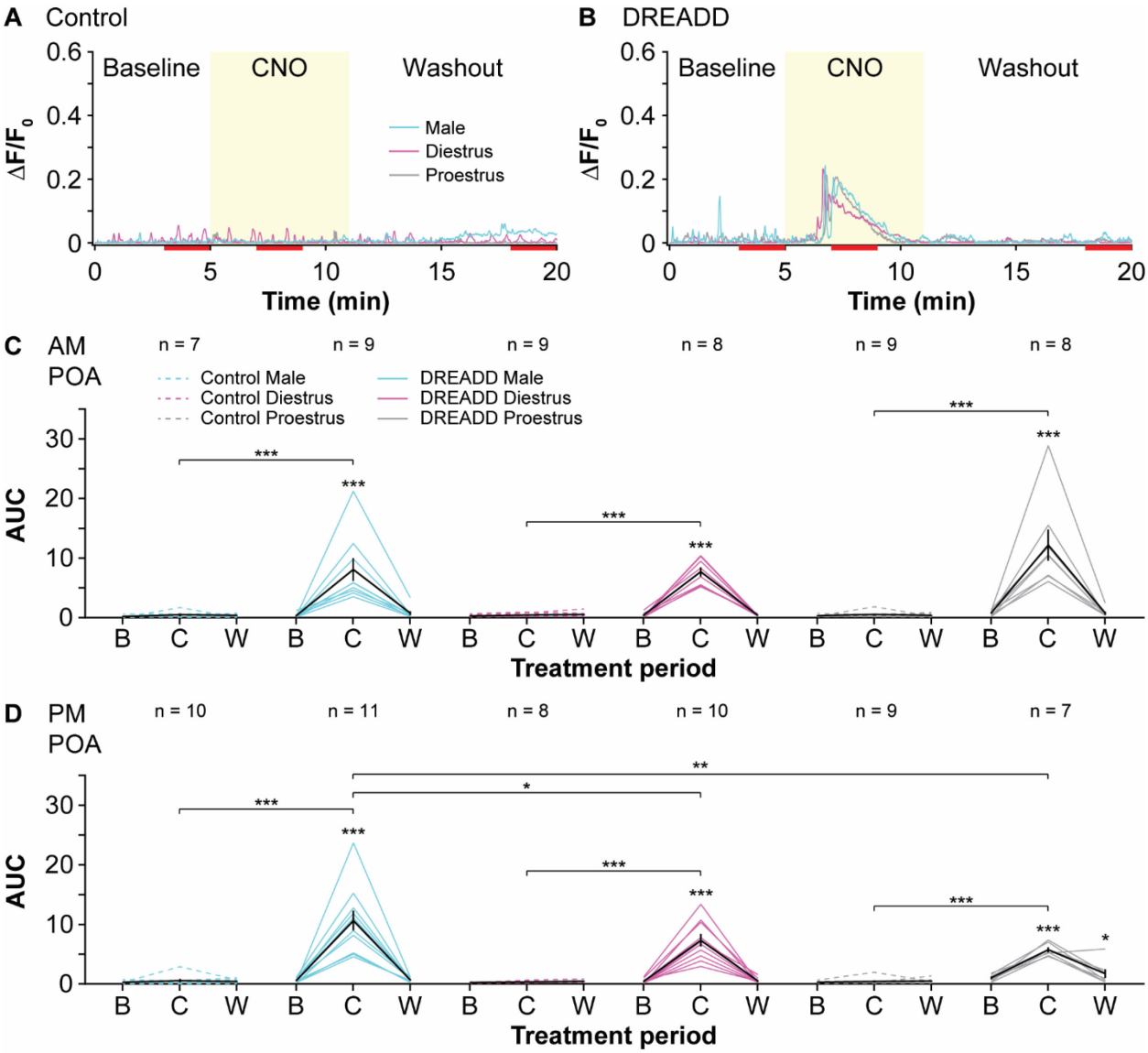


Figure 2.2: Activating Gq singaling in GFAP-expressing cells in the POA increases $[Ca^{2+}]_i$ regardless of sex, cycle stage, or time of day. **A and B,** Representative *ΔF/F₀* traces in brain slices from mice coinjected in the POA with AAV-GFAP-GCaMP6f and either AAV-GFAP-mCherry (A) or AAV-GFAP-hM3Dq (B). Red bars on the x-axis indicate the windows used for statistical comparisons. **C and D,** Quantification of AUC values in brain slices from control (dashed cyan, magenta, and grey lines) and DREADD (solid cyan, magenta, and grey lines) mice overlaid with mean ± SEM (black lines) in the AM and PM (C and D, respectively; three-way mixed-model ANOVAs with Bonferroni *post hoc*). B, baseline; C, 200 nM CNO; W, washout. Statistics are in Tables 2.4 and 2.5. Baseline-baseline and washout-washout pairwise comparisons are ommitted from the figure for clarity. *, $p < 0.05$; **, $p < 0.01$; ***, $p < 0.001$ for between-group comparisons indicated by bars, and for within-group comparisons to baseline indicated by stars alone.

To determine if calcium signaling properties in GFAP-expressing cells vary across different brain regions regulating reproduction, viral targeting and calcium imaging was also conducted at the ARC near KNDy neurons. Similar to the POA, AUC in ARC slices from control virus mice did not change during CNO treatment in the AM or PM (Figure 2.3C and D, respectively; Figure 2.3 statistical parameters in Tables 2.6 and 2.7) regardless of sex and cycle stage, whereas slices from DREADD virus mice exhibited an increase in AUC during CNO treatment in the AM (Figure 2.3C) and PM (Figure 2.3D) regardless of sex or cycle stage. In the PM, the CNO-induced increase in AUC was greater in slices from DREADD males and diestrous females than in proestrous females (Figure 2.3D). Despite these variations in amplitude, these calcium imaging data demonstrate efficacy of DREADD activation in augmenting $[Ca^{2+}]_i$ in GFAP-expressing cells in both brain regions of interest.

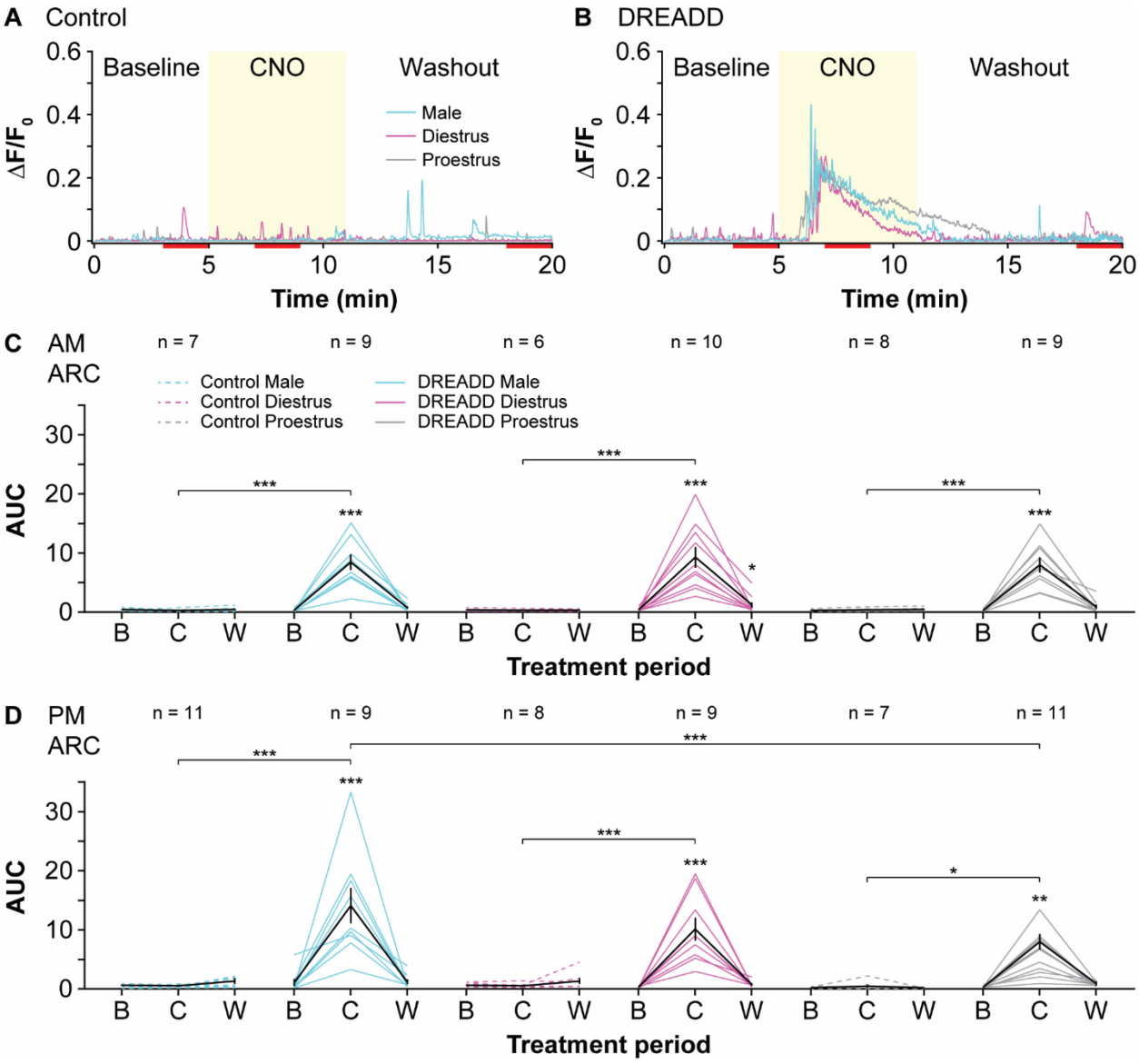


Figure 2.3: Activating Gq singaling in GFAP-expressing cells in the ARC increases $[Ca^{2+}]_i$ regardless of sex, cycle stage, or time of day. **A and B,** Representative $\Delta F/F_0$ traces in brain slices from mice coinjected in the ARC with AAV-GFAP-GCaMP6f and either AAV-GFAP-mCherry (A) or AAV-GFAP-hM3Dq (B). Red bars on the x-axis indicate the windows used for statistical comparisons. **C and D,** Quantification of AUC values in brain slices from control (dashed cyan, magenta, and grey lines) and DREADD (solid cyan, magenta, and grey lines) mice overlaid with mean ± SEM (black lines) during the AM and PM (C and D, respectively; three-way mixed-model ANOVAs with Bonferroni *post hoc*). B, baseline; C, 200 nM CNO; W, washout. Statistics are in Tables 2.6 and 2.7. Baseline-baseline and washout-washout pairwise comparisons are ommitted from the figure for clarity. *, $p < 0.05$; **, $p < 0.01$; ***, $p < 0.001$ for between-group comparisons indicated by bars, and for within-group comparisons to baseline indicated by stars alone.

Activation of Gq signaling in POA GFAP-expressing cells increases GnRH neuron firing rates in brain slices regardless of sex, time of day, or cycle stage. To determine if CNO-induced activation of GFAP-expressing cells has downstream effects on GnRH neuron firing, we performed extracellular recordings on GFP-tagged GnRH neurons. Brain slices were prepared from GnRH-GFP mice that received injections of either AAV-GFAP-mCherry (Figure 2.4A) or AAV-GFAP-hM3Dq (Figure 2.4B), and targeted extracellular recordings were made of firing activity in GnRH neurons within the infection sites. CNO treatment did not alter the firing rate of GnRH neurons in brain slices from control virus mice in the AM or PM (Figure 2.4C and D, respectively; Figure 2.4 statistical parameters in Tables 2.8 and 2.9) regardless of sex or cycle stage. In slices from DREADD virus mice, CNO treatment increased GnRH neuron firing rates increased in both the AM (Figure 2.4C) and PM (Figure 2.4D) regardless of sex and cycle stage. In the PM, the increase in GnRH neuron firing rates was greater during CNO treatment in slices from males than those from diestrous and proestrous females (Figure 2.4D); this may be at least in part attributed to the greater AUC measured in DREADD males compared to both female groups (Figure 2.2D). These data show that CNO-induced activation of POA GFAP-expressing cells can stimulate proximal GnRH neurons. This is notably different from previous work in which there was no effect of this paradigm on GnRH neuron firing rate in diestrous females studied in the PM. That work noted the major caveat that those mice were examined 18-22 weeks after stereotaxic surgery because of COVID 19-related laboratory closure. While that work was reported in the interest of transparency, the present work is a more rigorous and direct comparison of the response between the sexes.

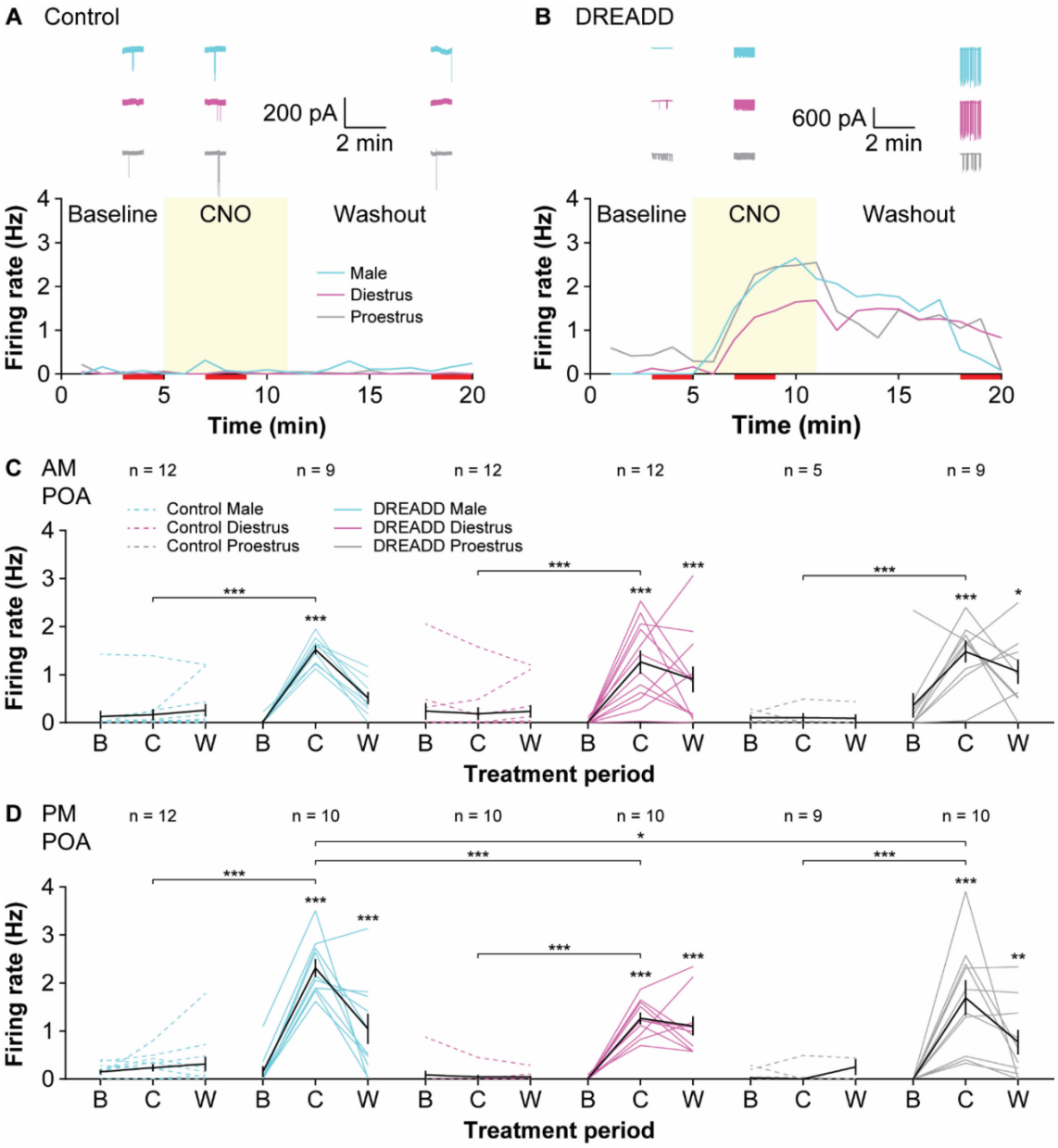


Figure 2.4: Activating Gq signaling in GFAP-expressing cells in the POA increases GnRH neuron firing regardless of sex, cycle stage, and time of day. **A and B,** Representative extracellular recording traces (top) and plots of firing rates binned at 1-min intervals (bottom) of GnRH neurons from mice injected with either AAV-GFAP-mCherry (A) or AAV-GFAP-hM3Dq (B) into the POA. Red bars on the x-axis indicate the windows used for statistical comparisons. **C and D,** Quantification of individual GnRH neuron firing rates for control (dashed cyan or magentia lines) and DREADD (solid cyan or magenta lines) brain slices overlaid with mean ± SEM (black lines) during the AM or PM (C and D, respectively; three-way mixed model ANOVAs with Bonferroni *post hoc*). B, baseline; C, 200 nM CNO; W, washout. Statistics are in Tables 2.8 and 2.9. Baseline-baseline and washout-washout pairwise comparisons are ommitted from the figure for clarity. *, $p < 0.05$; **, $p < 0.01$; ***, $p < 0.001$ for between-group comparisons indicated by bars, and for within-group comparisons to baseline indicated by stars alone.

Activation of Gq signaling in ARC GFAP-expressing cells has no effect on KNDy neuron firing rates in brain slices. To investigate if KNDy neurons are similarly stimulated following the activation of Gq signaling in proximal ARC GFAP-expressing cells, we performed extracellular recordings on GFP-tagged KNDy neurons from Tac2-GFP mice. CNO treatment did not alter the firing rates of KNDy neurons in brain slices from control virus mice in the AM or PM (Figure 2.5C and D, respectively; Figure 2.5 statistical parameters in Tables 2.10 and 2.11) regardless of sex or cycle stage. Unlike GnRH neurons, CNO treatment did not alter the firing rates of KNDy neurons in brain slices from DREADD virus mice in either the AM (Figure 2.5C) or PM (Figure 2.5D) regardless of sex or cycle stage. A minority of kisspeptin neurons increased in firing later into the wash period despite no contemporaneous change with CNO treatment; this increase with time of recording has been observed in the absence of a treatment in other studies of these cells, and has been attributed to a tendency for KNDy to sometimes become unstable during longer recordings[298,323,324]. These data suggest GFAP-expressing cells in the POA, but not in the ARC, are poised to stimulate reproductive neural circuits with no observed influence of sex, cycle stage, or the time of day.

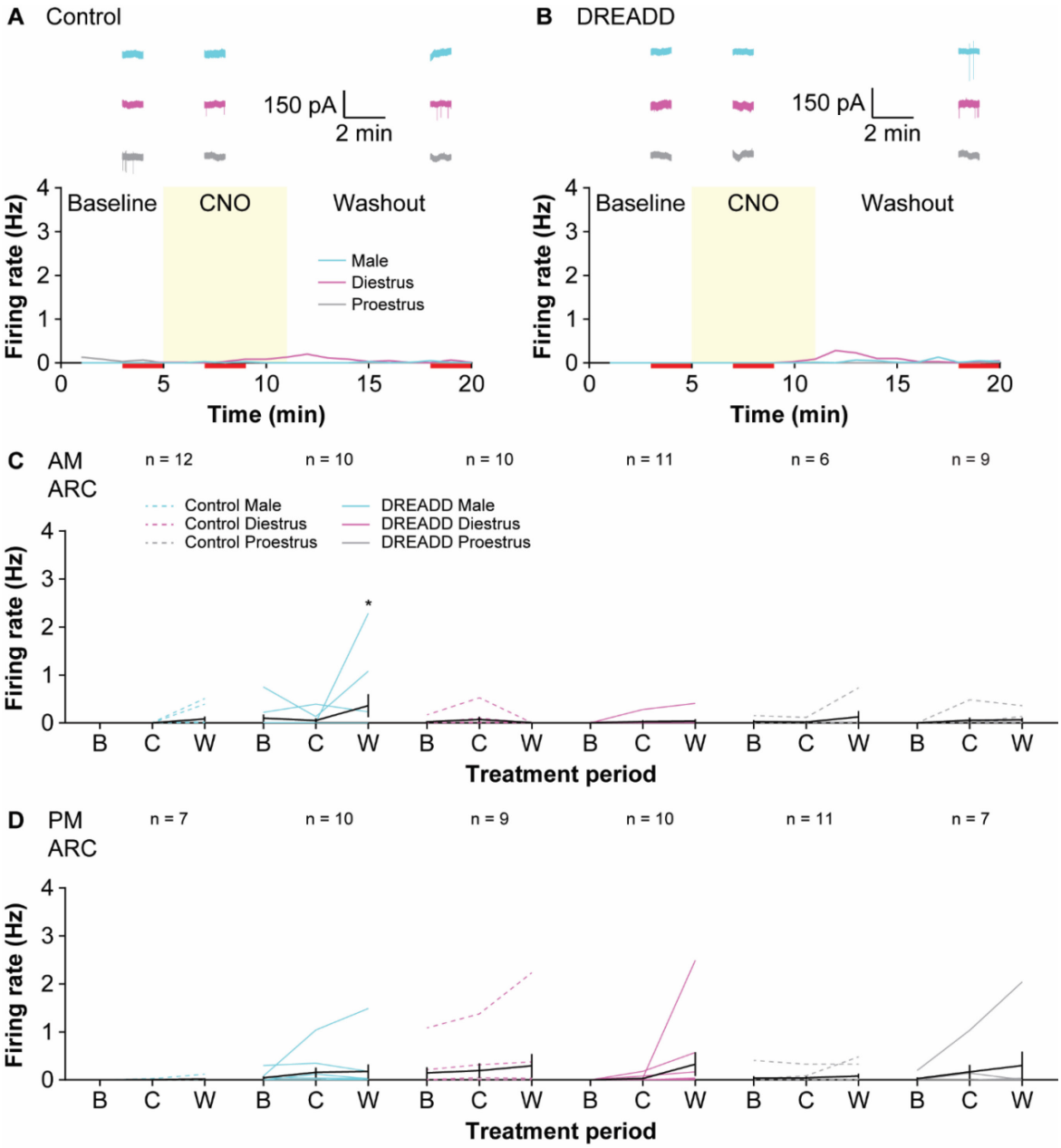


Figure 2.5: Activating Gq signaling in GFAP-expressing cells in the ARC does not alter KNDy neuron firing regardless of sex, cycle stage, and time of day. **A and B,** Representative extracellular recording traces (top) and plots of firing rates binned at 1-min intervals (bottom) of KNDy neurons from mice injected with either AAV-GFAP-mCherry (A) or AAV-GFAP-hM3Dq (B) into the ARC. Red bars on the x-axis indicate the windows used for statistical comparisons. **C and D,** Quantification of individual KNDy neuron firing rates for control (dashed cyan and magenta lines) and DREADD (solid, cyan, and magenta lines) brain slices overlaid with mean ± SEM (black lines) during the AM or PM (C and D, respectively; three-way mixed model ANOVAs with Bonferroni *post hoc*). B, baseline; C, 200 nM CNO; W, washout. Statistics are in Tables 2.10 and 2.11. Baseline-baseline comparisons are ommitted from the figure for clarity. *, $p < 0.05$ for the within-group comparison to baseline.

Activation of Gq signaling in POA GFAP-expressing cells increases LH release more in males than diestrous females. To determine the effect of activating Gq signaling in GFAP-expressing cells on GnRH neuron output, serial blood samples were obtained at 10-min intervals for LH measurement, which serves as a bioassay for GnRH release. There were no changes in LH levels following CNO treatment in mice injected with AAV-GFAP-mCherry in the POA regardless of sex or time of day (Figure 2.6; statistical parameters in Tables 2.12 through 2.15). In contrast, CNO increased LH in DREADD virus mice regardless of sex and time of day (Figure 2.6). Interestingly, although both sexes responded with increased LH following CNO administration, the LH response in DREADD virus males was greater than diestrous females in both the AM and PM (Figure 2.6C and D). LH levels in males peaked and plateaued within 20 min of CNO administration, whereas LH in diestrous females did not reach levels comparable to the plateau in males until 50 min after CNO injections in the AM and remained consistently lower than the male plateau in the PM (Figure 2.6C). This indicates that CNO-induced activation of POA GFAP-expressing cells augment GnRH neuron output in a sexually differentiated manner.

Activation of Gq signaling in ARC GFAP-expressing cells does not alter LH levels in diestrous females, but increases LH release in males. To determine if CNO-induced activation of GFAP-expressing neurons in the ARC has a similar effect as in the POA, blood collection procedures were conducted in mice that received viral injections in the ARC. Mice that received control virus injections exhibited no change in LH levels after CNO administration regardless of sex or time of day (Figure 2.7; statistical parameters in Tables 2.16 through 2.19). CNO also had no effect on LH levels in the AM or PM in diestrous females with DREADD viral injections (Figure 2.7). However, male mice with DREADD viral injections had increased LH levels following CNO administration in both the AM and PM (Figure 2.7). This LH rise is delayed by about 10 min compared to the response in POA DREADD-injected males.

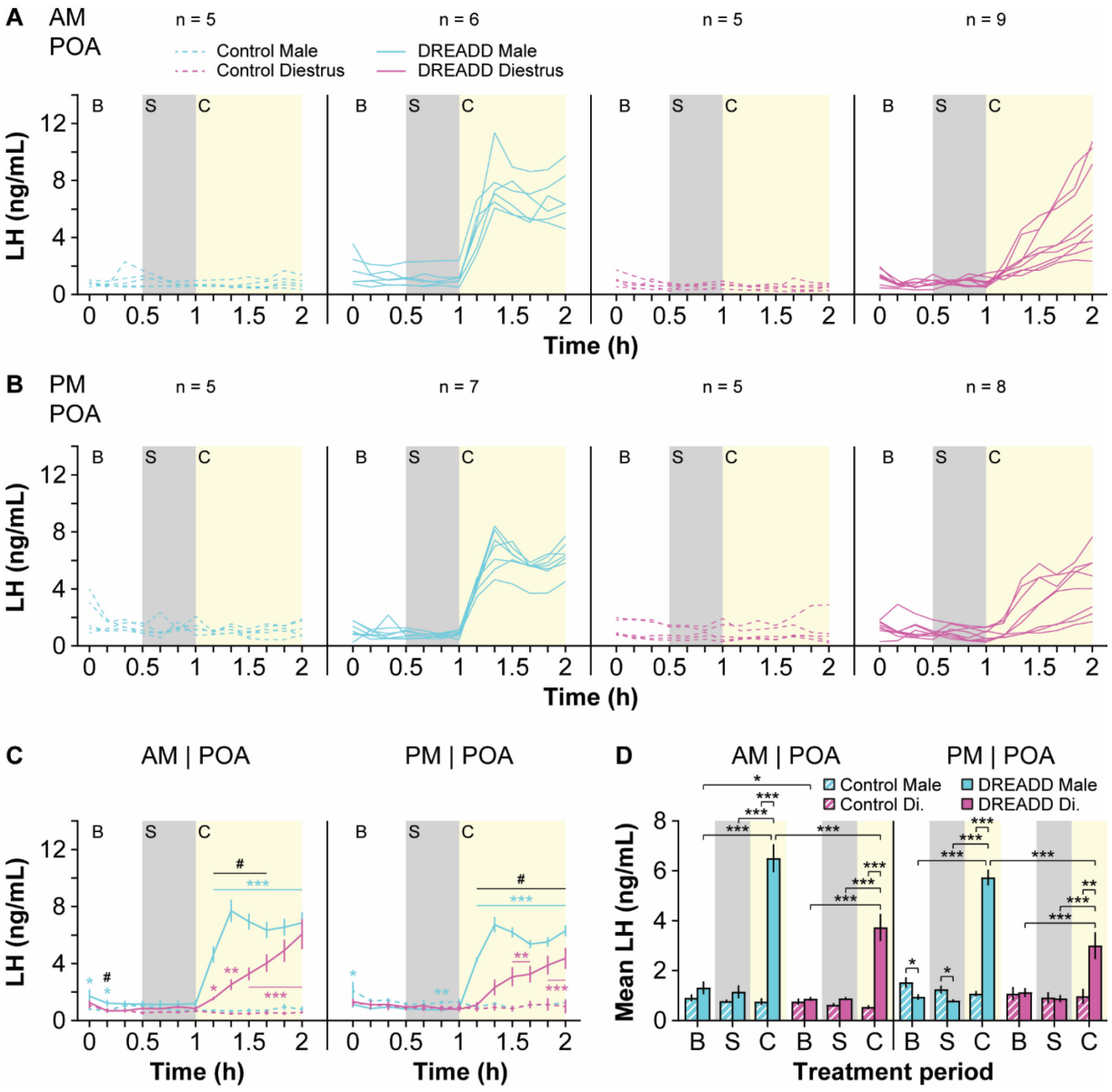


Figure 2.6: Activating Gq signaling in GFAP-expressing cells in the POA increases circulating LH levels more in males than diestrous females. **A and B,** Individual LH levels for control (dashed cyan or magenta lines) and DREADD (solid cyan or magenta lines) mice during in the AM (A) and PM (B). B, baseline; S, saline; C, 0.3 mg/kg CNO. **C,** Mean ± SEM LH levels at each sample time during the AM or PM (left and right, respectively; three-way mixed model ANOVAs with Bonferroni *post hoc*). Statistics are in Tables 2.12 and 2.13. Control-control LH level comparisons between the sexes and within-subject pairwise comparisons were omitted from the figure for clarity. *, $p < 0.05$; **, $p < 0.01$, ***, $p < 0.001$ comparing LH levels in DREADD virus mice with that in control virus mice of the same sex. #, $p < 0.05$ comparing LH between the sexes in DREADD virus mice.. **D,** Treatment period mean ± SEM LH levels during the AM or PM (left and right, respectively; three-way mixed model ANOVAs with Bonferroni *post hoc*). Statistics are in Tables 2.14 and 2.15. *, $p < 0.05$; **, $p < 0.01$; ***, $p < 0.001$.

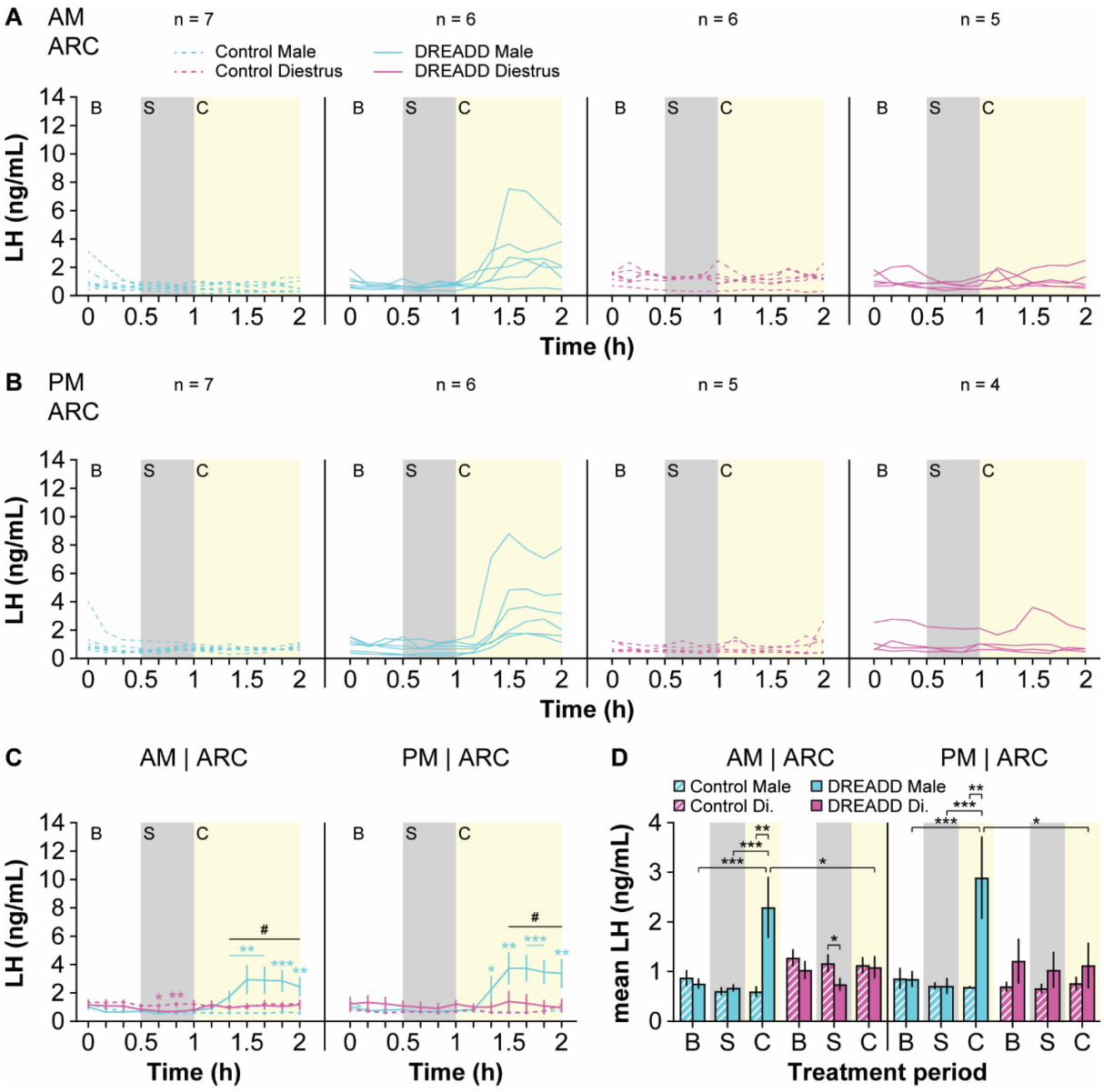


Figure 2.7: Activating Gq signaling in GFAP-expressing cells in the ARC increases circulating LH levels in males, but not diestrous females. **A and B,** Individual LH levels for control (dashed cyan or magenta lines) and DREADD (solid cyan or magenta lines) mice during the AM (A) and PM (B). B, baseline; S, saline; C, CNO. **C,** Mean ± SEM LH levels at each sample time during the AM or PM (left and right, respectively; three-way mixed model ANOVAs with Bonferroni *post hoc*). Statistics are in Tables 2.16 and 2.17. Control-control LH level comparisons between the sexes and within-subject pairwise comparisons were omitted from the figure for clarity. *, $p < 0.05$; **, $p < 0.01$; ***, $p < 0.001$ comparing LH levels in DREADD virus mice with that in control virus mice of the same sex. #, $p < 0.05$ comparing LH between between the sexes in DREADD virus mice. **D,** Treatment period mean ± SEM LH levels during the AM or PM (left and right, respectively; three-way mixed model ANOVAs with Bonferroni *post hoc*). Statistics are in Tables 2.18 and 2.19. *, $p < 0.05$; **, $p < 0.01$; ***, $p < 0.001$.

Knockdown of KNDy neurons does not alter the LH response to activating Gq signaling in ARC GFAP-expressing cells in males. The LH response to activation of GFAP-expressing cells in males was unexpected as it is in contrast to prior work in which no LH increase was observed[288]. This difference may be attributable to a greater viral injection volume to the arcuate in the present study (100 nL/virus) vs 50 nL/virus in prior work[288]; spread from the larger volume might engage additional regions like the median eminence in the response. To test if KNDy neurons are required for the LH increase observed in males under these conditions, we virally induced apoptosis in KNDy neurons within the injection region using targeted caspase-3 expression, then performed the same serial blood sample collection paradigm as above. Tac2-GFP mice were crossed with a Tac2-Cre strain and stereotaxically coinjected with a Cre-dependent caspase-3 (AAV-flex-taCasp3) and either AAV-GFAP-hM3Dq or AAV-GFAP-mCherry. Following Cre-dependent recombination in mice coinjected with caspase-3, GFP-expressing KNDy neurons within the mCherry-defined injection region were reduced more than 95% compared to mice injected only with the DREADD virus (Figure 2.8A and F; statistical parameters in Table 2.20). Interestingly, this marked reduction of KNDy neuron numbers had no effect on the LH response; LH levels still increased following CNO administration in mice coinjected with caspase-3 and DREADD viruses compared to mice coinjected with caspase-3 and control viruses (Figure 2.8B through E; statistical parameters in Tables 2.21 through 2.24). Though these experiments do not rule out technical limitations such as variations of craniometric parameters and brain volume between the sexes[325], these findings suggest that, unlike in females, activation of GFAP-expressing cells in the ARC/median eminence region in males can induce LH release in a manner that appears to not require KNDy neurons.

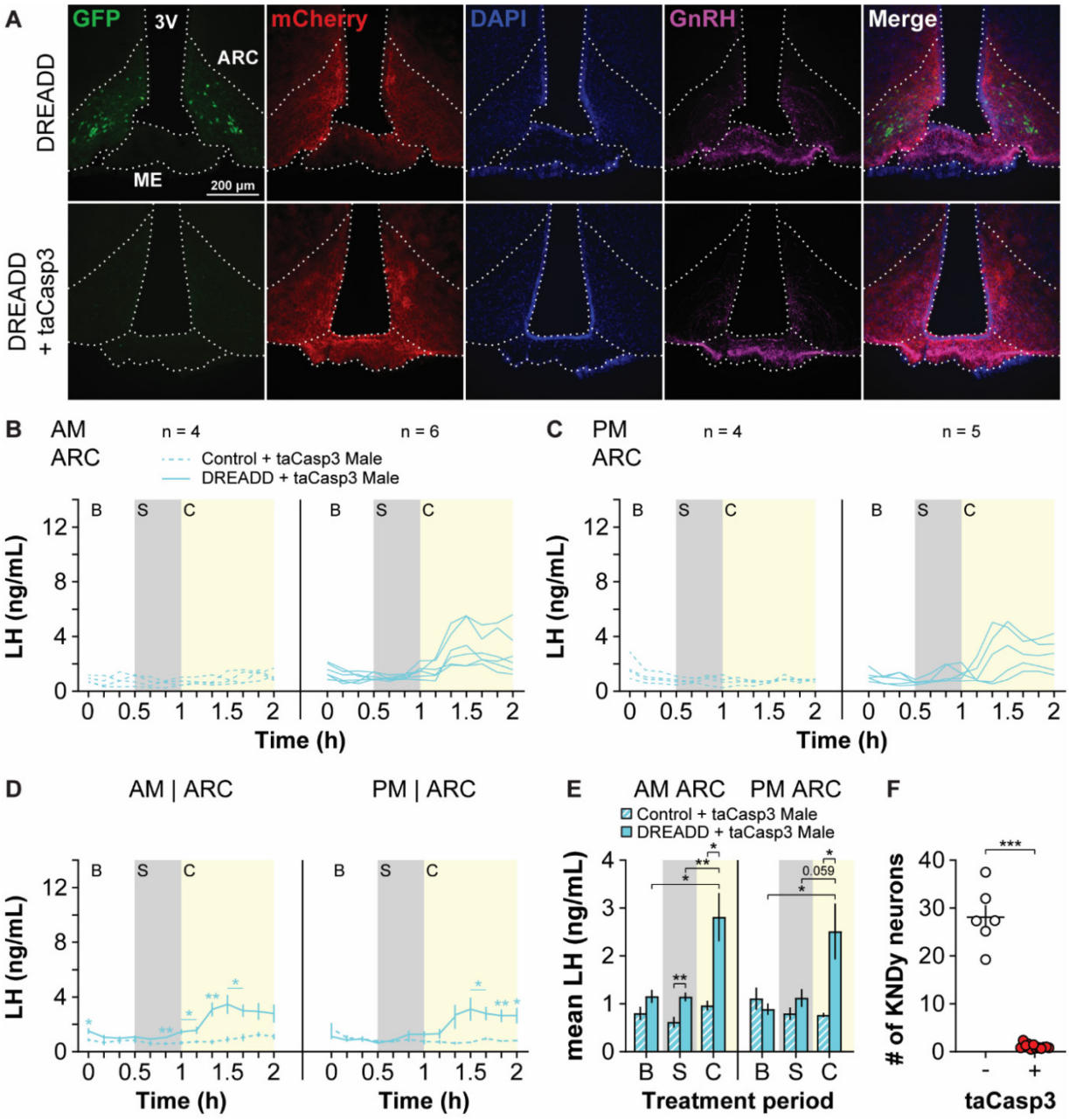


Figure 2.8: Viral knockdown of KNDy neurons in males does not abolish the increase in circulating LH levels induced by activating Gq signaling in GFAP-expressing cells in the ARC. **A,** Representative sections depicting expression of GFP (green) in KNDy neurons and mCherry (red) in cells expressing AAV-GFAP-hM3Dq. 3V, third ventricle; ME, median eminence. **B and C,** Individual LH levels during the AM (B) or PM (C) from mice with KNDy neuron attrition that were either coinjected with a control virus (dashed cyan line) or the DREADD virus (solid cyan line). B, baseline; S, saline; C, CNO. **D,** The mean ± SEM LH levels at each sample time during the AM or PM (left and right, respectively; 3-way mixed model ANOVAs with Bonferroni *post hoc*). Statistics are in Tables 2.21 and 2.22. Within-subject pairwise comparisons were omitted from the figure for clarity *, $p < 0.05$; **, $p < 0.01$; ***, $p < 0.001$ comparing LH levels in DREADD virus

mice with that in control virus mice. **E,** Treatment period mean ± SEM LH levels during the AM or PM (left and right, respectively; 3-way mixed model ANOVAs with Bonferroni *post hoc*). Statistics are in Tables 2.23 and 2.24. *, $p < 0.05$; **, $p < 0.01$. **F,** Mean ± SEM number of KNDy neurons per virus-expression ARC region per mouse (two-tailed, unpaired Student's t test with Welch's correction). Statistics are in Table 2.20[326]. ***, $p < 0.001$.

dmPGE2 activates GnRH neuron firing in males regardless of time of day, but females are less sensitive in the AM. Prior work showed that the CNO-induced increase in GnRH neuron firing in males is, at least in part, driven by activation of EP1 and/or EP2 receptors[288]. To test the possibility of sex differences in GnRH neuron responses to gliotransmitters, we bath applied the stable PGE2 analog dmPGE2 during extracellular recordings of GnRH neurons from male and diestrous female mice at different times of day. Brain slices were pretreated with vehicle (0.7% DMSO) or a cocktail of EP1 and EP2 antagonists (100 μM SC 19220 and 20 μM PF-04418948). In brain slices from males, 200 nM dmPGE2 increased GnRH neuron firing rate regardless of time of day; this response was blunted by blocking EP1 and EP2 receptors (Figure 2.9A and C; Figure 2.9 statistical parameters in Tables 2.25 through 2.27). In contrast, 200nM dmPGE2 increased GnRH neuron firing rate in the PM but not the AM in females; the increased firing rate in the PM was also blunted by blocking EP1 and EP2 receptors (Figure 2.9A and C). When brain slices from females were treated with 1 μM dmPGE2 in the AM, GnRH neuron firing rate was increased (Figure 2.9B), suggesting females are less sensitive to the activating effects of PGE2 in the AM.

Prior work showed no effect of dmPGE2 on KNDy neuron firing rates in males[288]. To determine if, as in GnRH neurons from females, a higher dose might be effective, dmPGE2 was bath applied during extracellular recordings of KNDy neurons pretreated with vehicle. There was no effect of either 200 nM or 1 μM dmPGE2 treatment on the firing rate of KNDy neurons in the AM (Figure 2.10A and B; Figure 2.10 statistical parameters in Tables 2.28 through 2.31) or PM (Figure 2.10C and D) in either sex. These data suggest that PGE2 action is directed through GnRH, but not KNDy, neurons, and that there are a sex-specific and diurnal effects modulating this action.

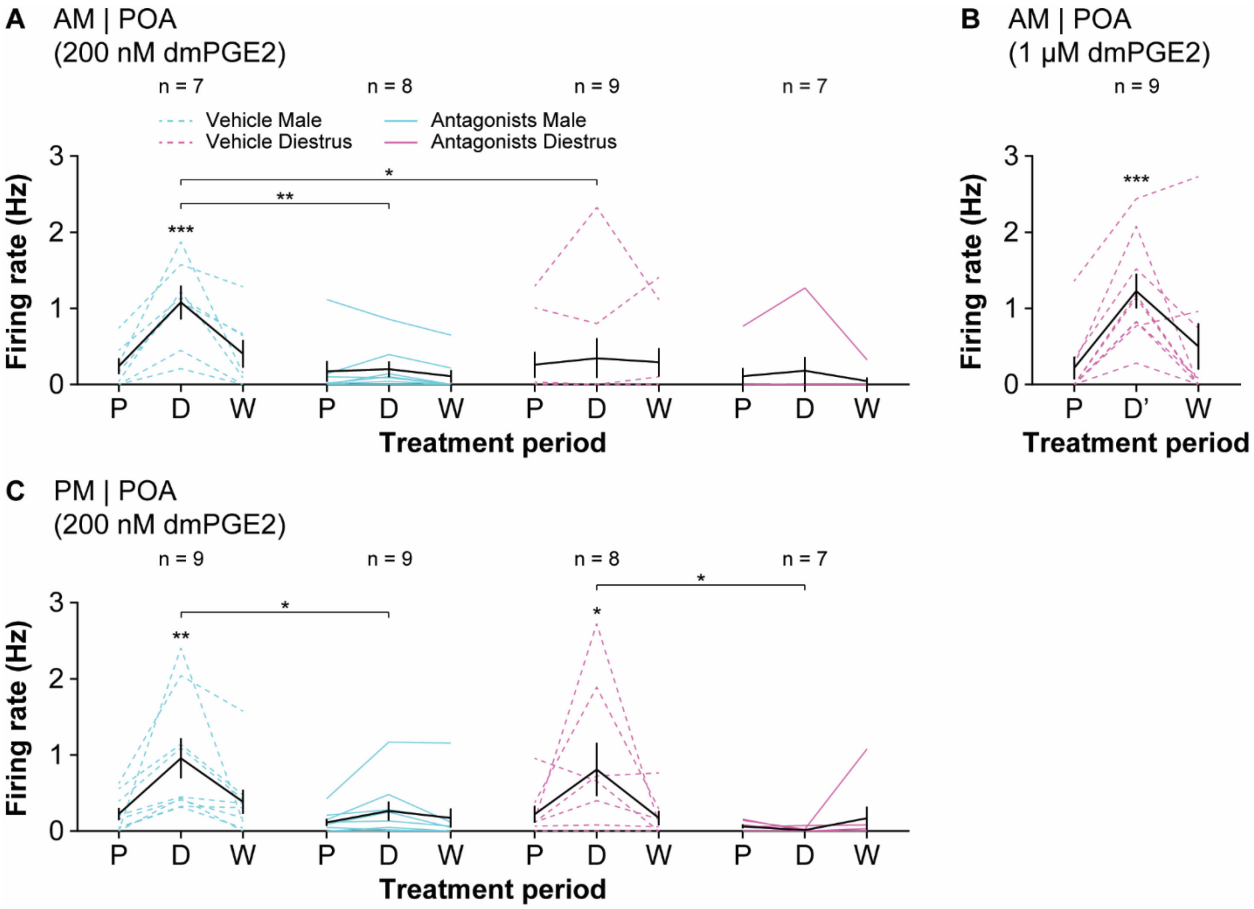


Figure 2.9: GnRH neurons from females are less sensitive to dmPGE2 than males. **A and C,** Firing rate of individual GnRH neurons pretreated with either vehicle (dashed cyan and magenta lines) or EP1 and EP2 antagonists SC 19220 and PF-04418948, (solid cyan and magenta lines) respectively, overlaid with mean ± SEM (black lines) during the AM or PM (A and C, respectively; three-way mixed model ANOVAs with Bonferroni *post hoc*). P, pretreatment with either vehicle or EP1 & EP2 antagonists; D, 200 nM dmPGE2 treatment; W, washout. Statistics are in Tables 2.25 and 2.27. *, $p < 0.05$; **, $p < 0.01$; ***, $p < 0.001$ for between-group comparisons indicated by bars, and for within-group comparisons to baseline indicated by stars alone. **B,** Firing rate of GnRH neurons treated with 1 μM dmPGE2 (one-way repeated measures ANOVA with Bonferroni *post hoc*). D', 1 μM dmPGE2. Statistics are in Table 2.26. ***, $p < 0.001$ for the within-group comparison to pretreatment period.

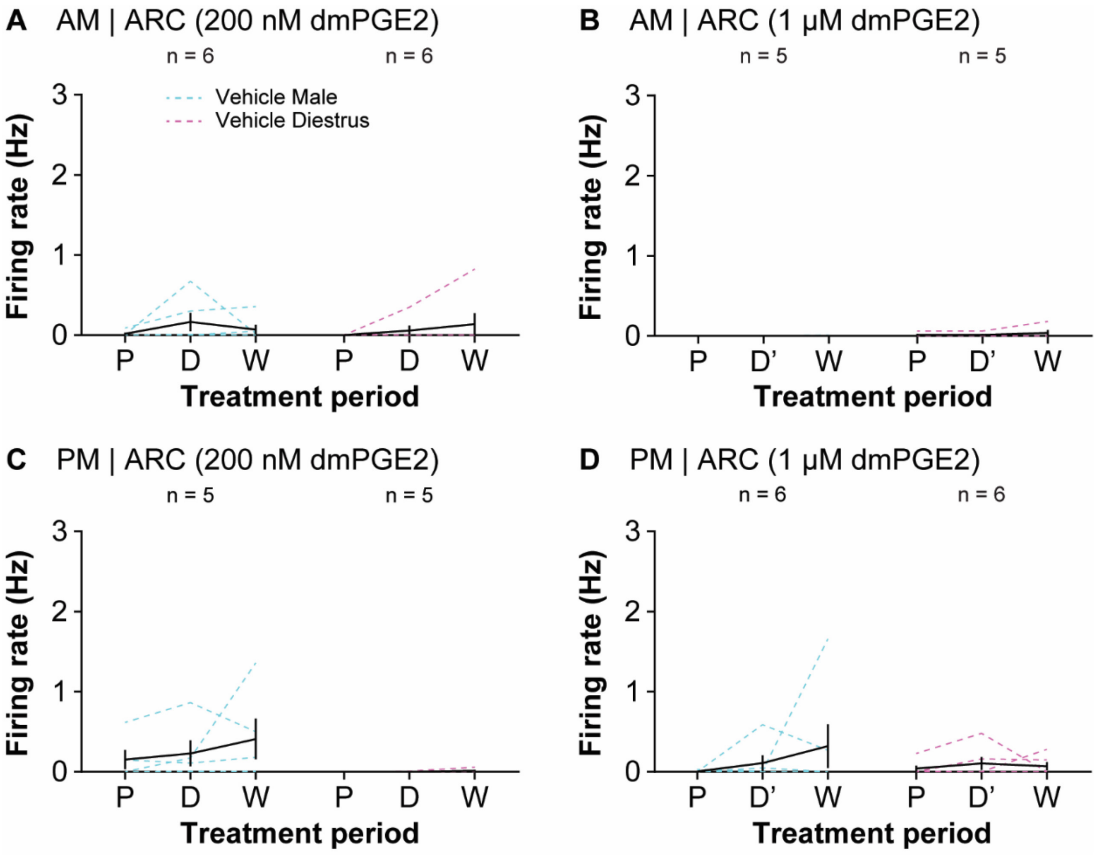


Figure 2.10: dmPGE2 does not alter KNDy neuron firing regardless of sex, time of day, or dose of drug. **A and C,** Firing rate of individual KNDy neurons pretreated with vehicle (dashed cyan and magenta lines) overlaid with mean ± SEM (black lines) during the AM or PM (A and C, respectively; two-way mixed model ANOVAs with Bonferroni *post hoc*). P, pretreatment with vehicle; D, 200 nM dmPGE2 treatment; W, washout. Statistics are in Tables 2.28 and 2.30. **B and D,** Firing rates of KNDy neurons treated with 1 µM dmPGE2 (two-way mixed model ANOVA with Bonferroni *post hoc*). D', 1 µM dmPGE2. Statistics are in Tables 2.29 and 2.31.

Blocking EP1 and EP2 receptors attenuates the increase in GnRH neuron firing induced by activating Gq signaling in both sexes in the morning but not in the afternoon.

Blocking EP1 and EP2 receptors in slices from males blunted the increase in GnRH neuron firing rate when GFAP-expressing cells in the POA were activated by CNO in the AM[288]. To establish if this mechanism differs with time of day and/or sex, we performed AM and PM extracellular recordings of GnRH neurons from mice injected with AAV-GFAP-hM3Dq in the POA. CNO increased firing rate of GnRH neurons in brain slices pretreated with DMSO vehicle in the AM (Figure 2.11A and B; Figure 2.11 statistical parameters in Tables 2.32 and 2.33) and PM (Figure 2.11C and D) regardless of sex. Pretreatment with EP1 and EP2 receptor antagonists attenuated this increase in the AM

in both sexes (Figure 2.11A and B). In contrast, there were no differences in the firing rate of GnRH neurons between vehicle and antagonist pretreatment groups in the PM regardless of sex. This suggests a time-of-day difference in how activation of GFAP-expressing cells increases firing rate of GnRH neurons.

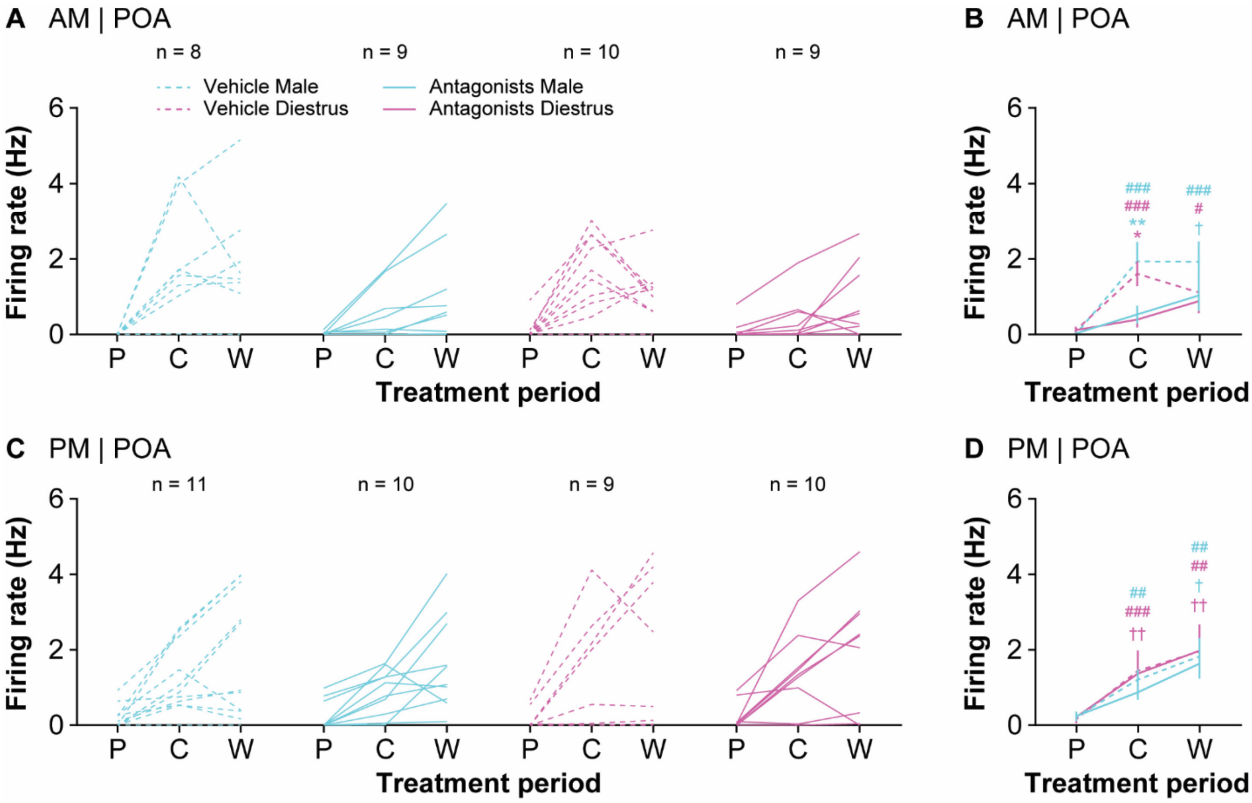


Figure 2.11: EP1 and EP2 antagonists blunt CNO-induced increases in GnRH neuron firing during the AM regardless of sex, but not in the PM. **A and C,** Firing rate of individual GnRH neurons during pretreatment with either vehicle (dashed cyan and magenta lines) or EP1 and EP2 antagonists SC 19220 and PF-04418948, respectively, (solid cyan and magenta lines) during the AM (A) or PM (C). P, pretreatment with either vehicle or EP1 & EP2 antagonists; C, 200 nM CNO treatment; W, washout. **B and D,** The mean ± SEM GnRH neuron firing rates during the AM or PM (B and D, respectively; three-way mixed model ANOVAs with Bonferroni *post hoc*). Statistics are in Tables 2.32 and 2.33. *, $p < 0.05$; **, $p < 0.01$ comparing firing rates between vehicle and antagonist pretreatment groups within a sex during a period; #, $p < 0.05$; ##, $p < 0.01$; ###, $p < 0.001$ for within-group comparisons to pretreatment period in vehicle slices. †, $p < 0.05$; ††, $p < 0.01$ for within-group comparisons to pretreatment period in antagonists slices.

Discussion

The network upstream of GnRH neurons is essential for regulating fertility. Astrocytes are an integral component of this network through gliotransmitters such as PGE2, which

stimulates GnRH neurons and LH release[235,250,287,288]. Here, we demonstrate that these interactions are region specific, sexually differentiated, and diurnally regulated.

The present work supports and expands on our understanding of how subsets of hypothalamic astrocytes alter reproductive neuroendocrine circuits. Specifically, chemogenetic activation of GFAP-expressing cells in the POA increases GnRH neuron firing rate in brain slices. A similar increase is observed when slices containing GnRH neurons are treated with a stable PGE2 analog. These responses were not observed in KNDy neurons regardless of sex, cycle stage, or the time of day. CNO increased $[Ca^{2+}]_i$ in Gq-DREADD-expressing GFAP-expressing cells in both the POA and ARC in the present work; this increase resembled that observed in other brain regions when astrocytes were activated with either DREADDs or by Gq-GPCR agonists[327–330]. These observations strongly indicate the failure of CNO to increase KNDy neuron firing rate is not attributable to ARC astrocytes being less responsive than POA astrocytes. In the POA, the onset of CNO-induced increases in astrocytic $[Ca^{2+}]_i$ occurred with a shorter latency than CNO-induced increases in GnRH neuron firing rate. Neither of these measures changed after CNO treatment of preparations infected with control virus, suggesting the GnRH neuron response is dependent upon the elevation of astrocytic $[Ca^{2+}]_i$ and subsequent gliotransmitter action. The duration of CNO-induced GnRH neuron firing was prolonged relative to the elevation of $[Ca^{2+}]_i$ in astrocytes. Together, these observations strongly suggest that astrocytes are poised to directly regulate elements of the reproductive circuit via GnRH, but not KNDy, neurons. This points to a mode of GnRH neuron output control that is likely separate from the putative KNDy-neuron centric GnRH pulse generator[331–333].

During development, GnRH neurons and their upstream network undergo sex-specific changes that enable the transition through the pubertal process to the functioning adult system[334–336]. In this regard, hypothalamic astrocytes exhibit sex differences in both morphological complexity and influence upon synaptic patterning[270,337]. These differences may underlie aspects of astrocytic regulation found in the present work, including increases in astrocyte $[Ca^{2+}]_i$ and correlated greater increases in GnRH neuron firing rate in males in the PM. There was a further sex difference in the time of

day at which dmPGE2 stimulates GnRH neuron firing. Specifically, stimulation in males did not depend on the time of day but GnRH neurons from diestrous females responded only in the PM. Interestingly, no sex differences in response to PGE2 were reported using a higher dose of 1 μM PGE2[287]. Consistent with that work, a five-fold increase in dmPGE2 to 1 μM in the present work successfully stimulated GnRH neurons from diestrous females in the AM, indicating a sex-dependent diurnal shift in sensitivity of GnRH neurons to this gliotransmitter.

Hypothalamic sex differences contribute to differential gonadotropin output from the pituitary. LH secretion in response to glial activation in the present studies was dependent upon not only sex, but also the time of day and the region of viral delivery. Notably, LH release in males injected in POA with the GFAP-driven DREADD virus sharply increases upon CNO administration, whereas increased LH release in diestrous females is more gradual; LH levels only become comparable between the sexes an hour after CNO treatment during the AM. In the PM, LH levels in females remain lower than males throughout the observation period, again suggesting sex and diurnal components of astrocyte regulation of GnRH neurons. Interestingly, this sex difference mirrors the results of earlier studies in which serum LH levels increased more rapidly in males following castration[281,338–341]. In those studies, there were no sex differences in LH secretion from pituitaries isolated from either gonadectomized or intact rats either basally or when perfused with physiologic GnRH-pulse frequencies[340,341]. The lack of sex differences at the level of the pituitary suggests that upstream central factors mediate these differences. Reported sex differences in the anatomical relationship between astrocytes and tanycytes lining the third ventricle/median eminence and GnRH neuron terminals could alter GnRH release patterns and/or its diffusion dynamics to the portal blood. The somata of hypothalamic neurons including GnRH and KNDy neurons have considerable astrocyte coverage, and the amount of coverage varies with the systemic steroid milieu and time of day[254,259,285,335,342]. Tanycyte endfeet also exhibit remarkable plasticity in response to circulating estradiol levels[278,303,343]. In diestrous female rats, tanycytes extend their endfeet and decrease the probability of GnRH neuron terminals being in apposition with the fenestrated capillaries in low estradiol conditions compared to the high estradiol conditions on proestrus[278,343–345].

In addition to structural effects, changes in steroid milieu can alter GnRH neuron firing rate in brain slices. Castration of male mice to remove negative feedback increases the number of peaks in GnRH neuron firing rate per hour[65]. The amount of hormone released in response to action-potential-clamp of GnRH neurons is also greater in orchiectomized than sham-operated male mice, attributable at least in part to an increase in Ca^{2+} currents induced during the spikes in castrate males[346]. Finally, repeated GnRH neuron depolarization mimicking action potentials transiently inhibits GABAergic inputs to that cell in an endocannabinoid- and prostaglandin-dependent manner that is modified by steroid feedback and sex[347]. This juxtaposition of steroid milieu and prostaglandins has been reported to be a driving force behind sexual function. Estrogen-mediated PGE2 signaling is a key component in masculinizing both behavior and the neuronal architecture in the developing hypothalamus[263,277]. Sex-dependent changes are also observed in other brain regions. For example, COX2 expression is transiently elevated in cortical astrocytes from males compared to females during the perinatal (P1) sex steroid surge[348]. These data suggest that sex differences in GnRH neurons themselves or their steroid-sensitive afferents include differential responses to a variety of inputs including gliotransmission.

One surprising sex difference between POA and ARC astrocyte activation was the LH response. ARC astrocyte activation increases LH levels in male, but not female, mice. This occurs despite an absence of changes in KNDy neuron firing rate following either ARC astrocyte activation or prostaglandin treatment. It is possible that KNDy neurons are induced to release neuromodulators in an action potential-independent manner, as has been observed in GnRH neurons and magnocellular neuroendocrine neurons[349,350]. We, however, favor the hypothesis that ARC astrocytes in males are not stimulating KNDy neurons but are instead activating GnRH neuron processes that terminate in the median eminence to release GnRH. The present LH results in males contrast with our prior work in which no change in LH was observed after activating GFAP-expressing cells in the ARC[288]. The present work utilized larger viral volumes and higher injection rate, and greater infiltration of AAVs into the median eminence was observed in both sexes than in the prior work[288]. Chemogenetic activation of POA astrocytes failed to stimulate GnRH neurons outside of the viral infection zone[288], but infection of the

median eminence bleeding over from the ARC could permit local gliotransmitters like PGE2 to reach GnRH neuron terminals. This postulate is supported by a report of PGE2-induced GnRH release from microdissected female rat median eminence tissue[351]. It is possible that the PGE2 released by ARC astrocytes in female mice and subsequent GnRH secretion is insufficient to induce an appreciable rise in LH levels during diestrus when tanycyte feet are extended. Tanycytes in males exhibit dynamic endfeet coverage of parvocellular axon terminals[352], though the extent of their influence specifically on reproduction is unknown. To attempt to eliminate a role for KNDy neurons in the present studies, caspace-3 was used to reduce KNDy neuron numbers; this did not alter the LH response to CNO. The lack of signal propagation beyond the infected area in the POA[288] suggests few KNDy neurons would have been in range of CNO-induced astrocytic modulator release. Taken together with the lack of effect of astrocyte activation on KNDy neuron firing rate, these data suggest that, in males, the terminal portions of GnRH neurons may be more sensitive to proximal astrocyte mediators than diestrous females, and/or that released GnRH may have easier access to the portal vasculature.

Consideration of additional mechanistic factors that could lead to the sex and time-of-day changes observed in the present study are somewhat hampered by a paucity of mechanistic work examining both variables, or even both sexes, under the same conditions. That said, involvement of a mechanism in one change (e.g., sex differences) does not preclude it participating in others (e.g., time-of-day changes). Factors of relevance reported to change with these variables include lipid metabolism[353] and astrocytic steroid receptor expression[268,354,355]. The latter is debated, however, as some evidence suggests sex-steroid-mediated differences in astrocyte morphology and synaptic organization may be driven indirectly via steroid-receptor-expressing neurons[270]. The types and amounts of gliotransmitters released when astrocytes are chemogenetically activated may be sexually differentiated or regulated by time of day. The suite of gliotransmitters released in the hypothalamus beyond PGE2 is incompletely understood. Astrocytes, like neurons, are capable of secreting numerous modulators such as ATP, glutamate, GABA, and D-serine[167]. Astrocytic D-serine has been shown to be a co-agonist of NMDARs in the supraoptic nucleus and critical for long-term

potentiation[356]. Interestingly, blocking EP1 and EP2 receptors in the present work attenuated the CNO-induced increase in GnRH neuron firing rates in the AM but not PM in both sexes, strongly suggesting the existence of other glial-derived factors that can activate GnRH neurons. It is possible that a combination of these and other intrinsic factors may explain the sex and time of day differences in astrocytic $[Ca^{2+}]_i$ and GnRH neuron firing rate response when activating POA astrocytes.

The approach used allowed cell-specific activation of signaling glia in specific brain regions, but there are still several caveats to consider in interpreting the results. First, chemogenetic manipulation does not phenocopy activation of GFAP-expressing cells by endogenous factors, which remain to be elucidated. Second, although EP2 receptor expression (*Ptger2)* is enriched in GnRH neurons of adult mice[357], we did not examine possible changes in *Ptger2* expression in GnRH neurons or COX2 expression in POA astrocytes that could shed light on the sex and time of day differences. Third, the 10-min sampling interval used for LH measurements are not sufficiently frequent to reveal changes in the pulsatile pattern, which could inform interpretation. Fourth, the natural cyclical changes in LH release in females precluded effective use of LH as a bioassay for time-of-day effects in proestrous mice. Finally, extracellular recordings allow examination of the neural response without altering intracellular milieu, but these cannot reveal underlying synaptic or intrinsic mechanisms.

The work presented supports the hypotheses that sex and the time of day both play a role in regulating how astrocytes communicate with proximal GnRH neurons through, at least in part, PGE2 signaling. The greater release in LH in males and the lower responsiveness of GnRH neurons in females to PGE2 points to potential sex differences in intrinsic GnRH neuron sensitivity to astrocytic signaling. Further investigation into endogenous mechanisms eliciting gliotransmission and the gliotransmitter profiles of POA astrocytes will further our understanding of the role of glia in reproduction.

Table 2.4: Statistical parameters from three-way mixed model ANOVA assessing the effect of sex/cycle stage and AAV on ΔF/F0 during 200 nM CNO treatment from AM | POA mouse brain slices (Fig. 2.2C).

Property	Males		Diestrous females		Proestrous females	
	AAV-GFAP-mCherry	AAV-GFAP-hM3Dq	AAV-GFAP-mCherry	AAV-GFAP-hM3Dq	AAV-GFAP-mCherry	AAV-GFAP-hM3Dq
Brain slices (n)	7	9	9	8	9	8
Mice (n)	3	3	3	3	3	3

Three-way mixed model ANOVA		
Effect	Statistic	Partial η^2
Treatment period	$F_{(2,88)}$ = 67.924, ***p* < 0.001**	0.607
Sex/cycle stage	$F_{(2,44)}$ = 1.777, p = 0.181	0.075
AAV	$F_{(1,44)}$ = 54.948, ***p* < 0.001**	0.555
Treatment period * Sex/cycle stage	$F_{(4,88)}$ = 1.643, p = 0.204	0.069
Treatment period * AAV	$F_{(2,88)}$ = 64.226, ***p* < 0.001**	0.593
Sex/cycle stage * AAV	$F_{(2,44)}$ = 1.734, p = 0.188	0.073
Treatment period * Sex/cycle stage * AAV	$F_{(4,88)}$ = 1.560, p = 0.221	0.066

Table 2.5: Statistical parameters from three-way mixed model ANOVA assessing the effect of sex/cycle stage and AAV on ΔF/F0 during 200 nM CNO treatment from PM | POA mouse brain slices (Fig. 2.2D).

Property	Males		Diestrous females		Proestrous females	
	AAV-GFAP-mCherry	AAV-GFAP-hM3Dq	AAV-GFAP-mCherry	AAV-GFAP-hM3Dq	AAV-GFAP-mCherry	AAV-GFAP-hM3Dq
Brain slices (n)	10	11	8	10	9	7
Mice (n)	4	4	3	4	3	3

Three-way mixed model ANOVA		
Effect	Statistic	Partial η^2
Treatment period	$F_{(2,98)}$ = 78.199, ***p* < 0.001**	0.615
Sex/cycle stage	$F_{(2,49)}$ = 2.135, p = 0.129	0.080
AAV	$F_{(1,49)}$ = 92.628, ***p* < 0.001**	0.654
Treatment period * Sex/cycle stage	$F_{(4,98)}$ = 4.564, ***p* = 0.013**	0.157
Treatment period * AAV	$F_{(2,98)}$ = 74.861, ***p* < 0.001**	0.604
Sex/cycle stage * AAV	$F_{(2,49)}$ = 1.766, p = 0.182	0.067
Treatment period * Sex/cycle stage * AAV	$F_{(4,98)}$ = 4.000, ***p* = 0.021**	0.140

Table 2.6: Statistical parameters from three-way mixed model ANOVA assessing the effect of sex/cycle stage and AAV on ΔF/F0 during 200 nM CNO treatment from AM | ARC mouse brain slices (Fig. 2.3C).

Property	Males		Diestrous females		Proestrous females	
	AAV-GFAP-mCherry	AAV-GFAP-hM3Dq	AAV-GFAP-mCherry	AAV-GFAP-hM3Dq	AAV-GFAP-mCherry	AAV-GFAP-hM3Dq
Brain slices (n)	7	9	6	10	8	9
Mice (n)	3	3	3	4	3	3
Three-way mixed model ANOVA						
Effect			Statistic		Partial η^2	
Treatment period			$F_{(2,86)}$ = 63.059, ***p* < 0.001**		0.595	
Sex/cycle stage			$F_{(2,43)}$ = 0.194, p = 0.824		0.009	
AAV			$F_{(2,43)}$ = 58.678, ***p* < 0.001**		0.577	
Treatment period * Sex/cycle stage			$F_{(4,86)}$ = 0.099, p = 0.920		0.005	
Treatment period * AAV			$F_{(2,86)}$ = 65.021, ***p* < 0.001**		0.602	
Sex/cycle stage * AAV			$F_{(2,43)}$ = 0.211, p = 0.811		0.010	
Treatment period * Sex/cycle stage * AAV			$F_{(4,86)}$ = 0.115, p = 0.907		0.005	

Table 2.7: Statistical parameters from three-way mixed model ANOVA assessing the effect of sex/cycle stage and AAV on ΔF/F0 during 200 nM CNO treatment from PM | ARC mouse brain slices (Fig. 2.3D).

Property	Males		Diestrous females		Proestrous females	
	AAV-GFAP-mCherry	AAV-GFAP-hM3Dq	AAV-GFAP-mCherry	AAV-GFAP-hM3Dq	AAV-GFAP-mCherry	AAV-GFAP-hM3Dq
Brain slices (n)	11	9	8	9	7	11
Mice (n)	4	3	3	3	3	4
Three-way mixed model ANOVA						
Effect			Statistic		Partial η^2	
Treatment period			$F_{(2,98)}$ = 48.263, ***p* < 0.001**		0.496	
Sex/cycle stage			$F_{(2,49)}$ = 5.721, ***p* = 0.006**		0.189	
AAV			$F_{(1,49)}$ = 62.064, ***p* < 0.001**		0.559	
Treatment period * Sex/cycle stage			$F_{(4,98)}$ = 2.561, p = 0.084		0.095	
Treatment period * AAV			$F_{(2,98)}$ = 50.397, ***p* < 0.001**		0.507	
Sex/cycle stage * AAV			$F_{(2,49)}$ = 4.273, ***p* = 0.019**		0.149	
Treatment period * Sex/cycle stage * AAV			$F_{(4,98)}$ = 3.145, ***p* = 0.048**		0.114	

Table 2.8: Statistical parameters from three-way mixed model ANOVA assessing the effect of sex/cycle stage and AAV on GnRH neuron response to 200 nM CNO treatment from AM | POA mouse brain slices (Fig. 2.4C).

Property	Males		Diestrous females		Proestrous females	
	AAV-GFAP-mCherry	AAV-GFAP-hM3Dq	AAV-GFAP-mCherry	AAV-GFAP-hM3Dq	AAV-GFAP-mCherry	AAV-GFAP-hM3Dq
Brain slices (n)	12	9	12	12	5	9
Mice (n)	4	6	4	6	2	4
Three-way mixed model ANOVA						
Effect			Statistic		Partial η^2	
Treatment period			$F_{(2,106)} = 27.045$, $\mathbf{p < 0.001}$		0.338	
Sex/cycle stage			$F_{(2,53)} = 0.240$, $p = 0.788$		0.009	
AAV			$F_{(1,53)} = 33.802$, $\mathbf{p < 0.001}$		0.389	
Treatment period * Sex/cycle stage			$F_{(4,106)} = 0.710$, $p = 0.576$		0.026	
Treatment period * AAV			$F_{(2,106)} = 27.245$, $\mathbf{p < 0.001}$		0.340	
Sex/cycle stage * AAV			$F_{(2,53)} = 1.078$, $p = 0.348$		0.039	
Treatment period * Sex/cycle stage * AAV			$F_{(4,106)} = 1.048$, $p = 0.383$		0.038	

Table 2.9: Statistical parameters from three-way mixed model ANOVA assessing the effect of sex/cycle stage and AAV on GnRH neuron response to 200 nM CNO treatment from PM | POA mouse brain slices (Fig. 2.4D).

Property	Males		Diestrous females		Proestrous females	
	AAV-GFAP-mCherry	AAV-GFAP-hM3Dq	AAV-GFAP-mCherry	AAV-GFAP-hM3Dq	AAV-GFAP-mCherry	AAV-GFAP-hM3Dq
Brain slices (n)	12	10	10	10	9	10
Mice (n)	4	6	4	5	3	6
Three-way mixed model ANOVA						
Effect			Statistic		Partial η^2	
Treatment period			$F_{(2,110)} = 49.291$, $\mathbf{p < 0.001}$		0.473	
Sex/cycle stage			$F_{(2,55)} = 4.485$, $\mathbf{p = 0.016}$		0.140	
AAV			$F_{(1,55)} = 90.536$, $\mathbf{p < 0.001}$		0.622	
Treatment period * Sex/cycle stage			$F_{(4,110)} = 2.060$, $p = 0.104$		0.070	
Treatment period * AAV			$F_{(2,110)} = 47.776$, $\mathbf{p < 0.001}$		0.465	
Sex/cycle stage * AAV			$F_{(2,55)} = 0.679$, $p = 0.511$		0.024	
Treatment period * Sex/cycle stage * AAV			$F_{(4,110)} = 2.465$, $p = 0.061$		0.082	

Table 2.10: Statistical parameters from three-way mixed model ANOVA assessing the effect of sex/cycle stage and AAV on KNDy neuron response to 200 nM CNO treatment from AM | ARC mouse brain slices (Fig. 5C).

Property	Males		Diestrous females		Proestrous females	
	AAV-GFAP-mCherry	AAV-GFAP-hM3Dq	AAV-GFAP-mCherry	AAV-GFAP-hM3Dq	AAV-GFAP-mCherry	AAV-GFAP-hM3Dq
Brain slices (n)	12	10	10	11	6	9
Mice (n)	6	6	6	4	3	4
Three-way mixed model ANOVA						
Effect			Statistic		Partial η^2	
Treatment period			$F_{(2,104)} = 3.097$, $p = 0.076$		0.056	
Sex/cycle stage			$F_{(2,52)} = 1.384$, $p = 0.260$		0.051	
AAV			$F_{(1,52)} = 1.028$, $p = 0.315$		0.019	
Treatment period * Sex/cycle stage			$F_{(4,104)} = 1.808$, $p = 0.165$		0.065	
Treatment period * AAV			$F_{(2,104)} = 0.529$, $p = 0.502$		0.010	
Sex/cycle stage * AAV			$F_{(2,52)} = 1.872$, $p = 0.164$		0.067	
Treatment period * Sex/cycle stage * AAV			$F_{(4,104)} = 0.747$, $p = 0.501$		0.028	

Table 2.11: Statistical parameters from three-way mixed model ANOVA assessing the effect of sex/cycle stage and AAV on KNDy neuron response to 200 nM CNO treatment from PM | ARC mouse brain slices (Fig. 2.5D).

Property	Males		Diestrous females		Proestrous females	
	AAV-GFAP-mCherry	AAV-GFAP-hM3Dq	AAV-GFAP-mCherry	AAV-GFAP-hM3Dq	AAV-GFAP-mCherry	AAV-GFAP-hM3Dq
Brain slices (n)	7	10	9	10	11	7
Mice (n)	5	5	4	6	5	3
Three-way mixed model ANOVA						
Effect			Statistic		Partial η^2	
Treatment period			$F_{(2,96)} = 4.644$, $\mathbf{p = 0.031}$		0.088	
Sex/cycle stage			$F_{(2,48)} = 0.461$, $p = 0.634$		0.019	
AAV			$F_{(1,48)} = 0.280$, $p = 0.599$		0.006	
Treatment period * Sex/cycle stage			$F_{(4,96)} = 0.645$, $p = 0.550$		0.026	
Treatment period * AAV			$F_{(2,96)} = 1.425$, $p = 0.242$		0.029	
Sex/cycle stage * AAV			$F_{(2,48)} = 0.653$, $p = 0.525$		0.026	
Treatment period * Sex/cycle stage * AAV			$F_{(4,96)} = 0.202$, $p = 0.846$		0.008	

Table 2.12: Statistical parameters from three-way mixed model ANOVA assessing the effect of sex/cycle stage and AAV on LH levels during 0.3 mg/kg CNO treatment from AM | POA mice (Fig. 2.6C left).

Property	Males		Diestrous females	
	AAV-GFAP-mCherry	AAV-GFAP-hM3Dq	AAV-GFAP-mCherry	AAV-GFAP-hM3Dq
Mice (n)	5	6	5	9
Three-way mixed model ANOVA				
Effect		Statistic		Partial η^2
Sample		$F_{(12,252)}$ = 40.870, ***p* < 0.001**		0.661
Sex		$F_{(1,21)}$ = 10.068, ***p* = 0.005**		0.324
AAV		$F_{(1,21)}$ = 71.863, ***p* < 0.001**		0.774
Sample * Sex		$F_{(12,252)}$ = 5.688, ***p* = 0.012**		0.213
Sample * AAV		$F_{(12,252)}$ = 45.073, ***p* < 0.001**		0.682
Sex * AAV		$F_{(1,21)}$ = 6.156, ***p* = 0.022**		0.227
Sample * Sex * AAV		$F_{(12,252)}$ = 5.585, ***p* = 0.012**		0.210

Table 2.13: Statistical parameters from three-way mixed model ANOVA assessing the effect of sex/cycle stage and AAV on LH levels during 0.3 mg/kg CNO treatment from PM | POA mice (Fig. 2.6C right).

Property	Males		Diestrous females	
	AAV-GFAP-mCherry	AAV-GFAP-hM3Dq	AAV-GFAP-mCherry	AAV-GFAP-hM3Dq
Mice (n)	5	7	5	8
Three-way mixed model ANOVA				
Effect		Statistic		Partial η^2
Sample		$F_{(12,252)}$ = 47.682, ***p* < 0.001**		0.694
Sex		$F_{(1,21)}$ = 8.472, ***p* = 0.008**		0.287
AAV		$F_{(1,21)}$ = 32.094, ***p* < 0.001**		0.604
Sample * Sex		$F_{(12,252)}$ = 8.463, ***p* < 0.001**		0.287
Sample * AAV		$F_{(12,252)}$ = 54.976, ***p* < 0.001**		0.724
Sex * AAV		$F_{(1,21)}$ = 3.446, p = 0.077		0.141
Sample * Sex * AAV		$F_{(12,252)}$ = 11.389, ***p* < 0.001**		0.352

Table 2.14: Statistical parameters from three-way mixed model ANOVA assessing the effect of sex/cycle stage and AAV on LH levels during 0.3 mg/kg CNO treatment from AM | POA mice (Fig. 2.6D left).

Property	Males		Diestrous females	
	AAV-GFAP-mCherry	AAV-GFAP-hM3Dq	AAV-GFAP-mCherry	AAV-GFAP-hM3Dq
Mice (n)	5	6	5	9
Three-way mixed model ANOVA				
Effect		Statistic		Partial η^2
Sample		$F_{(2,42)}$ = 66.820, ***p* < 0.001**		0.761
Sex		$F_{(1,21)}$ = 9.843, ***p* = 0.005**		0.319
AAV		$F_{(1,21)}$ = 62.819, ***p* < 0.001**		0.749
Sample * Sex		$F_{(2,42)}$ = 6.706, ***p* = 0.015**		0.242
Sample * AAV		$F_{(2,42)}$ = 74.792, ***p* < 0.001**		0.781
Sex * AAV		$F_{(1,21)}$ = 5.442, ***p* = 0.030**		0.206
Sample * Sex * AAV		$F_{(2,42)}$ = 5.903, ***p* = 0.022**		0.219

Table 2.15: Statistical parameters from three-way mixed model ANOVA assessing the effect of sex/cycle stage and AAV on LH levels during 0.3 mg/kg CNO treatment from PM | POA mice (Fig. 2.6D right).

Property	Males		Diestrous females	
	AAV-GFAP-mCherry	AAV-GFAP-hM3Dq	AAV-GFAP-mCherry	AAV-GFAP-hM3Dq
Mice (n)	5	7	5	8
Three-way mixed model ANOVA				
Effect		Statistic		Partial η^2
Sample		$F_{(2,42)}$ = 74.714, ***p* < 0.001**		0.781
Sex		$F_{(1,21)}$ = 6.796, ***p* = 0.016**		0.244
AAV		$F_{(1,21)}$ = 19.604, ***p* < 0.001**		0.483
Sample * Sex		$F_{(2,42)}$ = 11.531, ***p* = 0.002**		0.354
Sample * AAV		$F_{(2,42)}$ = 89.697, ***p* < 0.001**		0.810
Sex * AAV		$F_{(1,21)}$ = 1.512, p = 0.232		0.067
Sample * Sex * AAV		$F_{(2,42)}$ = 17.242, ***p* < 0.001**		0.451

Table 2.16: Statistical parameters from three-way mixed model ANOVA assessing the effect of sex/cycle stage and AAV on LH levels during 0.3 mg/kg CNO treatment from AM | ARC mice (Fig. 2.7C left).

Property	Males		Diestrous females	
	AAV-GFAP-mCherry	AAV-GFAP-hM3Dq	AAV-GFAP-mCherry	AAV-GFAP-hM3Dq
Mice (n)	7	6	6	5
Three-way mixed model ANOVA				
Effect		Statistic		Partial η^2
Sample		$F_{(12,240)} = 4.252$, $\mathbf{p = 0.029}$		0.175
Sex		$F_{(1,20)} = 0.014$, $p = 0.907$		0.001
AAV		$F_{(1,20)} = 2.432$, $p = 0.135$		0.108
Sample * Sex		$F_{(12,240)} = 3.031$, $p = 0.070$		0.132
Sample * AAV		$F_{(12,240)} = 5.266$, $\mathbf{p = 0.014}$		0.208
Sex * AAV		$F_{(1,20)} = 6.882$, $\mathbf{p = 0.016}$		0.256
Sample * Sex * AAV		$F_{(12,240)} = 3.590$, $\mathbf{p = 0.046}$		0.152

Table 2.17: Statistical parameters from three-way mixed model ANOVA assessing the effect of sex/cycle stage and AAV on LH levels during 0.3 mg/kg CNO treatment from PM | ARC mice (Fig. 2.7C right).

Property	Males		Diestrous females	
	AAV-GFAP-mCherry	AAV-GFAP-hM3Dq	AAV-GFAP-mCherry	AAV-GFAP-hM3Dq
Mice (n)	7	6	5	4
Three-way mixed model ANOVA				
Effect		Statistic		Partial η^2
Sample		$F_{(12,216)} = 5.499$, $\mathbf{p = 0.015}$		0.234
Sex		$F_{(1,18)} = 1.226$, $p = 0.283$		0.064
AAV		$F_{(1,18)} = 5.780$, $\mathbf{p = 0.027}$		0.243
Sample * Sex		$F_{(12,216)} = 4.422$, $\mathbf{p = 0.030}$		0.197
Sample * AAV		$F_{(12,216)} = 5.727$, $\mathbf{p = 0.013}$		0.241
Sex * AAV		$F_{(1,18)} = 1.033$, $p = 0.323$		0.054
Sample * Sex * AAV		$F_{(12,216)} = 5.543$, $\mathbf{p = 0.015}$		0.235

Table 2.18: Statistical parameters from three-way mixed model ANOVA assessing the effect of sex/cycle stage and AAV on LH levels during 0.3 mg/kg CNO treatment from AM | ARC mice (Fig. 2.7D left).

Property	Males		Diestrous females	
	AAV-GFAP-mCherry	AAV-GFAP-hM3Dq	AAV-GFAP-mCherry	AAV-GFAP-hM3Dq
Mice (n)	7	6	6	5
Three-way mixed model ANOVA				
Effect		Statistic		Partial η^2
Sample		$F_{(2,40)} = 5.554$, $\mathbf{p = 0.020}$		0.217
Sex		$F_{(1,20)} = 0.478$, $p = 0.497$		0.023
AAV		$F_{(1,20)} = 1.033$, $p = 0.322$		0.049
Sample * Sex		$F_{(2,40)} = 3.462$, $p = 0.066$		0.148
Sample * AAV		$F_{(2,40)} = 8.029$, $\mathbf{p = 0.006}$		0.286
Sex * AAV		$F_{(1,20)} = 6.647$, $\mathbf{p = 0.018}$		0.249
Sample * Sex * AAV		$F_{(2,40)} = 4.224$, $\mathbf{p = 0.043}$		0.174

Table 2.19: Statistical parameters from three-way mixed model ANOVA assessing the effect of sex/cycle stage and AAV on LH levels during 0.3 mg/kg CNO treatment from PM | ARC mice (Fig. 2.7D right).

Property	Males		Diestrous females	
	AAV-GFAP-mCherry	AAV-GFAP-hM3Dq	AAV-GFAP-mCherry	AAV-GFAP-hM3Dq
Mice (n)	7	6	5	4
Three-way mixed model ANOVA				
Effect		Statistic		Partial η^2
Sample		$F_{(2,36)} = 5.550$, $\mathbf{p = 0.026}$		0.236
Sex		$F_{(1,18)} = 0.629$, $p = 0.438$		0.034
AAV		$F_{(1,18)} = 5.015$, $\mathbf{p = 0.038}$		0.218
Sample * Sex		$F_{(2,36)} = 4.507$, $\mathbf{p = 0.044}$		0.200
Sample * AAV		$F_{(2,36)} = 5.499$, $\mathbf{p = 0.027}$		0.234
Sex * AAV		$F_{(1,18)} = 0.375$, $p = 0.548$		0.020
Sample * Sex * AAV		$F_{(2,36)} = 6.413$, $\mathbf{p = 0.018}$		0.263

Table 2.20: Statistical parameters assessing the viral ablation efficiency of KNDy neuron in male mice (Fig. 2.8F).

Property	Control	Ablation	
Mice (n)	6	12	
Two-tailed independent samples Welch's t-test			
Property		Statistic	η^2
KNDy neuron count		t(10.67), df = 5.04, ***p* < 0.001**	0.958

Table 2.21: Statistical parameters from two-way mixed model ANOVA assessing the effect of KNDy neuron ablation on LH levels during 0.3 mg/kg CNO treatment from AM | ARC male mice (Fig. 2.8D left).

Property	Males		
	AAV-GFAP-mCherry + AAV-flex-taCasp3	AAV-GFAP-hM3Dq + AAV-GFAP-hM3Dq	
Mice (n)	4	6	
Two-way mixed model ANOVA			
Effect		Statistic	Partial η^2
Sample		$F_{(12,96)}$ = 7.682, ***p* = 0.007**	0.490
AAV		$F_{(1,8)}$ = 11.074, ***p* = 0.010**	0.581
Sample * AAV		$F_{(12,96)}$ = 4.466, ***p* = 0.037**	0.358

Table 2.22: Statistical parameters from two-way mixed model ANOVA assessing the effect of KNDy neuron ablation on LH levels during 0.3 mg/kg CNO treatment from PM | ARC male mice (Fig. 2.8D right).

Property	Males		
	AAV-GFAP-mCherry + AAV-flex-taCasp3	AAV-GFAP-hM3Dq + AAV-GFAP-hM3Dq	
Mice (n)	4	5	
Two-way mixed model ANOVA			
Effect		Statistic	Partial η^2
Sample		$F_{(12,84)}$ = 3.624, p = 0.078	0.341
AAV		$F_{(1,7)}$ = 7.321, ***p* = 0.030**	0.511
Sample * AAV		$F_{(12,84)}$ = 5.024, ***p* = 0.041**	0.418

Table 2.23: Statistical parameters from two-way mixed model ANOVA assessing the effect of KNDy neuron ablation on LH levels during 0.3 mg/kg CNO treatment from AM | ARC male mice (Fig. 2.8E left).

Property	Males	
	AAV-GFAP-mCherry + AAV-flex-taCasp3	AAV-GFAP-hM3Dq + AAV-GFAP-hM3Dq
Mice (n)	4	6
Two-way mixed model ANOVA		
Effect	Statistic	Partial η^2
Sample	$F_{(2,16)}$ = 9.625, ***p* = 0.014**	0.546
AAV	$F_{(1,8)}$ = 12.009, ***p* = 0.009**	0.600
Sample * AAV	$F_{(2,16)}$ = 5.220, ***p* = 0.050**	0.395

Table 2.24: Statistical parameters from two-way mixed model ANOVA assessing the effect of KNDy neuron ablation on LH levels during 0.3 mg/kg CNO treatment from PM | ARC male mice (Fig. 2.8E right).

Property	Males	
	AAV-GFAP-mCherry + AAV-flex-taCasp3	AAV-GFAP-hM3Dq + AAV-GFAP-hM3Dq
Mice (n)	4	5
Two-way mixed model ANOVA		
Effect	Statistic	Partial η^2
Sample	$F_{(2,14)}$ = 3.043, p = 0.116	0.303
AAV	$F_{(1,7)}$ = 6.830, ***p* = 0.035**	0.494
Sample * AAV	$F_{(2,14)}$ = 5.399, ***p* = 0.045**	0.435

Table 2.25: Statistical parameters from three-way mixed model ANOVA assessing the effect of sex and antagonists to receptors EP1 and EP2 on GnRH neuron firing during 200 nM dmPGE2 treatment from AM | POA mice (Fig. 2.9A).

Property	Males		Diestrous females	
	Vehicle	EP1 & E2 antagonists	Vehicle	EP1 & EP2 antagonists
Brain slices (n)	7	8	9	7
Mice (n)	5	4	4	3
Three-way mixed model ANOVA				
Effect	Statistic			Partial η^2
Treatment period	$F_{(2,54)}$ = 12.681, ***p* < 0.001**			0.320
Sex	$F_{(1,27)}$ = 1.102, p = 0.303			0.039
Pretreatment	$F_{(1,27)}$ = 3.792, p = 0.062			0.123
Treatment period * Sex	$F_{(2,54)}$ = 5.457, ***p* = 0.018**			0.168
Treatment period * Pretreatment	$F_{(2,54)}$ = 6.640, ***p* = 0.009**			0.197
Sex * Pretreatment	$F_{(1,27)}$ = 0.546, p = 0.466			0.020
Treatment period * Sex * Pretreatment	$F_{(2,54)}$ = 6.959, ***p* = 0.008**			0.205

Table 2.26: Statistical parameters from one-way repeated measures ANOVA assessing the effect of 1 μM dmPGE2 treatment on GnRH neuron firing from AM | POA diestrous female mice (Fig. 2.9B).

Property	Diestrous females	
	Vehicle	
Brain slices (n)	9	
Mice (n)	4	
One-way repeated measures ANOVA		
Effect	Statistic	Partial η^2
Treatment period	$F_{(2,16)}$ = 14.694, ***p* = 0.001**	0.647

Table 2.27: Statistical parameters from three-way mixed model ANOVA assessing the effect of sex and antagonists to receptors EP1 and EP2 on GnRH neuron firing during 200 nM dmPGE2 treatment from PM | POA mice (Fig. 2.9C).

Property	Males		Diestrous females	
	Vehicle	EP1 & E2 antagonists	Vehicle	EP1 & EP2 antagonists
Brain slices (n)	9	9	8	7
Mice (n)	6	4	5	5
Three-way mixed model ANOVA				
Effect		Statistic		Partial η^2
Treatment period		$F_{(2,58)}$ = 7.583, ***p* = 0.004**		0.207
Sex		$F_{(1,29)}$ = 0.902, p = 0.350		0.030
Pretreatment		$F_{(1,29)}$ = 7.770, ***p* = 0.009**		0.211
Treatment period * Sex		$F_{(2,58)}$ = 0.384, p = 0.618		0.013
Treatment period * Pretreatment		$F_{(2,58)}$ = 6.925, ***p* = 0.006**		0.193
Sex * Pretreatment		$F_{(1,29)}$ = 0.007, p = 0.933		0.000
Treatment period * Sex * Pretreatment		$F_{(2,58)}$ = 0.383, p = 0.618		0.013

Table 2.28: Statistical parameters from two-way mixed model ANOVA assessing the effect of sex on KNDy neuron firing during 200 nM dmPGE2 treatment from AM | ARC mice (Fig. 2.10A).

Property	Males	Diestrous females
Brain slices (n)	6	6
Mice (n)	4	3
Two-way mixed model ANOVA		
Effect	Statistic	Partial η^2
Treatment period	$F_{(2,20)}$ = 1.409, p = 0.268	0.124
Sex	$F_{(1,10)}$ = 0.049, p = 0.829	0.005
Treatment period * Sex	$F_{(2,20)}$ = 0.806, p = 0.458	0.075

Table 2.29: Statistical parameters from two-way mixed model ANOVA assessing the effect of sex on KNDy neuron firing during 1 μM dmPGE2 treatment from AM | ARC mice (Fig. 2.10B).

Property	Males	Diestrous females	
Brain slices (n)	5	5	
Mice (n)	3	3	
Two-way mixed model ANOVA			
Effect		Statistic	Partial η^2
Treatment period		$F_{(2,16)} = 1.166$, $p = 0.312$	0.127
Sex		$F_{(1,8)} = 0.933$, $p = 0.362$	0.104
Treatment period * Sex		$F_{(2,16)} = 0.834$, $p = 0.388$	0.094

Table 2.30: Statistical parameters from two-way mixed model ANOVA assessing the effect of sex on KNDy neuron firing during 200 nM dmPGE2 treatment from PM | ARC mice (Fig. 2.10C).

Property	Males	Diestrous females	
Brain slices (n)	5	5	
Mice (n)	3	4	
Two-way mixed model ANOVA			
Effect		Statistic	Partial η^2
Treatment period		$F_{(2,16)} = 0.767$, $p = 0.413$	0.088
Sex		$F_{(1,8)} = 3.637$, $p = 0.093$	0.313
Treatment period * Sex		$F_{(2,16)} = 0.615$, $p = 0.464$	0.071

Table 2.31: Statistical parameters from two-way mixed model ANOVA assessing the effect of sex on KNDy neuron firing during 1 μM dmPGE2 treatment from PM | ARC mice (Fig. 2.10D).

Property	Males	Diestrous females	
Brain slices (n)	6	6	
Mice (n)	3	3	
Two-way mixed model ANOVA			
Effect		Statistic	Partial η^2
Treatment period		$F_{(2,20)} = 0.987$, $p = 0.356$	0.090
Sex		$F_{(1,10)} = 0.481$, $p = 0.504$	0.046
Treatment period * Sex		$F_{(2,20)} = 0.795$, $p = 0.411$	0.074

Table 2.32: Statistical parameters from three-way mixed model ANOVA assessing the effect of sex and antagonists to receptors EP1 and EP2 on GnRH neuron firing during 200 nM CNO treatment from AM | POA mice (Fig. 2.11B).

Property	Males		Diestrous females	
	Vehicle	EP1 & E2 antagonists	Vehicle	EP1 & EP2 antagonists
Brain slices (n)	8	9	10	9
Mice (n)	4	5	6	6
Three-way mixed model ANOVA				
Effect		Statistic		Partial η^2
Treatment period		$F_{(2,64)}$ = 30.563, ***p* < 0.001**		0.489
Sex		$F_{(1,32)}$ = 0.873, p = 0.357		0.027
Pretreatment		$F_{(1,32)}$ = 7.951, ***p* = 0.008**		0.199
Treatment period * Sex		$F_{(2,64)}$ = 1.525, p = 0.226		0.046
Treatment period * Pretreatment		$F_{(2,64)}$ = 8.101, ***p* < 0.001**		0.202
Sex * Pretreatment		$F_{(1,32)}$ = 0.413, p = 0.525		0.013
Treatment period * Sex * Pretreatment		$F_{(2,64)}$ = 0.547, p = 0.572		0.017

Table 2.33: Statistical parameters from three-way mixed model ANOVA assessing the effect of sex and antagonists to receptors EP1 and EP2 on GnRH neuron firing during 200 nM CNO treatment from PM | POA mice (Fig. 2.11D).

Property	Males		Diestrous females	
	Vehicle	EP1 & E2 antagonists	Vehicle	EP1 & EP2 antagonists
Brain slices (n)	11	10	9	10
Mice (n)	6	6	5	4
Three-way mixed model ANOVA				
Effect		Statistic		Partial η^2
Treatment period		$F_{(2,72)}$ = 37.452, ***p* < 0.001**		0.510
Sex		$F_{(1,36)}$ = 0.693, p = 0.411		0.019
Pretreatment		$F_{(1,36)}$ = 0.292, p = 0.592		0.008
Treatment period * Sex		$F_{(2,72)}$ = 0.911, p = 0.383		0.025
Treatment period * Pretreatment		$F_{(2,72)}$ = 0.513, p = 0.550		0.014
Sex * Pretreatment		$F_{(1,36)}$ = 0.007, p = 0.936		0.000
Treatment period * Sex * Pretreatment		$F_{(2,72)}$ = 0.041, p = 0.921		0.001

Chapter 3: Investigation of the Endogenous Activators of Preoptic Area Astrocyte in Reproductive Function[2]

Introduction

Glia were once considered to play only a supportive role within the neural circuitry underlying animal physiology. Research over the past few decades, however, has uncovered the many functional contributions that glia, and particularly astrocytes, have in these circuits. Astrocytes are a core component of the tripartite synapse, which utilizes a variety of glia-to neuron and glia-to-glia signaling modalities[162]. This bidirectional communication between glia and neurons is important in a variety of systems including, but not limited to, long-term memory, sleep-wake cycles, sensory and motor regulation, respiration, and even reproduction. Uncovering the mechanisms that describe how glia contribute to these important neuronal circuits is thus important.

Recent work has begun to elucidate the mechanisms of astrocyte modulation of the central reproductive neuroendocrine circuit within the hypothalamic-pituitary-gonadal (HPG) axis. Gonadotropin-releasing hormone (GnRH) neurons in the medial preotic area (POA) compose the final central output within the HPG axis. Hypothalamic astrocytes modulate GnRH neuron function through morphological plasticity and gliotransmission, which are predominately induced by changes in intracellular calcium levels ($[Ca^{2+}]_i$). The gliotransmitter prostaglandin E_2 (PGE2) is a potent activator of GnRH neurons, as these neurons express PGE2 receptor 2 (EP2), allowing direct astrocytic PGE2 signaling[287]. Diets deficient in fatty acids, precursors to prostaglandin synthesis, delayed puberty onset in female mice[228]. Inhibiting PGE2 synthesis via disruption of erbB receptor signaling pathways similarly compromises reproductive capacity in mice[243,246,250]. Recent work activating astrocytes with designer receptors

[2] Co-authored by Chrystian D. Phillips, Laura L. Burger, Nick Rossiter, R. Anthony DeFazio, and Suzanne M. Moenter.

exclusively activated by designer drugs (DREADDs) found that astrocyte communication with the GnRH neuron network via PGE2 was sex dependent[288].

Stimulation of Gq-associated G-protein-coupled receptors (GPCRs) is a major route of astrocyte activation *in vivo*; this was the impetus behind utilizing Gq-coupled DREADDs in prior work. However, utilization of chemogenetic and optogenetic tools comes with its own caveats[358], as their effects on cells do not fully recapitulate native cellular function. This is the basis for elucidating the endogenous activators of POA astrocytes. Although little is known about the receptor makeup of these astrocytes, there are several candidate activators worth investigation. First, Ca^{2+} signaling in astrocytes can be achieved by activation of metabotropic glutamate receptors (mGluRs) *in vitro* and *in situ*. The group I mGluRs, particularly subtype 5, are Gq GPCRs that have been implicated in glia-neuron communication. Second, endocannabinoids can also alter neurotransmitter uptake in astrocytes, and astrocytes across the limbic system, including the hypothalamus, express the endocannabinoid receptor CB1[359,360]. Although CB1 signal transduction is canonically through $G_{i/o}$ GPCRs, specific agonists like WIN 55,212-2 can change CB1 coupling to Gq receptors[361]. Interestingly, GnRH neurons synthesize endocannabinoids, and prostaglandins including the gliotransmitter PGE2 are reported to modulate the effect of these endocannabinoids on GABAergic post synaptic current frequencies in GnRH neurons[347]. Third, ATP is known not only for being the primary intracellular energy molecule, but it, along with ADP, also acts as an intercellular signal. Purines act on the ionotropic P_2X and metabotropic P_2Y receptors, and both glutamate and ATP are purported to mediate autocrine and paracrine stimulation at the tripartite synapse[362].

Here, we interrogated candidate modulators of astrocytic $[Ca^{2+}]_i$. We also examine if attenuation of Ca^{2+} signaling is capable of altering murine reproductive parameters *in vivo*. Finally, we initiated CRISPR-Cas9-mediated knock down of a candidate receptor in astrocytes to determine potential deleterious effects on reproductive function.

Materials & Methods

All chemicals were purchased from Sigma-Aldrich (St. Louis, MO USA) unless otherwise noted.

Animals. Mouse strains are listed in Table 3.1. C57BL/6 mice were obtained from the Jackson Laboratory (000664) and propagated in our colony for Ca^{2+} imaging and Ca^{2+} signaling attenuation experiments. Mice expressing Cre recombinase under control of the glial fibrillary acidic protein (*Gfap)* promoter were bred to Lox-Stop-Lox Cas9/eGFP mice (Jax 024858). Mice were maintained under a 14-hour light, 10-hour dark photoperiod (lights out at 0300 h) with *ad libitum* access to Teklad 2916 chow (Envigo, Madison, WI USA) and water. Adult mice aged 2 to 6 months were used for stereotaxic injections. In females, estrous cycle stage was determined by vaginal lavage and confirmed by uterine mass at euthanasia (50-80 mg for diestrus). Animals were randomized among experimental groups. The Institutional Animal Care and Use Committee at the University of Michigan approved all procedures.

Table 3.1: Mouse strain used.

Strain name	Shorthand	Ref.	Supplier	Catalog number	RRID
C57BL/6J	Wild Type	[309]	The Jackson Laboratory	000664	IMSR_JAX:000664

Stereotaxic injections. Adeno-associated viruses (AAVs) and the purpose of each are listed in Table 3.2. Preferential targeting to astrocytes was achieved using either the long or short forms of the *Gfap* promoter; GFAP is expressed in most astrocytes[132,363]. Mice aged between 2-6 months were anesthetized with isoflurane (30 s at 5% for induction, and 1.5% for maintenance) and given carprofen (Zoetis, Inc., 5 mg/kg, sc) before surgery and 24 h post-surgery for analgesia. Scalp hair was removed with clippers (559A, Oster). Anesthetized mice were placed on a stereotaxic instrument (David Kopf Instruments) using ear bars. Body temperature was maintained at 36°C using a feedback-controlled heating pad (TCAT-2LV Controller, Physitemp Instruments). Ophthalmic ointment (Optixcare) was applied to the eyes to prevent ulceration. Under

magnification (Model 310187, Zeiss), an incision was made along the interfrontal and sagittal sutures, and the skin was peeled back to reveal bregma and lambda. Craniotomies were created using a high-speed drill (Model 1100, Dremel) to target the POA (1.2 mm anterior to bregma, 0.2 mm from the midline, 5 mm ventral from the skull surface at bregma). Bilateral injections of 150 nL of AAV were performed at the POA at ~50 nL/min with the use of a Kopf stereotaxic frame (Model 942, David Kopf Instruments). The injection pipette was left in place for 8 min after injection to allow the virus to diffuse into the brain, then raised 200 µm and left in place for 2 min more. Surgical sites were closed with liquid wound sealant (3M Vetbond) and monitored daily for 10 days for signs of infection or dehiscence. For Ca^{2+} imaging experiments, viral transduction proceeded for 3-6 weeks before mice were used for experiments.

Table 3.2: Viruses used.

AAV	Shorthand	Ref	Purpose	Addgene number	RRID
pZac2.1 gfaABC1D-cyto-GCaMP6f	AAV-GFAP-GCaMP6f	[310]	Ca imaging	52925-AAV5	Addgene_52925
pAAV-GFAP104-mCherry	AAV-GFAP-mCherry	[311]	Ca attenuation control	58909-AAV5	Addgene_58909
pZac2.1-GfaABC1D-mCherry-hPMCA2w/b	AAV-GFAP-hPMCA2w/b	[364]	Ca attenuation	111568-AAV5	Addgene_111568

Free floating immunofluorescence. Antibodies are listed in Table 3.3. Mice were deeply anesthetized with isoflurane and transcardially perfused with PBS for 5 min (~15 mL) followed by 10% neutral-buffered formalin for 5 min (~15 mL). Brains were harvested and placed in the same fixative overnight at 4°C on a rocker. Brains were transferred to 30% sucrose for at least 24 h until brains sank in the solution. Brains were sectioned (30 µm, four series) on a cryostat (Leica CM1860) and stored at -20°C in antifreeze solution (25% ethylene glycol and 25% glycerol in PBS). Sections used for immunostaining were first washed once with PBS containing 0.1% TritonX-100 (PBST), then treated with 0.1% $NaBH_4$ in PBST for 10 min to reduce background autofluorescence. Sections were washed with PBST (3 times, 5 min each) and then

placed in blocking solution (PBST containing 10% normal goat serum, Jackson ImmunoResearch) for 1 h at room temperature. Sections were then incubated in primary antibodies diluted in blocking solution for 48 h at 4°C. Sections were washed (3 times, 5 min each) and incubated with secondary antibodies in PBST for 1.5 h at room temperature. Sections were mounted, set to dry overnight, and coverslipped (VWR International 48393 251). Images were collected on a Nikon Eclipse TE200 (lower magnification) or a Nikon A1 confocal microscope (colocalization verification). The number of GCaMP6f-only, S100β-only, mCherry-only, GCaMP6f/S100β, and GCaMP6f/mCherry coexpressing cells were counted from images (signal observed by eye, 3 fields/mouse in the infected region).

Table 3.3: Antibodies used.

Antibody	Species	Working dilution	Reference	Supplier	Catalog number	RRID
Anti-S100β	Rabbit	1:500	[313]	GeneTex	GTX129573	AB_2886037
Anti-mCherry	Rat	1:3,000	[314]	Thermo Fisher Scientific	M11217	AB_2536611
Anti-GFP	Chicken	1:1,000	[316]	Abcam	ab13970	AB_300798
Anti-rabbit, Alexa Fluor 488	Goat	1:500	-	Thermo Fisher Scientific	A-11008	AB_143165
Anti-chicken, Alexa Fluor 488	Goat	1:500	-	Thermo Fisher Scientific	A-11039	AB_142924
Anti-rat, Alexa Fluor 594	Goat	1:500	-	Thermo Fisher Scientific	A-11007	AB_141374

Brain slice preparation. All solutions were bubbled with 95% O_2/5% CO_2 for at least 15 min before being exposed to tissue. Brains were rapidly removed (9:00-10:00 EST) and placed in ice-cold sucrose saline solution containing the following (in mM): 250 sucrose, 3.5 KCl, 25 $NaHCO_3$, 10 D-glucose, 1.25 Na_2HPO_4, 1.2 $MgSO_4$, and 3.8 $MgCl_2$; the

solution was adjusted to pH 7.6 and 345 mOsm. Coronal brain slices (300 μm) were cut with a VT1200S vibrating microtome (Leice Biosystems). Slices were incubated for 30 min at room temperature (21-23°C) in 50% sucrose saline and 50% artificial cerebrospinal fluid (ACSF) containing the following (in mM): 135 NaCl, 3.5 KCl, 26 $NaHCO_3$, 10 D-glucose, 1.25 Na_2HPO_4, 1.2 $MgSO_4$, and 2.5 $CaCl_2$; the solution was adjusted to pH 7.4 and 305 mOsm. Slices were transferred to 100% ACSF for at least another 30 min before experiment recordings. Individual slices were transferred to a recording chamber that sits below a mounted Olympus BX51WI upright fluorescent microscope (Evident). Slices were perfused with ACSF (3 mL/min) using a peristaltic pump (MINIPULS 3, Gilson) at 29-32°C with an inline heating unit (Warner Instruments). Slices were used within 6 h of preparation. No differences in results associated with time after brain slice preparation were observed.

Ca^{2+} imaging. Brain slices were imaged under a 20x objective with an ORA-FLASH4.0 V3 CMOS camera (Hamamatsu) mounted on the microscope. Images were acquired at 500 ms intervals with 50 ms exposure times using Olympus cellSense software (Evident). Slices first were imaged during 5-min stabilization period where it was verified that no overt motion artifacts were present. To assess the response to these activators, the area under the curve (AUC) was calculated from $\Delta F/F_0$ traces as a proxy for elevations in $[Ca^{2+}]_i$. Spontaneous $[Ca^{2+}]_i$ events in astrocytes were observed in all brain slices during baseline measurements. Slices were then imaged for a 5-min baseline period to monitor spontaneous Ca^{2+} signaling. Slices were then treated for 6 min with one of the following pharmacological agents administer via bath perfusion: mGluR5 agonist chlorohydroxyphenylglycine (CHPG, 300 μM; Cayman), group I and II mGluR agonist 1-aminocyclopentane-1,3-dicarboxylic acid (ACPD, 100 μM; Cayman), cannabinoid receptor agonist WIN 55,212-2 (10 μM; Cayman), ATP (100-500 μM), and ADP (100-500 μM). To enhance the stability of ATP in solution, its pH was adjusted using NaOH to physiological levels and was prepared within one month of Ca^{2+} imaging. A subset of slices also underwent a 6 min pretreatment period with an antagonist to the respective candidate receptor or a vehicle. Imaging was concluded with an 8- or -9-min washout period. In addition, the following blockers were perfused

for the duration of recordings to mitigate the effects of candidate activators on neuronal activity: AMPA receptor antagonist CNQX (20 μM), NMDA receptor antagonist AP5 (20 μM), $GABA_A$ receptor antagonist picrotoxin (100 μM), and action-potential-inhibitor tetrodotoxin (TTX, 500 nM). Up to three slices were used per mouse, and a minimum of three mice were studied per group.

Table 3.4: Specificity of *P2ry1* sgRNAs and off-targeting predictions.

sgRNA	*Specificity score	†Mismatches (MMs) between sgRNA and gene locus	Gene	#Off-target score	Locus
P2ry1-g1	88	3MMs [3:5:18]	*Dnmt1*	0.63	chr9:-20829215-20829237
		4MMs [3:4:15:20]	*Dus3l*	0.18	chr17:+57072601-57072623
		4MMs [1:5:16:20]	*Arhgap33os*	0.12	chr7:-30220251-30220273
P2ry1-g2	96	4MMs [6:11:13:19]	*Txnip*	0.06	chr3:-96467355-96467377
		4MMs [1:2:7:14]	*Gga1*	0.16	chr15:-78761693-78761715
		4MMs [1:10:12:19]	*Lmtk2*	0.24	chr5:+144121712-144121734
		4MMs [4:7:11:18]	*Dtnb*	0.12	chr12:-3622784-3622806
		4MMs [6:12:15:18]	*Cpsf1*	0.02	chr15:-76481866-76481888

*Value ranges from 0 to 100 index to assess the specificity of the guide, with 100 being the most specific guide to *P2ry1*.
†3MMs [3:5:18] indicates nucleotides 3, 5, and 18 of the sgRNA do not match the off-target gene locus.
#Value ranges from 0 to 100, with 100 being the value for *P2ry1*.

sgRNA constructs. Generation of single guide RNAs (sgRNA) involved identifying gN20-nt target sequences preceding SpCas9-specific 5'-NGG-3' protospacer-adjacent motif

(PAM) sequences. In order to minimize off target effects, the CRISPOR design tool was used to target exon 1 of mouse *P2ry1*[365,366]. Two candidates were selected based on the lowest predicted off-target effects (Table 3.4), hence called sgRNA1 and sgRNA2. *P2ry1* targeting sgRNAs (5' to 3'): sgRNA1 - GACTCGAGACCCAGCCGAGCG; sgRNA2 - GAGCTCGTCTCCGCGCTCGGC. After synthesis of the gN20-nt target and complement sequences with BsmBI overhangs, the oligonucleotides were annealed and phosphorylated. The oligonucleotides were then ligated in the lentiCRISPRv2 puro plasmid ("lentiCRISPRv2", Addgene 98290) after BsmBI digestion. A control sgRNA sequence was designed to target *lacZ* gene from *Escherichia coli* (5'-TGCGCAGCCTGAATGGCGAA-3'). All plasmids were verified by sequencing. Plasmids (lentiCRISPRv2) containing the sgRNA sequences were then sent to the University of Michigan Vector Core for lentiviral production.

Cell line culture and transduction. The mouse-derived microglial cell line BV-2 (generous gift of Dr. Sebastian Werneberg) was grown in Dulbecco's Modified Eagle's Medium (DMEM) containing 5% fetal bovine serum (FBS; Invitrogen, Carlsbad, CA USA) and 1% penicillin and streptomycin (Invitrogen, Carlsbad, CA USA). Cells were maintained at 37°C in 5% CO_2 atmosphere. DMEM was replaced every 3 days, and cell passaging occurred every 6 days. For transduction, $2x10^6$ BV-2 cells were plated in DMEM into each well in a 6 well plate. Polybrene (10 µg) and 250 µL undiluted lentriviral particles were mixed with the cells per plate. Cells underwent lentiviral spinfection at 37°C for 45 min at 1,200 g, then were left to incubate overnight. Cells were then selected for 6 days with DMEM containing 2 µg/mL puromycin.

Quantitative PCR. Total RNA was isolated from transduced and puromycin-selected BV-2 cells (RNeasy Plus Micro Kit with on column DNasing, QIAGEN) and 1 µg RNA was reverse transcribed into cDNA (Superscript Vilo, Invitrogen, Fisher Scientific). Quantitative Taqman PCR (TaqMan Gene Expression Master Mix, Applied Biosystems, Fisher Scientific) was performed on duplicates of 25ng cDNA for *P2ry1*, *Actb*, and *Rps29*. A standard curve was made from a serial dilution (1:5) of BV-2 control cDNA. Data were analyzed by the ΔΔCT method[367], normalized to *Actb* and *Rps29* and

reported relative to control BV-2. Primers and Taqman probes were purchased from Integrated DNA Technologies (Coralville, IA) and are reported in Table 3.5.

Table 3.5: Primer probes used for qPCR.

Gene	IDT assay	Forward primer 5' → 3'	Probe 5' → 3'	Reverse primer 5' → 3'
P2ry1	Mm.PT.58.33326673	TCAAGCAGAATGGAGACACG	TTGTGAAGGCACGAGATCCTAGCTC	TGGTCAATAGAGTGTTGCTTCT
Actb	Mm.PT.39a.22214843.g	GATTACTGCTCTGGCTCCTAG	CTGGCCTCACTGTCCACCTTCC	GACTCATCGTACTCCTGCTTG
Rps29	custom	TGAAGGCAAGATGGGTCAC	AGTCACCCACGGAAGTTCGG	GCACATGTTCAGCCCGTATT
P2ry1 sequencing	custom	CCTTTTGTTCTGACCACTGA		AACCACCTCCTCTCTGATCA

Sanger Sequencing. Genomic DNA was isolated from BV-2 cells (Quick-DNA Miniprep Plus Kit, Zymo). Approximately 50 ng genomic DNA was used to amplify a 470bp product encompassing the 5' end of the first exon of the *P2ry1* gene (chr3:60909983-60910452, GRCm39). The PCR products were gel extracted (QIAquick Gel Extraction Kit, Qiagen) and Sanger sequenced (Azenta Life Sciences, Burlington, MA) from both the forward and reverse primers. DNA sequences were imported into SeqMan Ultra (DNASTAR Lasergene, Madison, WI) and aligned against the mouse consensus genomic sequence to look for DNA disruption (indels) with BV-2 samples transduced with lentiviral sgRNA constructs.

Ca^{2+} signaling attenuation. To ensure wider coverage of POA astrocytes with AAV-GFAP hPMCA2w/b, double bilateral injections were performed (1.2 mm anterior to bregma, 0.2 mm from the midline, 5 mm ventral from the skull surface at bregma; 1.0 mm anterior to bregma, 0.2 mm from the midline, 5.5 mm ventral from the skull at bregma) for both AAV-GFAP-mCherry and AAV-GFAP-hPMCA2w/b injections. Estrous cycle stage was monitored by daily vaginal cytology for ten days before and 8 weeks following stereotaxic injections. Viral targeting was verified via immunofluorescence after cycling.

Data analyses. Imaging data were transferred to Igor Pro 9 (Sutter Instruments) for analysis.The algorithm used to calculate Ca^{2+} signals ($\Delta F/F_0$) was derived from prior research analyzing Ca^{2+} signals[320]. In brief, mean fluorescence *F(t)* of an ROI was

calculated for each time point *t*. The time-dependent baseline $F_0(t)$ for that ROI was then calculated; $F_0(t)$ was defined as the minimum value of the smoothed $F(t)$ during a user-defined time window of duration τ (500 s) extending from $t - \tau$ to *t.* The relative change of fluorescent signal between $F(t)$ and $F_0(t)$ was calculated and filtered to yield $\Delta F/F_0$. To quantify the effect of treatment on Ca^{2+} signaling, the area under the curve (AUC) from each ROI's $\Delta F/F_0$ curve was calculated. The AUCs obtained from 27 independent ROIs were averaged to yield the average AUC of the slice.

Statistical analyses. Statistical analyses were performed using Prism 10 (GraphPad Software; 10.4.1 [627]) or SPSS (IBM; 31.0.0.0 [117]). Shapiro-Wilk was used to test normality of data distributions; most experiments included one or more groups that were not normally distributed. Data are all plotted as mean ± SEM and were compared among animal groups with statistical tests as indicated in the figure legends. The level accepted as significant was set to $p < 0.05$.

Results

GCaMP6f successfully delivered to POA astrocytes. To characterize the effects of candidate activators of endogenous astrocytic Gq GPCRs, we injected the POA with AAV5 bearing the calcium indicator GCaMPf driven by the GFAP promoter (AAV-GFAP-GCaMP6f; Fig. 3.1A). A subset of mice was perfused and dual immunofluorescence of GCaMP6f and the astrocytic cytoplasmic marker S100β were used to examine if viral expression was appropriately targeted (Fig. 3.1B). GCaMP6f expression was found to overlap with S100β signals in 94.7 ± 1.0% of POA astrocytes counted (n = 3 mice).

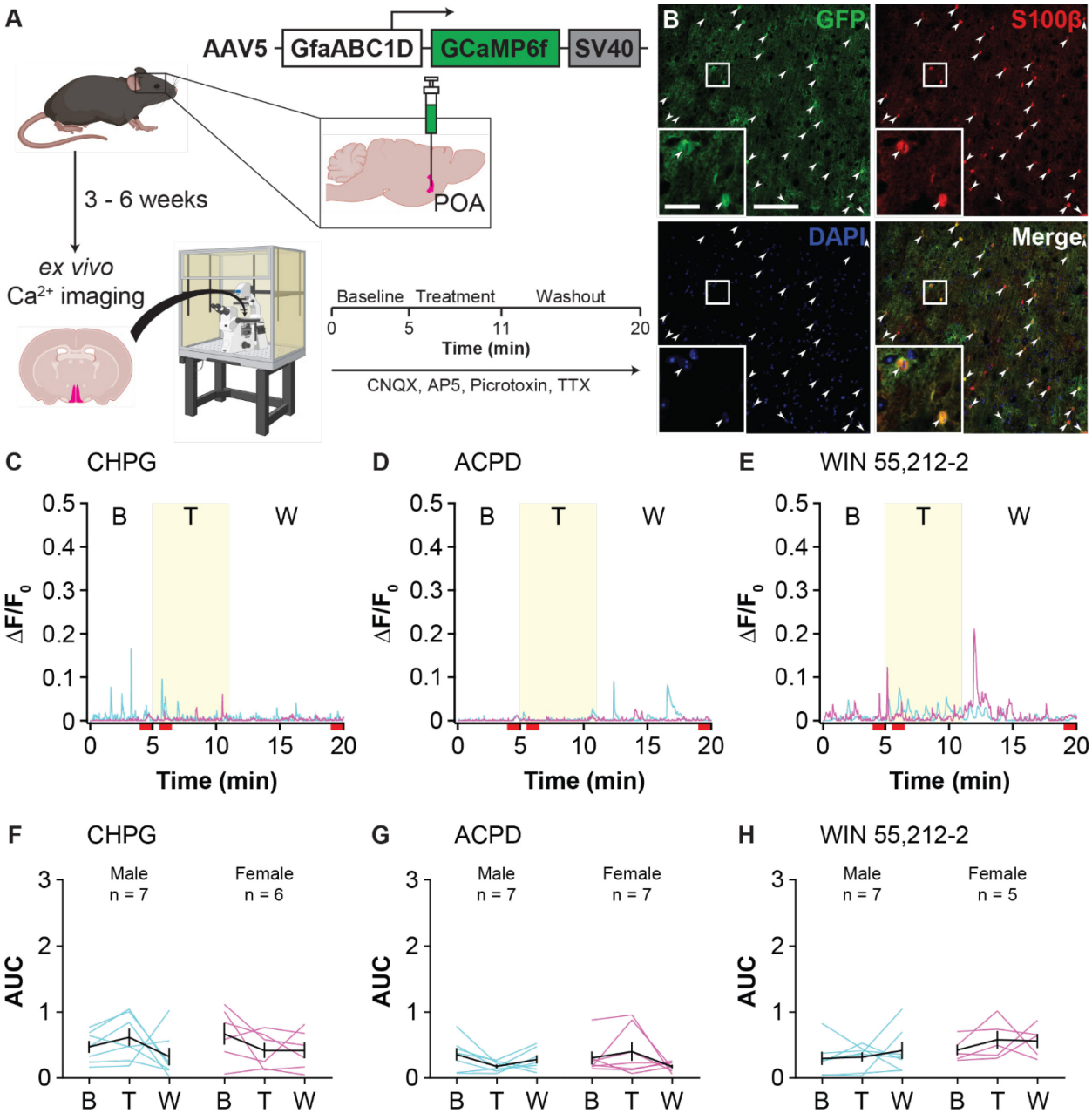


Figure 3.1: mGluR and CB1 agonists fail to induce Ca^{2+} signaling in POA astrocytes. **A,** Representative dual immunofluorescent images of GFP+ cells (for GCaMP6f) stained with the glial marker S100β to show colocalization of the two signals in POA-containing mouse brain sections. White arrowheads point to instances of colocalization. For all panels, scale bar in full image: 100 μm; scale bar in inset: 20 μm. **B-D,** Representative *ΔF/F₀* traces in brain slices from male (cyan) and diestrous female (magenta) mice injected with AAV5-GFAP-GCaMP6f. Red bars on the x-axis indicate the windows used for statistical comparison. B, baseline; T, treatment with agonist; W, washout. **E-G,** Quantification of AUC values in brain slices (cyan and magenta lines) overlaid with mean ± SEM (black lines; two-way mixed-model ANOVAs with Sidak *poc hoc*; statistics are in Tables 3.6-3.8).

Agonists for metabotropic glutamatergic receptors (mGluRs) and cannabinoid receptor 1 (CB1) fail to induce Ca^{2+} signaling in POA GFAP-expressing cells. We next tested if astrocytic Ca^{2+} signaling could be evoked in brain slices containing the POA by candidate activators. First, we attempted to augment $[Ca^{2+}]_i$ in astrocytes by activation of metabotropic glutamatergic receptor 5 (mGluR5) using the agonist CHPG. Bath application of CHPG (300 μM) did not alter the AUC for calcium traces in brain slices compared to baseline readings regardless of sex (Fig. 3.1C and F; statistical parameters in Table 3.6). Similar responses were obtained when the group I and group II mGluR agonist ACPD (100 μM) was used (Fig. 3.1D and G; statistical parameters in Table 3.7). We next tested if activation of CB1 was sufficient to augment $[Ca^{2+}]_i$ in astrocytes. Bath application of the CB1 agonist WIN 55,212-2 (10 μM) did not alter AUC compared to baseline readings regardless of sex (Fig. 3.1E and H; statistical parameters in Table 3.8). These results demonstrate that POA astrocytes in adult male and diestrous female mice do not respond to glutamate and endocannabinoids with elevated $[Ca^{2+}]_i$.

The purines ATP and ADP induce Ca^{2+} signaling in POA GFAP-expressing cells, with P_2Y_1 partially mediating the response. The lack of response of POA astrocytes to endocannabinoids then led to the investigation of purinergic signaling as a potential mechanism of activation. Brain slices were perfused with ATP (500 μM) at a concentration previously shown to evoke Ca^{2+} signaling in cortical and hippocampal astrocytes *ex vivo*[368]. ATP significantly increased AUC in brain slices compared to baseline and this effect was reversible during washout levels. There were no sex differences in response to ATP (Fig. 3.2A and D; statistical parameters in Table 3.9).

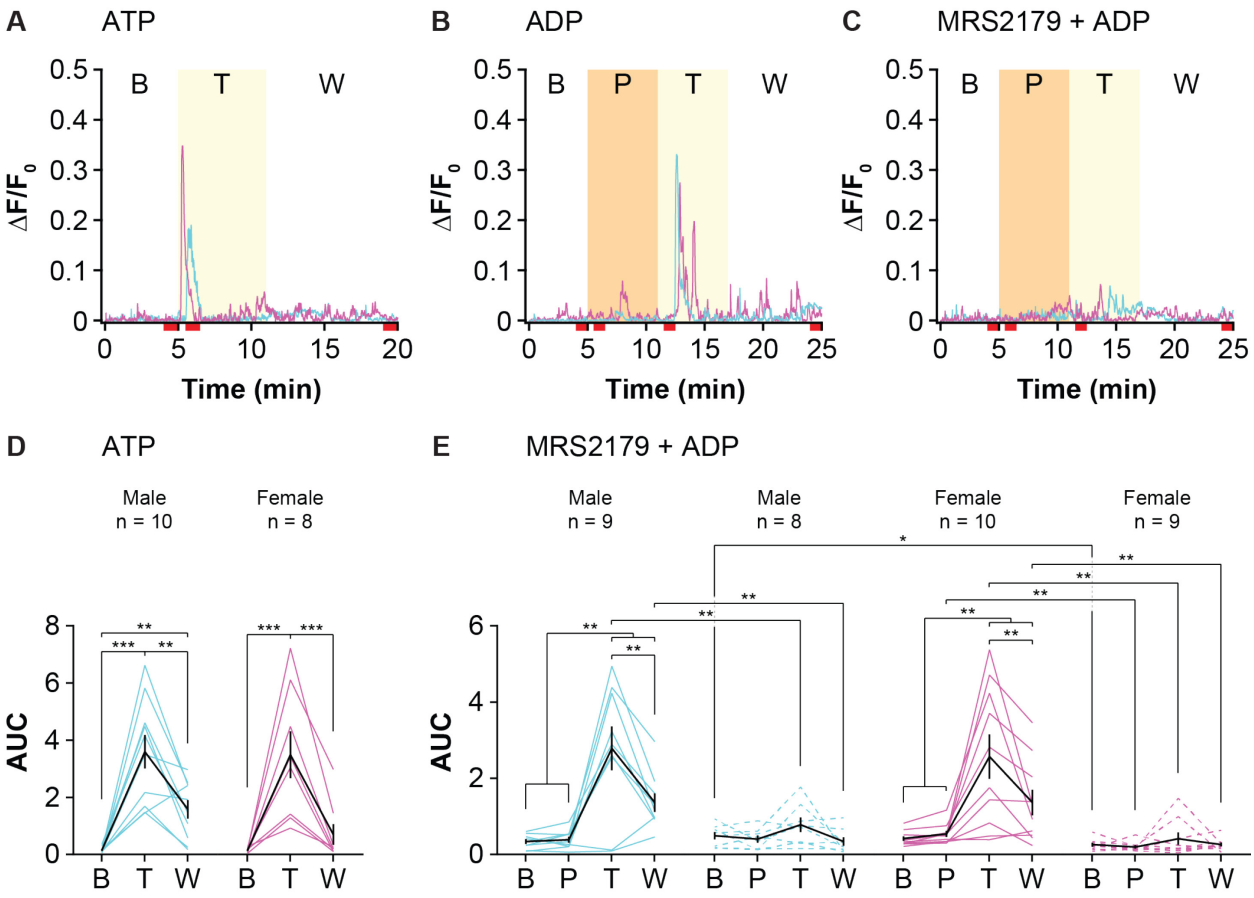


Figure 3.2: Purines ATP and ADP increase $[Ca^{2+}]_i$ in astrocytes, with the latter partially being mediated via P_2Y_1. **A-C,** Representative *ΔF/F₀* traces in brain slices from male (cyan) and diestrous female (magenta) mice injected with AAV5-GFAP-GCaMP6f. Red bars on the x-axis indicate the windows used for statistical comparison. B, baseline; T, treatment with agonist; W, washout. **D,** Quantification of AUC values in brain slices (cyan and magenta lines) overlaid with mean ± SEM (black lines; two-way mixed-model ANOVA with Sidak *poc hoc*; statistics are in Table 3.9). **E,** Quantification of AUC values in brain slices for vehicle-pretreated (solid cyan and magenta lines) and MRS2179-pretreated (dashed cyan and magenta lines) overlaid with mean ± SEM (three-way mixed-model ANOVA with Sidak *post hoc*; statistics are in Table 3.10). P, pretreatment with vehicle or MRS2179. * $p < 0.05$; ** $p < 0.01$; *** $p < 0.001$.

Because ATP serves as an agonist of both ionotropic P_2X and metabotropic P_2Y receptor classes, we next perfused brain slices with the P_2Y agonist ADP to attempt to isolate the mode of astrocytic activation. Bath application of ADP (500 μM) similarly increased AUC in brain slices compared to baseline and washout levels in both sexes, and no sex differences were detected (Fig. 3.2 B and E; statistical parameters in Table 3.10). Receptor subtypes P_2Y_1, P_2Y_6, and P_2Y_{12} are primarily activated by nucleoside diphosphates[369–371], and P_2Y_1 has been implicated in mediating astrocytic Ca^{2+}

signaling in various brain regions of rodents[372–374]. Thus, we next performed Ca^{2+} imaging on brain slices during which the P_2Y_1 antagonist MRS2179 (10 μM) was bath-applied before and during ADP treatment. The AUC levels during cotreatment with ADP and MRS2179 were significantly attenuated compared to levels observed in brain slices only treated with ADP in both males and females, and no sex differences in the response were measured except for baseline levels between the male and female antagonist groups (Fig. 3.2B, C, and E; statistical parameters in Table 3.10). Although not significant, a few brain slices from both males and females displayed increased AUC levels during ADP treatment in the presence of MRS2179 (Fig. 3.2E), indicating potentially the presence of other purinergic receptors being targeted by ADP. Nonetheless, these data indicate that purinergic signaling via P_2Y_1 is a mechanism by which Ca^{2+} signaling can be induced in POA astrocytes.

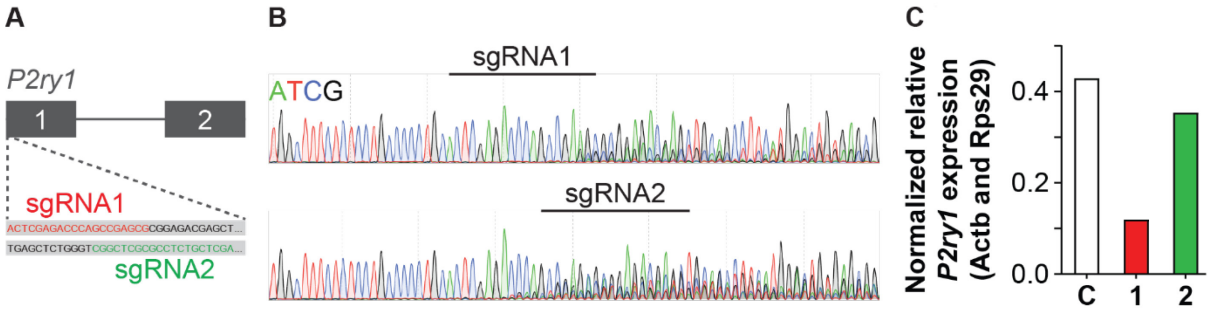


Figure 3.3: *In vitro* validation of *P2ry1* single guide RNAs. **A,** Depiction of sgRNAs targeting exon 1 of *P2ry1*. **B,** Sanger sequencing from BV2 cells transduced with lentivirus carrying sgRNAs targeting *P2ry1*. **C,** Relative *P2ry1* mRNA transcript expression from BV2 cells. C: control (no virus); 1, sgRNA1; 2, sgRNA2.

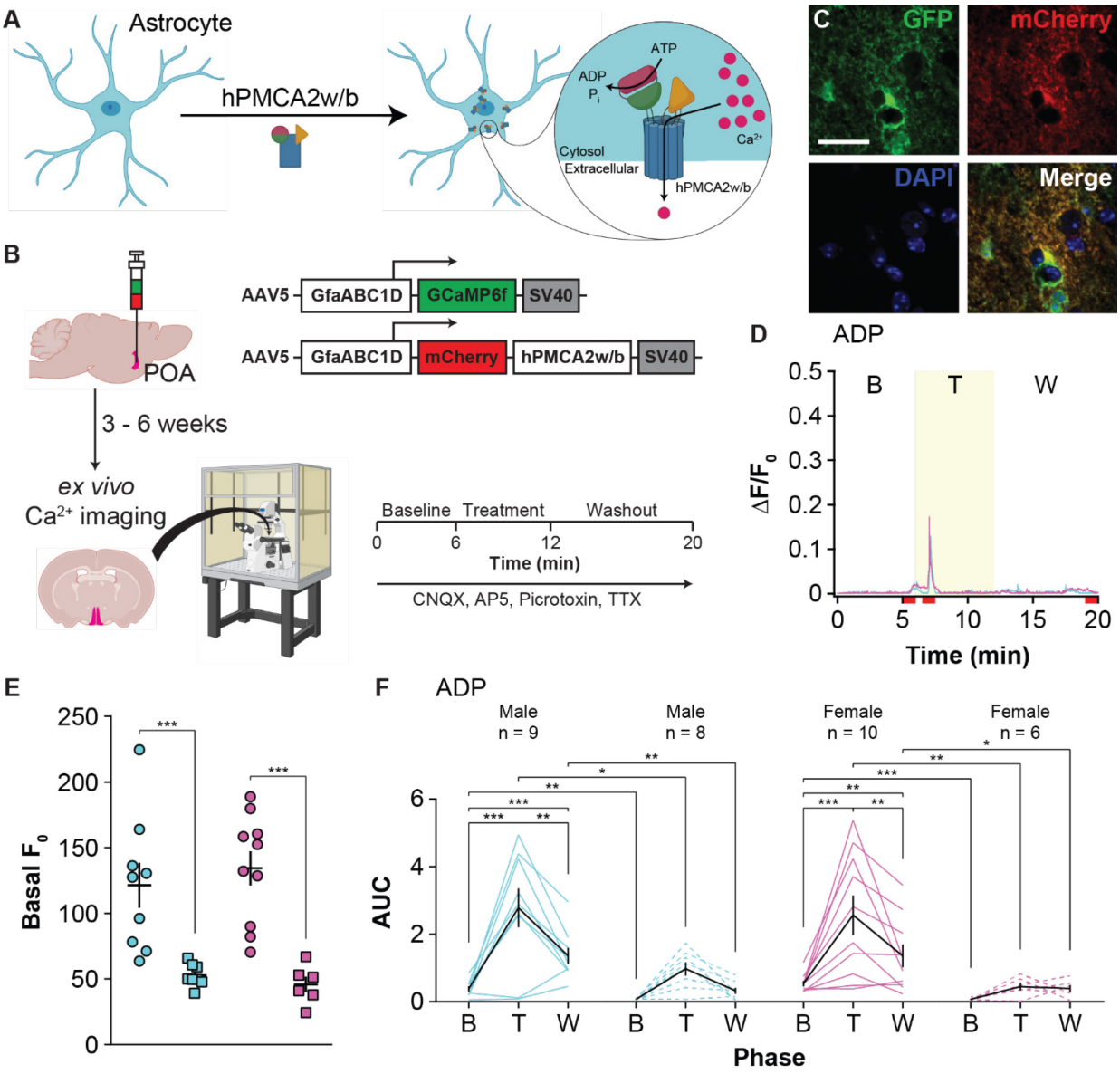


Figure 3.4: Reducing Ca^{2+} signaling in POA astrocytes with hPMCA2w/b. **A,** Schematic of hPMCA2w/b to reduce $[Ca^{2+}]_i$ in astrocytes. **B,** Paradigm for expressing AAV-GFAP-hPMCA2w/b with GCaMPf in POA astrocytes and subsequently recording Ca^{2+} signals. **C,** Representative dual immunofluorescent images of GFAP cells stained with GFP (for GCaMP6f) and mCherry (for hPMCA2w/b)to show colocalization of the two signals in POA-containing mouse brain sections. Scale bar: 20 µm. **D,** Representative *ΔF/F₀* traces in brain slices from male (cyan) and diestrous female (magenta) mice injected with AAV5-GFAP-GCaMP6f and AAV-GFAP-hPMCA2w/b. Red bars on the x-axis indicate the windows used for statistical comparison. B, baseline; T, treatment with agonist; W, washout. **E,** Quantification of F_0 values 10 s after start of *ex vivo* recordings in brain slices from males (cyan) and diestrous females (magenta) injected with only AAV-GFAP-CaMP6f (circles) or both viruses (squares) overlaid with mean ± SEM (black lines; two-way ANOVA with Sidak *post hoc*; statistics are in Table 3.11). **F,** Quantification of AUC values in brain slices from mice injected with only AAV-GFAP-CaMP6f (solid

cyan and magenta lines) or both viruses (dashed cyan and magenta lines) overlaid with mean ± SEM (black lines; three-way mixed model ANOVA with Sidak *post hoc*; statistics are in Table 3.12). * $p < 0.05$; ** $p < 0.01$; *** $p < 0.001$.

In vitro validation of synthetic guide RNAs (sgRNAs) for knock down of P2ry1 gene expression. With the identification of P_2Y_1 as an endogenous mediator of astrocytic Ca^{2+} signaling in the POA, our next goal was to utilize clustered, regularly interspaced, short palindromic repeats (CRISPR) and associated endonuclease (Cas9) to achieve spatial and temporal control over *P2ry1* knockdown. Two sgRNAs (sgRNA1 and sgRNA2) were designed to target exon 1 of *P2ry1* (Fig. 3.3A), which will enable Cas9-mediated double-stranded breaks resulting in frameshifting insertions and/or deletions (indels). These indels often result in gene disruption due to DNA repair errors during non-homologous end joining (NHEJ). The sgRNAs were individually subcloned into lentiCRISPRv2 puro plasmids. Following production of lentiviral particles from the plasmids, BV-2 cells were transduced and selected for using puromycin. BV-2 cells expressing either sgRNA exhibited peak-on-peak sequences, which are an indicator of gene disruption (Fig. 3.3B). Furthermore, preliminary quantification of *P2ry1* mRNA expression shows that sgRNA1 reduced expression by about 75% compared to control, while sgRNA2 was only about 15% effective (Fig. 3.3C). These *in vitro* data indicate that sgRNA1 is potentially a potent guide to knock down *P2ry1* expression, which will be addressed in ongoing experiments aiming at packaging the sgRNA into AAVs for *in vivo* study.

Ex vivo validation of Ca^{2+} signaling attenuation using hPMCA2w/b. While development of the CRISPR-Cas9 approach to knock down *P2ry1 in vivo* was underway, we tested another method of disrupting Ca^{2+} signaling in POA astrocytes. The human isoform type 2 plasma membrane Ca^{2+} pump PMCA lacking cytosolic interaction domains and expressing mCherry (hPMCA2w/b) was selected to attenuate Ca^{2+} signaling events. This pump is a Ca^{2+}-ATPase that constitutively extrudes Ca^{2+} from the cytosol into the extracellular space (Fig. 3.4A). hPMCA2w/b effectively reduces astrocytic Ca^{2+} signaling amplitudes and durations, and these changes are associated with modifications of grooming behavior and contextual memory[364,375].

To deliver hPMCA2w/b to the POA, it was packaged in an AAV driven by GFAP (AAV-GFAP-hPMCA2w/b) and stereotaxically injected along with AAV-GFAP-GCaMP6f (Fig.

3.4B). hPMCA2w/b expression overlapped with GCaMP6f signals in 94.1 ± 2.7% of POA astrocytes (n = 3 mice; Fig. 3.4C). *Ex vivo* Ca^{2+} signaling experiments revealed that hPMCA2w/b-expressing astrocytes exhibited reduced basal fluorescent intensity (F_0) compared to control slices in both sexes; this effect was not sexually differentiated (Fig. 3.4E; statistical parameters in Table 3.11). We next evaluated the efficacy of hPMCA2w/b in reducing ADP-evoked $[Ca^{2+}]_i$ elevations. hPMCA2w/b reduced ADP-induced rises in AUC levels compared to those in control slices in both sexes, and there were no sex differences in this effect (Fig. 3.4D and F; statistical parameters in Table 3.12). Perfusion with ADP still increased AUC levels in slices expressing hPMCA2w/b, confirming that the pump attenuates but does not abolish evoked Ca^{2+} signaling in astrocytes.

Reducing astrocytic Ca^{2+} signaling in the POA does not alter adult female estrous cyclicity. We next investigated if expression of hPMCA2w/b in POA astrocytes affected estrous cyclicity, which is a readily measurable marker of many reproductive functions in females. Cycles were monitored daily from 10 days before stereotaxic injections with either a control AAV (AAV-GFAP-mCherry) or AAV-GFAP-hPMCA2w/b until 8 weeks after surgery (Fig. 3.5A and B). Females expressing hPMCA2w/b did not exhibit disrupted cyclicity; these mice entered estrus, diestrus, and proestrus as frequencies similar to those observed in control females during the post-operative period (Fig. 3.5C, statistical parameters in Table 3.13). The frequency of entry into proestrus was also measured on a week-by-week basis, as a trend appeared wherein hPMCA2w/b-expressing females were transiently entering proestrus less frequently near weeks 3 and 4 (Fig. 3.5D). This effect was not significant at any week when corrections for multiple comparisons were used (Fig 3.5D, statistical parameters in Table 3.14). These results suggest that attenuation of Ca^{2+} signaling in POA astrocytes does not disrupt female reproductive cyclicity.

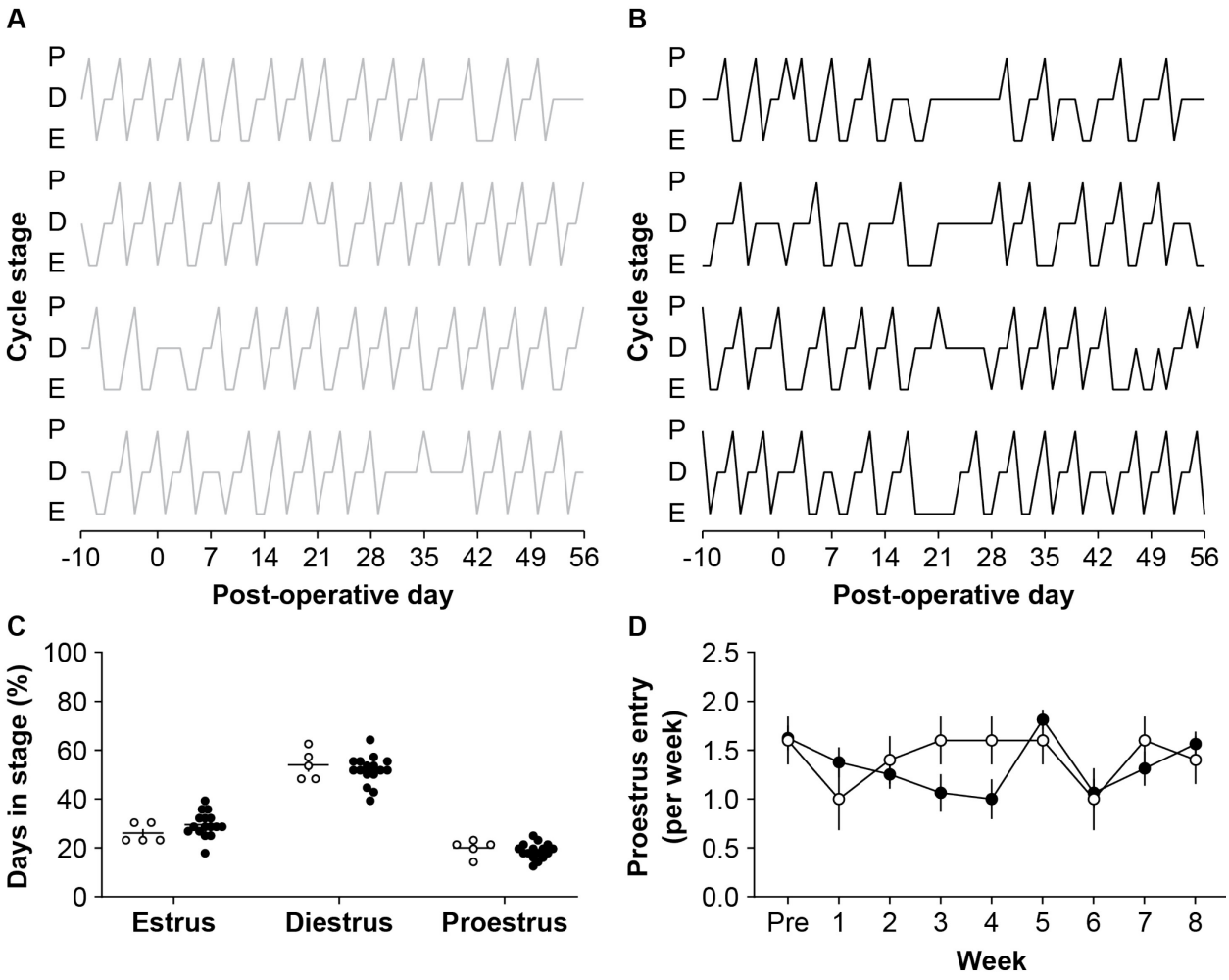


Figure 3.5: Attenuation of $[Ca^{2+}]_i$ in POA astrocytes fails to alter reproductive cyclicity in females. **A and B,** Representative reproductive cycles of female mice that received injections of AAV-GFAP-mCherry (A) or AAV-GFAP-hPMCA2w/b (B) in the POA. E, estrus; D, diestrus; P, proestrus. Day 0 is the day of stereotaxic surgery. **C,** Individual values of the percentage of days females injected with AAV-GFAP-mCherry (white circles) or AAV-GFAP-hPMCA2w/b (black circles) spend in each cycle stage overlaid with mean ± SEM (black lines; χ^2 test with adjusted Pearson standardized residuals; statistics are in Table 3.13). **D,** Weekly proestrus entry frequency by females injected with AAV-GFAP-mCherry (white circles) or AAV-GFAP-hPMCA2w/b (black circles; mean ± SEM; two-way mixed model ANOVA with Sidak *post hoc*, statistics are in Table 3.14).

Discussion

Astrocyte-neuron communication underlies numerous physiological functions including reproduction. Outbound signals from POA astrocytes such as PGE2 can directly modulate GnRH neuron activity, but less is understood about the endogenous activators of Ca^{2+} signaling events within astrocytes that initiate these signals. Here, we began to

elucidate the endogenous mechanisms of POA astrocyte stimulation utilizing *ex vivo* Ca^{2+} imaging.

Among the candidate Gq GPCR activators tested with Ca^{2+} imaging, neither mGluR agonists CHPG nor ACPD augmented astrocytic $[Ca^{2+}]_i$, indicating that these hypothalamic astrocytes do not directly receive glutamatergic signaling via Gq GPCRs in both sexes. This was initially a surprise, as there is extensive literature on the topic of mGluR5 activation leading to increased $[Ca^{2+}]_i$ *in situ* and *in vitro*[151,152,328,376–380]. The earliest work investigating astrocytic Ca^{2+} responses to neurotransmitters found glutamate as one of these activators[150]; this contributed to the development of the tripartite synapse model[144]. A purported role of astrocytes at synapses is the rapid uptake of neurotransmitters to mitigate excitatory post-synaptic transmission. Removal of glial coverage around the synaptic cleft increases excitatory transmission in the cerebellum[381], and it causes more glutamate spillover in the hippocampus[382]. GnRH neurons receive glutamatergic transmission, and the number of dendritic spines, which are indirect markers of glutamatergic inputs, is lower in juveniles rats compared to adults[383,384]. Conversely, transcriptomic data of murine forebrain astrocytes has shown that expression levels of the mGluR genes *Grm5* and *Grm1* decrease with age[172]. Given that most work investigating glutamatergic transmission as a method of glial activation has been performed using brain tissue harvested from juvenile rodents[150,385], this indicates that astrocytes in adults may display different signaling modalities. Indeed, astrocytes in mouse pup cortices are strongly activated by both ACPD and group I mGluR agonist DHPG *in vivo*, while the same astrocytes in adults are insensitive to these agonists[368].

A similar failure to evoke astrocytic Ca^{2+} signaling was observed using the CB1 agonist WIN 55,212-2. Endocannabinoids typically induce synaptic depression by reducing pre-synaptic neurotransmitter release[386]. This phenomenon is observed at GABAergic terminals apposed to GnRH neurons when the latter's depolarization causes transitory depression of GABAergic currents via endocannabinoid signaling[347]. Although originally thought to be solely expressed by neurons, CB1 is also expressed by hippocampal astrocytes and its activation induces astrocytic glutamate release[387]. Of note, inhibition

of COX activity with indomethacin reverses endocannabinoid-mediated suppression of GABAergic post-synaptic transmission to GnRH neurons[347].

The lack of POA astrocyte response to mGluR and, in particular, CB1 agonists raises the question whether these astrocytes and GnRH neurons engage in reciprocal communication, or if astrocytes are activated by other cell populations to alter GnRH neuron function in a linear, top-down communication pathway. In this regard, we performed pilot *ex vivo* Ca^{2+} imaging experiments using GnRH as a candidate activator, but it had no effect on astrocyte $[Ca^{2+}]_i$. Similarly, the neuropeptide kisspeptin, which is a strong activator of GnRH neurons, failed to induce Ca^{2+} signaling in POA astrocytes despite expression of the kisspeptin receptor transcript *Kiss1r* by these cells[388]. These early findings do not, however, exclude other mechanisms of neuron-glia bidirectional communication. For example, GnRH neuron terminals and both astrocytes and tanycytes exhibit remarkable plasticity at the median eminence. The homophilic and heterophilic interactions of cell-surface adhesion molecules like SynCAM1 and RPTPβ, respectively, contribute to the level of glial coverage of GnRH neuron terminals[303,389]. PGE2 synthesis is also induced by SynCAM1-mediated activation of astrocytic erbB4 receptors, and disruption of SynCAM1 delays puberty onset in female mice[390]. Further investigation is required to elucidate how elements of the GnRH neuronal network communication with proximal glia.

An encouraging finding was the augmentation of astrocytic $[Ca^{2+}]_i$ by the purines ATP and ADP to a similar extent in both sexes. These findings in the POA mirror those observed in response to ATP in cortical and hippocampal astrocytes in both juvenile and adult mice[368]. In fact, purinergic signaling is observed in nearly all non-neuronal tissues[391,392]. The ability of purines to activate a large and spatially heterogeneous population of glia, while glutamate and endocannabinoids fail, suggests purinergic signaling as a more common mode of communication among neuron-glia and glia-glia networks. The cellular responses to purinergic signaling are diverse on account of the numerous receptor subtypes between the P_1, P_2X, and P_2Y classes. For example, P_2Y_1 is an important signaling pathway in various neuropathologies. During brain injuries such as ischemia and hypoxia, ATP, among other compounds, is released by intact and

damaged cells into the extracellular space[393]. This recruits microglia to the injury site and induces astrocytes to undergo reactive astrogliosis[374], and microglial signaling through astrocytic P_2Y_1 regulates the level of scar formation. Interestingly, astrogliosis-like phenotypes can be mimicked by injection of P_2Y_1 agonists in rat brains[393]. Our findings indicate that ADP-evoked Ca^{2+} signaling events in brain slices are inhibited by pretreatment with P_2Y_1 antagonist MRS2179, which suggest that ADP signaling in POA astrocytes may be a prerequisite for glial response to various types of brain trauma in this region. Moreover, the utilization of hyperphysiologic concentrations of ATP and ADP to elicit Ca^{2+} signaling may further suggest that this mode of communication with POA astrocytes is normally engaged in neuropathological conditions. This will be addressed using the CRISPR-Cas9 approach to knock down *P2ry1* expression in POA astrocytes *in vivo* and measuring reproductive biometrics.

Data from the *in vivo* attenuation of astrocytic Ca^{2+} signaling via hPMCA2w/b suggests that POA astrocyte activity, regardless of the mechanism inducing Ca^{2+} signaling, is not necessary for female reproductive function. Females with attenuated POA astrocytic Ca^{2+} signaling did not dwell in any individual cycle stage at frequencies different to control females over the entire post-operative period. *Ex vivo* verification of Ca^{2+} attenuation in hPMCA2w/b-expressing brain slices, as well as previous studies utilizing the AAV[364,394], suggests that reduction of $[Ca^{2+}]_i$ in these astrocytes is insufficient to alter GnRH neuron function. There are caveats to these findings, however, as POA astrocytes engage in signal pathways that directly activate GnRH neurons including PGE2. One consideration that must be made is whether compensatory mechanisms are engaged following hPMCA2w/b expression in astrocytes. This idea is motivated by a trend, although not significant, that was observed during postoperative weeks 3 and 4 where female entry into proestrus in the hPMCA2w/b mice appeared blunted. Expression of transgenes via AAVs can be detected as early as 1 week following injections, and peak expression around week 3[395]. The correlation between typical peak expression and potential transient disruption in female cyclicity followed by normalization of cycle patterns lends credence to compensation, though a candidate mechanism for this is unknown. One explanation could be that hPMCA2w/b does not sufficiently decrease $[Ca^{2+}]_i$ in POA astrocytes enough to halt gliotransmitter synthesis

and signaling to GnRH neurons. Furthermore, potential compensatory signaling pathways can arise from these astrocytes themselves, whereby Ca^{2+}-independent release of gliotransmitters could be upregulated. For example, hemichannel connexin and purinergic receptor P_2X_7 are capable of releasing gliotransmitters glutamate and ATP in a Ca^{2+}-independent manner[188–194]. Expression of several different purinergic receptors could allow for self-sufficient mechanisms of ensuring POA astrocyte responsiveness to extracellular signals while also maintaining the capacity of gliotransmission even with blunted $[Ca^{2+}]_i$.

In conclusion, these findings indicate that purinergic signaling via P_2Y_1 is a mechanism of POA astrocyte activation in mice, which will inform future CRISPR-Cas9 methods to genetically block *P2ry1* expression. *In vivo* attenuation of $[Ca^{2+}]_i$ in these astrocytes failed to cause long-term disruption in female reproduction, which may be attributable to a lack of necessity of these glia in adult reproduction, or perhaps an insufficiency of hPMCA2w/b at mitigating astrocyte activation. Future work will aim to expand these findings by disrupting general astrocyte functionality in the POA.

Table 3.6: Statistical parameters from two-way mixed model ANOVA assessing the effect of CHPG on $[Ca^{2+}]_i$ in *ex vivo* POA astrocytes (Fig. 3.1F).

Property	Males	Diestrous females	
Brain slices (n)	7	6	
Mice (n)	5	6	
Two-way mixed model ANOVA			
Effect		Statistic	Partial η^2
Treatment period		$F_{(2,22)} = 1.413$, $p = 0.266$	0.114
Sex		$F_{(1,11)} = 0.078$, $p = 0.785$	0.007
Treatment period * Sex		$F_{(2,22)} = 1.403$, $p = 0.268$	0.113

Table 3.7: Statistical parameters from two-way mixed model ANOVA assessing the effect of ACPD on $[Ca^{2+}]_i$ in *ex vivo* POA astrocytes (Fig. 3.1G).

Property	Males	Diestrous females	
Brain slices (n)	7	7	
Mice (n)	5	4	
Two-way mixed model ANOVA			
Effect		Statistic	Partial η^2
Treatment period		$F_{(2,24)} = 0.830$, $p = 0.440$	0.065
Sex		$F_{(1,12)} = 0.076$, $p = 0.788$	0.006
Treatment period * Sex		$F_{(2,24)} = 2.404$, $p = 0.117$	0.167

Table 3.8: Statistical parameters from two-way mixed model ANOVA assessing the effect of WIN 55,212-2 on $[Ca^{2+}]_i$ in *ex vivo* POA astrocytes (Fig. 3.1H).

Property	Males	Diestrous females	
Brain slices (n)	7	5	
Mice (n)	3	3	
Two-way mixed model ANOVA			
Effect		Statistic	Partial η^2
Treatment period		$F_{(2,20)} = 0.715$, $p = 0.455$	0.067
Sex		$F_{(1,10)} = 4.093$, $p = 0.071$	0.290
Treatment period * Sex		$F_{(2,20)} = 0.220$, $p = 0.722$	0.022

Table 3.9: Statistical parameters from two-way mixed model ANOVA assessing the effect of ATP on $[Ca^{2+}]_i$ in *ex vivo* POA astrocytes (Fig. 3.2D).

Property	Males	Diestrous females	
Brain slices (n)	10	8	
Mice (n)	7	4	
Two-way mixed model ANOVA			
Effect		Statistic	Partial η^2
Treatment period		$F_{(2,32)} = 38.679$, $\mathbf{p < 0.001}$	0.707
Sex		$F_{(1,16)} = 0.574$, $p = 0.460$	0.035
Treatment period * Sex		$F_{(2,32)} = 0.717$, $p = 0.449$	0.043

Table 3.10: Statistical parameters from three-way mixed model ANOVA assessing the effect of ADP and the P_2Y_1 antagonist MRS2179 on $[Ca^{2+}]_i$ in *ex vivo* POA astrocytes (Fig. 3.2E).

Property	Males		Diestrous females	
	Vehicle + ADP	MRS2179 + ADP	Vehicle + ADP	MRS2179 + ADP
Brain slices (n)	9	8	10	9
Mice (n)	3	5	4	7
Three-way mixed model ANOVA				
Effect		Statistic		Partial η^2
Treatment period		$F_{(3,96)} = 27.325$, $\mathbf{p < 0.001}$		0.461
Sex		$F_{(1,32)} = 0.407$, $p = 0.528$		0.013
Pretreatment		$F_{(1,32)} = 23.687$, $\mathbf{p < 0.001}$		0.425
Treatment period * Sex		$F_{(3,96)} = 0.287$, $p = 0.680$		0.009
Treatment period * Pretreatment		$F_{(3,96)} = 17.804$, $\mathbf{p < 0.001}$		0.357
Sex * Pretreatment		$F_{(1,32)} = 0.445$, $p = 0.510$		0.014
Treatment period * Sex * Pretreatment		$F_{(3,96)} = 0.084$, $p = 0.861$		0.003

Table 3.11: Statistical parameters from two-way mixed model ANOVA assessing the effect of AAV-GFAP-hPMCA2w/b on basal F_0 levels in *ex vivo* POA astrocytes (Fig. 3.4E).

Property	Males		Diestrous females	
	No virus	AAV-GFAP-hPMCA2w/b	No virus	AAV-GFAP-hPMCA2w/b
Brain slices (n)	9	8	10	6
Mice (n)	3	3	4	3
Two-way mixed model ANOVA				
Effect		Statistic		Partial η^2
Sex		$F_{(3,29)} = 0.053$, $p = 0.820$		0.002
Virus		$F_{(3,29)} = 37.319$, $\mathbf{p < 0.001}$		0.563
Sex * Virus		$F_{(3,29)} = 0.608$, $p = 0.442$		0.021

Table 3.12: Statistical parameters from three-way mixed model ANOVA assessing the effect of AAV-GFAP-hPMCA2w/b on ADP-induced elevations in $[Ca^{2+}]_i$ in *ex vivo* POA astrocytes (Fig. 3.4F).

Property	Males		Diestrous females	
	No virus	AAV-GFAP-hPMCA2w/b	No virus	AAV-GFAP-hPMCA2w/b
Brain slices (n)	9	8	10	6
Mice (n)	3	3	4	3

Three-way mixed model ANOVA		
Effect	Statistic	Partial η^2
Treatment period	$F_{(2,58)}$ = 27.825, ***p* < 0.001**	0.490
Sex	$F_{(1,29)}$ = 0.130, p = 0.721	0.004
Virus	$F_{(1,29)}$ = 21.757, ***p* < 0.001**	0.429
Treatment period * Sex	$F_{(2,58)}$ = 0.810, p = 0.414	0.027
Treatment period * Virus	$F_{(2,58)}$ = 8.558, ***p* = 0.002**	0.228
Sex * Virus	$F_{(1,29)}$ = 0.077, p = 0.783	0.003
Treatment period * Sex * Virus	$F_{(2,58)}$ = 0.123, p = 0.815	0.004

Table 3.13: Statistical parameters from χ^2 test assessing the effect of AAV-GFAP-hPMCA2w/b on female mouse estrous cycle staging post-operatively (Fig.3.5C).

Property	Diestrous females	
	AAV-GFAP-mCherry	AAV-GFAP-mCherry + AAV-GFAP-hPMCA2w/b
Mice (n)	5	16

χ² Test				
Effect	Statistic	Estrus	Diestrus	Proestrus
		Adj. res. (p value)	Adj. res. (p value)	Adj. res. (p value)
Estrous cycle stage distribution	χ^2 (2, N = 1176) = 1.219, p = 0.544	-1.10 (0.271)	0.63 (0.528)	0.46 (0.645)

Adj. res.: Adjusted residual of hPMCA2w/b group

Table 3.14: Statistical parameters from two-way mixed model ANOVA assessing the effect of AAV-GFAP-hPMCA2w/b on frequency of entry into proestrus (Fig. 3.5D).

Property	Diestrous females	
	AAV-GFAP-mCherry	AAV-GFAP-mCherry + AAV-GFAP-hPMCA2w/b
Mice (n)	5	16

Two-way mixed model ANOVA		
Effect	Statistic	Partial η^2
Week	$F_{(8,152)}$ = 1.782, p = 0.085	0.086
Virus	$F_{(1,19)}$ = 0.534, p = 0.474	0.027
Week * Virus	$F_{(8,152)}$ = 1.168, p = 0.322	0.058

Chapter 4: Conclusion

Introduction

The field of reproductive neuroendocrinology emerged following centuries of parallel investigations into the origin of internal secretions and the nature of nervous tissue. The pioneering 1849 gonadal transplantation study by Arnold Berthold is widely considered the start of endocrinology. Despite the slow initial pace, the field has seen tremendous growth over the last 50 years ever since the sequencing of the GnRH decapeptide. Glial research arguably mirrors the recent advances in reproductive neuroendocrinology, as the development of fluorescent imaging techniques in the latter half of the 20th century has allowed for the characterization of glial activation through the observation of Ca^{2+} signaling. The work outlined in this dissertation aimed to add to the understanding of how glia contribute to reproductive function by determine if sex, estrous cycle stage, or time-of-day-dependent factors altered astrocyte communication with elements of the GnRH neuronal network. This work also interrogated what endogenous mechanisms of Ca^{2+} signaling were present in POA astrocytes, and if disruption of Ca^{2+} signaling can alter *in vivo* reproductive function in mice.

Astrocyte Regulation of the HPG Axis is Modified by Sex-Dependent Factors and the Heterogeneous Regulatory Capacity of Different Astrocyte Populations

The initial goal of this dissertation work was to assess the extent to which factors including sex, time of day, hormonal state, and brain region informed how astrocytes and elements of the HPG axis communicate, if at all. The investigation of these factors was initially motivated by previous work in our lab[288]. Similar to the work in this dissertation, Vanacker and colleagues manipulated astrocytic Ca^{2+} dynamics by virally expressing excitatory Gq DREADDs in POA and ARC GFAP-expressing cells[288]. A considerable amount of the findings pertained to males; activation of Gq signaling in

POA astrocytes increased both GnRH neuron firing rate and LH release. ARC astrocyte activation did not stimulate KNDy neurons. The induced GnRH neuron firing, moreover, appeared to be, in part, dependent upon PGE2-mediated signaling, as inhibiting EP1 and EP2 reduced CNO-induced GnRH neuron firing. Strikingly, limited data collected from diestrous females indicated that activation of Gq signaling in POA astrocytes failed to cause GnRH neuron firing, but LH release did increase. Technical concerns stemming from prolonged (>18 weeks) induction time in females because of the COVID pandemic shutdown reduces confidence in this work. Further, the effect of ARC astrocytes activation on KNDy neuron firing was not assessed in females. These results raised questions as to the nature of astrocyte communication with the reproductive neuroendocrine axis, particularly regarding potential sex differences. We hypothesized that the sex of the mouse and the location of these astrocytes inform glial regulation of the GnRH neuronal network.

Consistent with the previous work, we found that activation of ARC astrocytes via Gq signaling did not change proximal KNDy neuron firing in males or in diestrous females. Astrocytic Ca^{2+} signaling was verified to be induced following Ca^{2+} imaging recordings in the ARC, as well as the POA, and the effect of CNO treatment on $[Ca^{2+}]_i$ mirrors induced Ca^{2+} transients seen in other brain regions[327–330]. Thus, the lack of response by KNDy neurons is likely caused by an absence of astrocyte-KNDy neuron signaling. Consistent with this, *ex vivo* administration of the prostaglandin analog dmPGE2 failed to stimulate KNDy neurons regardless of sex. These data suggest that astrocyte communication via PGE2 with the GnRH neuronal network is not directed at the putative GnRH/LH “pulse generator” postulated to reside in KNDy neurons. Of note, these findings do not exclude one-way kisspeptin neuron communication with astrocytes. POA and ARC astrocytes express kisspeptin receptor gene *Kiss1r*, and knockout of *Kiss1r* in GFAP-expressing cells altered astrocyte-GnRH-neuron appositions and potentially disrupted LH secretion patterns[388]. In preliminary *ex vivo* Ca^{2+} imaging recordings performed on GCaMP6f-expressing POA and ARC astrocytes, kisspeptin failed to significantly increase $[Ca^{2+}]_i$, though only a few slices were measured and a concentration curve for kisspeptin was not established. More work

needs to be conducted to elucidate astrocytes as a potential relay for kisspeptin neuron communication with GnRH neurons.

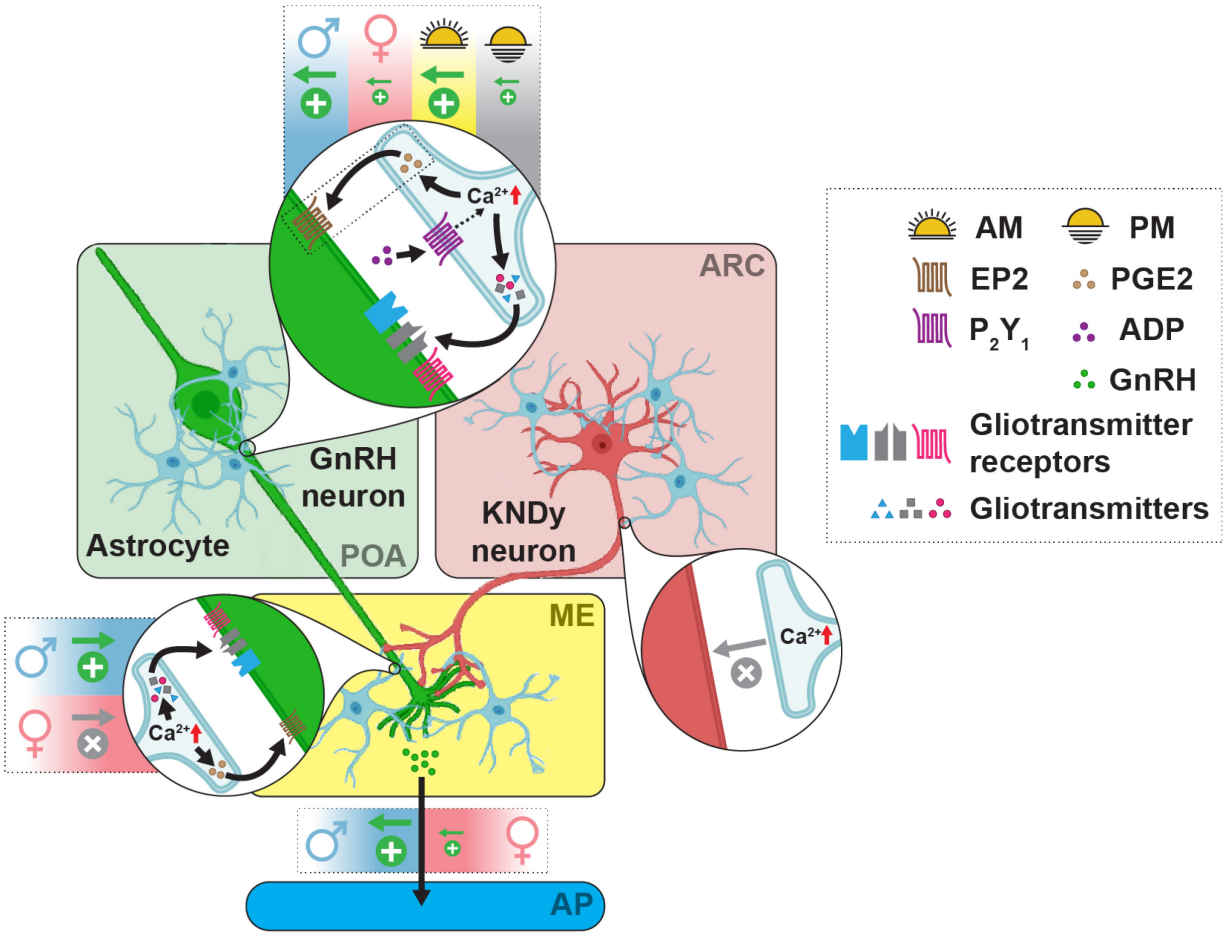


Figure 4.1: Working model of astrocyte contribution to the central reproductive neural circuit in male and diestrous female mice. POA astrocytes communicate with GnRH neurons through, in part, PGE2 signaling in a sex-dependent and time-of-day-dependent manner. Other gliotransmitter likely contribute, although their identity is unknown. While P_2Y_1 is sufficient to induce Ca^{2+} signaling in POA astrocytes, whether this is a pathway for gliotransmitter release is unknown. Astrocytes in the median eminence likely signal to GnRH neurons in males but not diestrous females. ARC astrocytes do not appear to directly communicate with KNDy neurons via gliotransmission. ME, median eminence; AP, anterior pituitary.

Interestingly, we found that activating Gq signaling in POA astrocytes increased GnRH neuron firing in both males and diestrous females, contrary to prior findings[288]. *In vivo* activation of Gq signaling in POA astrocytes also increased LH secretion in both males and diestrous females, which harmonized with the results from the *ex vivo* GnRH neuron recordings in the present work. The sex differences previously observed cannot

be ascribed to sex differences in glial Gq signaling properties in the DREADD model, as the current work found that activation of Gq signaling can successfully increase $[Ca^{2+}]_i$ in both males and diestrous females. Rather, the present work supports the concerns regarding prolonged viral transduction in females, which were studied 18-22 weeks following stereotaxic injections versus 3-6 weeks in males. The ability to exclude brain slices from analysis heavily relied on visual observation of DREADD-expressing cells exhibiting neuronal morphology, which is a criteria that was not applied to the *in vivo* LH assays. It is unknown whether prolonged incubation of AAV increases off-target expression of DREADDs. Related to this, AAVs are a valuable tool for gene delivery on account of their remarkable stability in varying environmental conditions including temperature, pH, and medium of storage[396]. Their infectiousness remains nearly unchanged after several months even at room temperature[396], which may permit for continued ectopic neuronal expression in longer experimental timelines. More investigation is required to determine the discrepancy in these findings.

In the present work, the increase in LH secretion upon glial activation was sexually differentiated despite similar GnRH neuron firing responses between sexes. Specifically, LH release in males was greater and more rapid than in diestrous females. Determining at what level – the anterior pituitary and/or the hypothalamus – this sex difference contributes to the present findings is challenging, although a central component is at least likely. Previous *in vitro* an *in vivo* studies have investigated the effect of gonadectomy on LH release in rodents; both LH secretion from pituitary explants and serum LH levels from gonadectomized males are considerably elevated compared to females, mirroring the present findings[338,340,341]. One appealing explanation for these findings points to intrinsic sex differences in the anterior pituitary. Gonadectomy is reported to increase GnRH receptor expression in gonadotropes in males, but not females[397]. However, it's important to note that administration of GnRH at physiologic frequencies and amplitudes *in vitro* or *in vivo* still does not cause greater LH release in males compared to females[340,341]. Although it has been reported that LH content in the pituitary is similar between sexes[338], other studies report a slightly higher LH content in males[398]. Lastly, studies utilizing single-cell RNA sequencing (scRNA-seq) on mouse anterior pituitary tissue have also found sex differences in cell-type diversity and

functionality within the context of reproduction[399,400]. For example, the gene *Spp1*, which encodes for a protein that is involved in the GnRH signaling pathway, was slightly enriched in a cluster of male pituitary cells compared to females[399].

Another explanation for the sex differences in LH release in the present work includes upstream factors in the hypothalamus. One potential mechanism may involve intrinsic sex differences in GnRH neurons. A study using enzyme-linked immunosorbent assay (ELISA) to measure murine releasing hormone content in hypothalamic tissue homogenate found GnRH content to be about 2.5-fold higher in males compared to females, though the cycle stage of the females was not reported[401]. GnRH neurons may also be differentially activated by afferent signals. In the present work, extracellular recordings conducted on GnRH neurons treated with dmPGE2 resulted in reliable increases in GnRH neuron firing in males, while the diestrous female responses were not as great at the same concentration of dmPGE2; firing rates in females were recapitulated with a 5-fold increase in dmPGE2 concentration. This indicates that there may be a difference in sensitivity of GnRH neurons to PGE2.

We further pursued this question regarding GnRH neuron sensitivity to gliotransmitters after making the observations that Gq signaling activation in ARC astrocytes induces LH release in males but not diestrous females. These results were a surprise given that KNDy neurons are unresponsive to ARC astrocyte activation regardless of sex. No viral expression was found to spill over into the POA in either sex, indicating that the astrocyte action was likely directed at local reproductive circuits in and near the ARC. This is in line with previous findings indicating that GnRH neurons located outside of the DREADD expression region do not respond to CNO-induced astrocyte activation *ex vivo*[288]. We hypothesized that KNDy neurons do not relay this astrocytic signaling through action-potential-independent mechanisms, which have been observed in GnRH and magnocellular neurons[349,350]. Targeted viral ablation of KNDy neurons in males did not reduce the rise in LH following ARC astrocyte activation. These data suggest that astrocytes in the ARC activate GnRH neurons through KNDy-neuron-independent circuits in a sex-dependent manner.

Direct stimulation of GnRH neuron terminals is thus an appealing mechanism for ARC astrocyte regulation of the male reproductive circuit. Kisspeptin and glutamate are capable of directly activating GnRH neurons through their terminals[402,403]. Moreover, glia including astrocytes and tanycytes form appositions with GnRH neuron soma and terminals as they descend to the median eminence[264,280,303,404]. Viral expression of DREADDs in the present work was observed to spread into the median eminence, opening the possibility of glia to induce GnRH release in males. Indeed, PGE2 is secreted from rodent median eminence explants in both males and females, and this is sufficient to stimulate GnRH release[213,231,351]. Whether GnRH neurons release more GnRH in males in the presence of PGE2, however, is unknown. Given the possibility that higher amplitudes of GnRH secretion in males may explain the LH sex differences observed in the present work, it is imperative that future directions quantify GnRH secretion in males and diestrous females following astrocyte-mediated GnRH neuron activation. Our lab has successfully adapted fast scan cyclic voltammetry (FSCV), which is a technology that permits the detection of electrochemically active molecules[405], to quantify the amount of GnRH released in brain slices containing the median eminence[406]. Implementation of FSCV could elucidate intrinsic sex differences in GnRH release following PGE2 action.

An important factor regarding the ability of astrocytes to stimulate GnRH neuron terminals includes sexual differences in both synaptic patterning and glia-neuronal architecture in the ARC and POA. For context, the sexually idiosyncratic maturation of reproductive circuits in the ARC and POA primarily depends upon timely peri- and postnatal exposure to gonadal steroids[270,336,407–409]. Perinatal exposure to testosterone in male rats increases GFAP expression, astrocyte process length, and the frequency of fully differentiated astrocytes. This increases the level of glial ensheathment of ARC neurons as well as decreases dendritic spine density[264,335]. The greater contact between these astrocytes and ARC neuronal elements in males could permit more efficient PGE2 action on GnRH neuron terminals. This is also applicable to the POA. Astrocytes in males exhibit greater morphological complexity compared to females[270,276], which may explain the greater LH release observed in males following Gq signaling activation in POA astrocytes compared to diestrous females.

The influence of sex steroids on the structural relationship between glial processes and the reproductive circuit was a contributing factor behind our decision to include proestrous females as an experimental group[410,411]. Tanycytes exhibit remarkable plasticity, and their level of ensheathment of GnRH neuron terminals changes as a function of circulating estradiol levels[412]. Elevated estradiol levels, such as during the GnRH/LH surge, cause tanycyte endfeet to retract, increasing the interface of GnRH neuron terminals with the pericapillary space and, ostensibly, allowing more GnRH to reach the pituitary portal vasculature[278]. Interestingly, we found that extracellular recordings of GnRH neurons following activation of Gq signaling in POA astrocytes did not differ between proestrous and diestrous females, although this is not a direct measure of GnRH release. The presence of the LH surge in the afternoon of proestrous females prevented them from being included in the LH assays, so it is difficult to ascertain if elevated estradiol levels in these mice facilitates greater glia-mediated GnRH/LH release.

Although both gonadal steroids and PGE2 are critical for early developmental maturation of the reproductive circuit, it remains poorly understood to what physiological extent these steroids modulate glia-to-GnRH-neuron PGE2 signaling in adult mice. Future studies can continue the *ex vivo* recordings measuring the effect of dmPGE2 on GnRH neuron firing in brain slices from proestrus females. Additionally, future work can utilize both OVX and OVX+E mouse models to interrogate whether alteration of the native steroid environment modifies downstream GnRH neuron responsiveness to either dmPGE2 or astrocyte activation via Gq-DREADD-induced signaling compared to diestrus. The OVX+E model is particularly interesting to investigate this question; while OVX females exhibit higher LH pulse frequencies and amplitudes compared to intact diestrous females due to loss of negative feedback, OVX+E recapitulates the pulse frequency to a comparable level seen in diestrus, but the LH release amplitude remains augmented[413].

Despite the insights gained pertaining to the sexual differentiation and regional specificity in astrocyte regulation of the central reproductive circuit, the mechanisms that underlie these differences are still poorly understood. It is only speculated from the

findings in the present study that GnRH neurons in males exhibit greater sensitivity to PGE2 signaling compared to diestrous females. In addition, the present findings suggest that sex differences in LH secretion may be caused, in part, by intrinsic differences in gonadotropic and/or GnRH neuron function. A promising way to distinguish the phenotype of a cell, as well as determining potential variation in gene expression profiles, is by sequencing mRNAs associated with ribosomes. We have piloted an experiment utilizing this method, called translating ribosome affinity purification (TRAP)[414], to isolate mRNAs from GFAP-expressing cells. To do so, GFAP-Cre mice were crossed with the Cre-dependent enhanced-GFP-fused ribosomal protein subunit L10a (EGFP-L10a) mouse line. Hypothalamic tissue punches from these GFAP-Cre::EGFP-L10a progeny were then processed for TRAP. Importantly, tissue was collected from both males and diestrous females, and collection was done in the morning (AM) or afternoon (PM). Though we have yet to follow up with these isolated mRNAs from GFAP-expressing cells, we have identified numerous promising genetic markers that may underlie the sex differences observed. Markers considered for qPCR include the COX1 and 2 genes *Ptgs1* and *Ptgs2*, respectively, the P_2Y_1 gene *P2ry1*, and both the androgen and estradiol α receptor genes *Ar* and *Esr1*, respectively. Finally, this methodology can also be applied to gonadotropes by crossing the EGFP-L10a mice with a GnRH receptor Cre line (GnRHR-Cre) to assess potential sex differences in response to GnRH at the level of the pituitary.

Finally, a major gap in knowledge left in the present work questions the role of AVPV astrocytes in regulating the reproductive circuit. Kisspeptin neurons in the AVPV are the primary mediator of sex steroid positive feedback, which initiates the GnRH/LH surge[415]. Although activation of Gq signaling in ARC astrocytes failed to induce KNDy neuron firing in proestrous females, a more apt assessment of the effects of elevated estradiol levels on glial-neuron communication would interrogate AVPV astrocyte signaling to kisspeptin neurons. Some studies already suggest that AVPV astrocytes are capable of synthesizing neuroprogesterone, which acts directly on kisspeptin neurons to drive the LH surge and ovulation[416–418]. Given the close proximity of the AVPV to the POA, future work can also assess whether astrocytes in the former region also directly communicate with GnRH neurons via PGE2.

Diurnal Factors Appear to Influence Gliotransmission Action on GnRH Neurons

In Chapter 2, the main findings indicated that potent sex differences underlie astrocyte communication with the GnRH neuronal network, and that POA astrocytes are primarily poised to modulate this reproductive circuit. It is also important to note that diurnal effects were measured in various experiments. CNO-induced $[Ca^{2+}]_i$ were deemed to be slightly elevated in males compared to females only in the PM. dmPGE2-induced GnRH neuron firing rates increased in the AM and PM for males, but only in the PM for diestrous females. Critically, when CNO-induced GnRH neuron firing was recorded *ex vivo* in the presence of EP1 and EP2 antagonists, firing rates were attenuated in the AM, but not in the PM. These data indicate that gliotransmission, particularly PGE2 signaling, is likely temporally regulated.

Similar to the future work proposed to interrogate the underlying sex differences in astrocytes, we designed the TRAP pilot study with diurnal regulation in mind. Male and diestrous female hypothalamic tissue were harvested at AM and PM timepoints to determine if key genetic markers for putative gliotransmitter synthesis pathways experienced diurnal fluctuations in expression among GFAP-expressing cells. Candidate markers included genes for glutamate transmission *Vglut2*, GABA transporter VIAAT *Slc32a1*, *Ptgs1*, *Ptgs2*, and *Gfap*. The density of GFAP immunoreactivity in the suprachiasmatic nucleus (SCN) and around it, including near the 3rd ventricle, was found to decrease in the PM in OVX and OVX+E females compared to the AM[419]. The SCN nuclei send efferent projections to numerous brain regions including the POA, AVPV, and ARC[420]. Of note, SCN astrocytes exhibit circadian rhythms of $[Ca^{2+}]_i$, and they regulate local glutamatergic transmission via glutamate uptake[421]. These results suggest that glia in the rostral hypothalamus could be important for linking circadian rhythms with sexual differences in the intrinsic properties of various elements of the HPG axis.

Currently, the strongest evidence in the literature that points to diurnal factors as a contributor to glial regulation of the reproductive circuit is morphological plasticity of astrocytes and tanycytes varying as a function of daily estradiol levels in

females[264,285,342]. TRAP sequencing can be further leveraged to determine the putative expression pattern of steroid receptor genes *Ar* and *Esr1* in GFAP-expressing cells at different cycle stages. Less is known, however, about the interaction between sex steroids and diurnal factors that underlie glial regulation of the reproductive circuit in males. Tanycytes in males are known to contact parvocellular neuron terminals[352], though to what extent they dynamically impact GnRH neuron access to the portal blood vasculature, if at all, is unknown. One study does provide promising insight into this question; male, diestrous female, and androgenized female rats were given intravenous injections of saline or GnRH and were divided into three subgroups[398]. Injections were given to a subgroup at either 8 a.m., 4 p.m., or 12 a.m., and serum LH levels were measured 20 min post injection. Interestingly, GnRH-induced LH levels were noticeably lower in males and both female groups at 4 p.m. and 12 a.m. compared to induced LH levels at 8 a.m. This suggests that whatever diurnal factors that regulate glial interaction with the reproductive neuronal circuit in females is likely similar in males.

Purines, but not Glutamate or Endocannabinoid Signaling, Activate POA Astrocytes, Though Underlying Ca^{2+} Signaling is not Necessarily Important for Female Reproduction

The mGluR agonists ACPD and CHPG, as well as endocannabinoid agonist WIN 55,212-2, did not induce increases in POA astrocyte $[Ca^{2+}]_i$ *ex vivo.* The lack of mGluR response is likely due to the developmental regulation of mGluR1 and 5 transcripts *Grm1* and *Grm5*, respectively. Specifically, cortical and hippocampal astrocytes exhibit high expression of *Grm1* and *Grm5* prepubertally, particularly up to postnatal week 1, but this drops off afterwards[368]. Interestingly, the narrow window of mGluR expression in the rodent brain also coincides with important prenatal and prepubertal postnatal developmental milestones, including astrogenesis, in the hypothalamus[422]. During the prepubertal postnatal period, hypothalamic astrocytes experience rapid proliferation from their progenitors, which include radial glial cells, tanaycytes – themselves derived from radial glial cells – as well as through self-differentiation[423,424]. GnRH neurons recruit nearby astrocytes via prostaglandin D_2 (PGD2) signaling during astrogenesis within the first 2 weeks of postnatal life, and these astrocytes remain associated with

GnRH neurons into adulthood[425]. Moreover, astrogenesis is important for timely sexual maturation, as disrupting PGD2 receptor 1 (DP1) signaling in the POA slightly disrupts estrous cyclicity[425]. *In vitro* and *ex vivo* recordings have shown that glutamate spillover from active synapses stimulates astrocytic production of PGE2, which in turn activates GnRH neurons[200,426]. Taken together, these findings suggest that glutamate signaling may be an important component underlying astrogenesis and the eventual maturation of the GnRH neuronal network.

Both ATP and ADP emerged from our work as candidate activators of Ca^{2+} signaling pathways in POA astrocytes regardless of sex. Moreover, antagonizing the purinergic receptor P_2Y_1 reduced the ADP-induced increase in astrocytic $[Ca^{2+}]_i$. Although the AUC levels during ADP + MRS2179 cotreatment did not significantly differ from baseline levels, a couple of slices from each sex did increase in fluorescence. Given the broad diversity in purinergic receptor subtypes, it is possible other purinergic signaling pathways, including P_2Y_1, are being engaged to activate POA astrocytes, though the identity of these subtypes is incompletely understood. *In situ hybridization* has found mRNA expression of both P_2X_4 and P_2X_6 in the POA, though which cells express these purinergic receptor subtypes in unknown[427]. Interrogating these other receptor subtypes through *ex vivo* Ca^{2+} imaging will elucidate the purinergic signaling pathways that activate POA astrocytes. It is critical that as many astrocytic endogenous signaling pathways are identified, as failing to knockout enough of these mechanisms may lead to unaltered reproductive function following *in vivo* CRISPR-Cas9 deletion of known candidate receptors.

The lack of long-term reproductive changes observed with hPMCA2w/b expression targeted to astrocytes has several caveats, and these may be addressed by utilizing other experimental methods to elucidate the necessity of these astrocytes. If POA astrocytes engage in both Ca^{2+}-dependent and Ca^{2+}-independent mechanisms of activation, then targeted ablation of these glia can address their contribution to the GnRH neuronal network *in vivo*; one method may include the targeted expression of the apoptosis driver caspase 3 in GFAP-expressing cells within the POA. A caveat to this method, however, is that other physiological behaviors derived from the hypothalamus

that rely on glial regulatory input may also be compromised. For example, both body weight homeostasis and thermal regulation have neuronal circuits that, in part, reside in the POA[428]. Ablation of proximal glia may thus confound any potential disruptions seen in reproductive function, as metabolic state and reproductive maturation are intertwined[429,430].

Another consideration of the hPMCA2w/b study is that the importance of astrocyte regulation of reproductive function may change across development. Although activation of astrocytic signaling pathways involving erbB1 and erbB4, which stimulate PGE2 synthesis, appear necessary for timely puberty onset and normal reproductive capacity during early adulthood in female mice, these females are still fertile albeit with a propensity to conceive smaller litters[243,246]. This is in mirrored contrast with the kisspeptin neuronal populations, where deletion of *Kiss1* in mice causes stark infertility in adults[90,431]. Of note, both GnRH neuron migration from the nasal placode to the hypothalamus and pubertal onset are unaffected in these knockouts[431,432]. Given the importance of the recruitment of astrocyte progenitors during early developmental GnRH neuron migration[425], it is possible glia have a prominent role in regulating the HPG axis early in development up until puberty. Although glia play a crucial role in regulating GnRH neuron terminal access to portal blood vasculature at the median eminence, their role throughout adulthood may mostly be supplanted by other GnRH neuron afferents including kisspeptin-expressing neurons[433]. Interrogation of this hypothesis could be done by targeted Ca^{2+} attenuation or ablation of POA astrocytes in prepubertal mice, though there are technical limitations to accurate localization of AAVs in juveniles that need to be addressed.

EP2 Signaling as a Contributing Mechanism behind Female Reproductive Maturation

Extensive work has shown that PGE2 signaling activates GnRH neurons, even in adults. Prevot and colleagues showed that GnRH neurons are potently stimulated by PGE2 *ex vivo*, and this effect is directly exerted via EP2-G_S-cAMP/PKA signal transduction[287]. Given the abundance of data showing that blocking PGE2 signaling at

the level of astrocytes can disrupt reproductive parameters, we began a pilot experiment to develop a transgenic mouse model investigating the effect of knocking down EP2 expression in GnRH-expressing cells. To generate this model, we crossed $EP2^{fl/fl}$ mice (generous gift of Dr. Katrin Andreasson, Stanford University) with a GnRH-Cre mouse line to generate F1 single-floxed heterozygous progeny ($GnRH\text{-}Cre^{+/-}$::$EP2^{fl/+}$). The F1 were back-crossed with $EP2^{fl/fl}$ mice to generate a proportion of the double-floxed homozygous EP2 knockout ($GnRH\text{-}Cre^{+/-}$::$EP2^{fl/fl}$). Following weaning, mice from these crossings, including littermate controls, underwent daily observation for pubertal onset (vaginal opening in females, and preputial separation in males). Pubertal onset occurred approximately on postnatal days 31 and 34 in male and female littermate controls, respectively (Fig. 4.1A and B). Neither heterozygous nor homozygous males exhibited differences in preputial separation compared to littermate controls (Fig. 4.1A; statistical parameters in Table 4.1). In contrast, both female heterozygotes and homozygotes reached puberty several days after littermate controls (Fig. 4.1B; statistical parameters in Table 4.2). The body mass upon pubertal separation did not differ between controls and both mutant groups regardless of sex (Fig. 4.1C and D; statistical parameters in Tables 4.3 and 4.4).

The delay in vaginal opening among $GnRH\text{-}Cre^{+/-}$::$EP2^{fl/+}$ and $GnRH\text{-}Cre^{+/-}$::$EP2^{fl/fl}$ mice is consistent with previous work investigating the effect of disrupting astrocytic PGE2 signaling on puberty onset in female rodents. Importantly, both $GnRH\text{-}Cre^{+/-}$::$EP2^{fl/+}$ and $GnRH\text{-}Cre^{+/-}$::$EP2^{fl/fl}$ female groups had smaller body masses compared to littermate controls at the time of vaginal opening. Both body mass and food intake are important in timely puberty onset and day of first estrus in female rodents[434]. Fatty acid deficiency not only delays vaginal opening in female rats, but it also causes puberty to occur at a lower body mass[228]. Conversely, erbB signaling disruption in astrocytes does not reduce body mass in mice during the peripubertal stage compared to wild type controls[246]. It is thus possible that growth deficits pose a confound to our observations of delayed female puberty onset. This could be addressed by daily measurements of both body mass and food consumption in these mutants. Other future works could investigate whether leptin signaling, which is implicated in both energy homeostasis and reproduction[435], is altered in these EP2 knockouts.

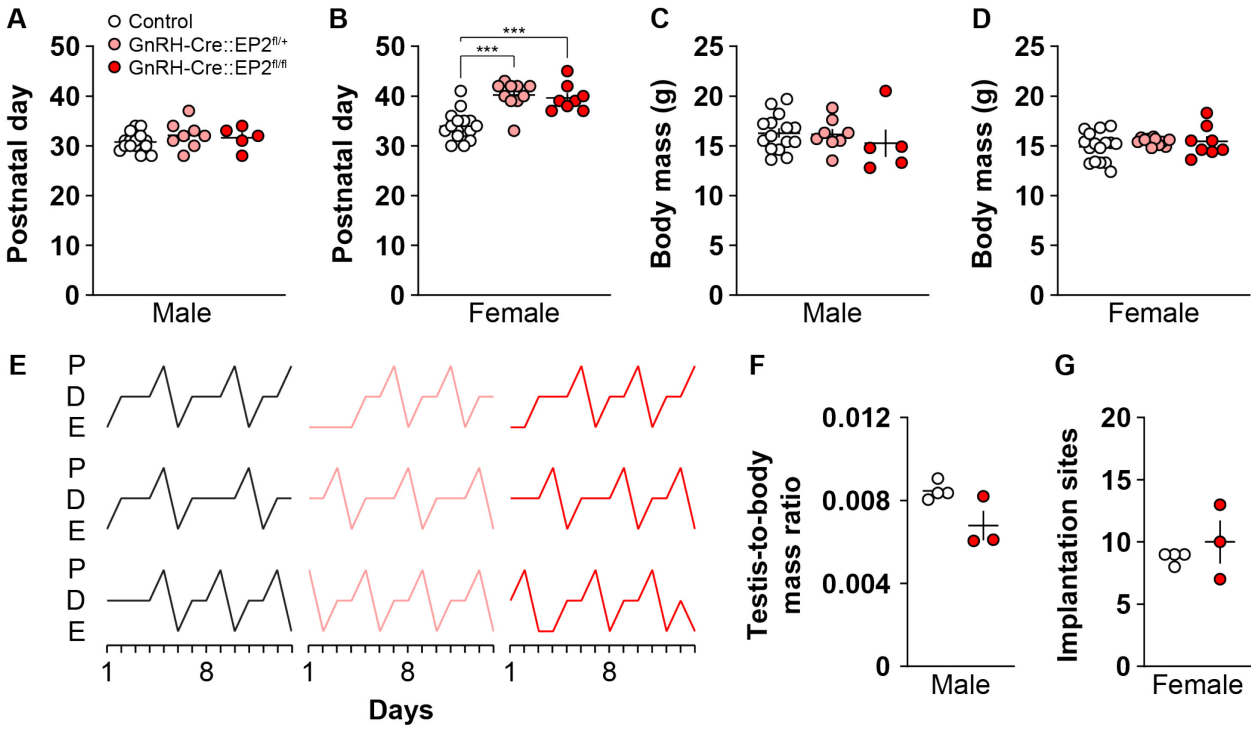


Figure 4.2: Preliminary data showing EP2 knockout in GnRH-expressing cells delaying female puberty but not disrupting long-term reproductive function. **A and B,** The age of male (A) and female (B) mice when exhibiting preputial separation and vaginal opening, respectively (one-way ANOVA with Sidak *post hoc*; statistics are in Tables 4.1 and 4.2). **C and D,** Mass of male (C) and female (D) mice upon puberty onset (one-way ANOVA with Sidak *post hoc*; statistics are in Tables 4.3 and 4.4). **E,** Representative reproductive cycles of control (left), GnRH-Cre::EP2$^{fl/+}$ (center), and GnRH-Cre::EP2$^{fl/fl}$ (right) females. E, estrus; D, diestrus; P, proestrus. **F,** Ratio of testis and body masses of sexually naive males (two-tailed, unpaired Student's t test with Welch's correction; statistics are in Table 4.5). **G,** Number of uterine implantation site in control females paired with either control (white) or GnRH-Cre::EP2$^{fl/fl}$ mice (red; two-tailed, unpaired Student's t test with Welch's correction; statistics are in Table 4.6). ***, $p < 0.001$.

Another consideration to be made with this transgenic model is whether the effects of EP2 knockout on female sexual maturation is caused by disruption of GnRH-expressing cells in extrahypothalamic regions[436]. Vertebrates are believed to express two or three isoforms of GnRH (GnRH-I, -II, -III), though over two dozen isoforms have been found[437]. GnRH-I (expressed by the eponymously named hypothalamic neurons) is also found throughout the CNS including the basal forebrain, striatum, and particularly the cerebellum[438,439]; the short half-life on GnRH, however, limits the range of GnRH action down to a local level[440], so these extrahypothalamic brain regions may have little impact on reproductive function. Although a substantial amount of GnRH expression in the

periphery derives from isoform II, GnRH-I and its receptor are found in peripheral reproductive tissues including the testes and ovaries in both humans and rodents[441–444]. Moreover, PGE2 and EP2 are highly expressed in the ovary, and autocrine and paracrine prostanoid signaling is identified as a key mediator of various ovulatory processes[445–448]. Given that the promoter of the GnRH-Cre line is derived from isoform I, we conducted pilot immunofluorescence of ovarian tissues using antibodies for GnRH (EL-14[449]) and EP2 (ab167171, abcam) to assess potential colocalization of the two signals. Interestingly, preliminary data show that there is sparse GnRH expression colocalized with EP2 signal in stromal cells, while no GnRH signal was detected in the ovarian parenchyma areas. Ovarian follicles mainly compose the parenchyma, while the stroma consists of a variety of cells such as immune cells, surface epithelium, and stem cells and that support the maintenance and development of the follicles[450]. Preliminary data gathered from ovulating GnRH-Cre$^{+/-}$::EP2$^{fl/fl}$ females on the day of estrus indicates that they release a similar number of oocytes during ovulation compared to littermate controls. More work is still required to determine if EP2 knockout in stromal GnRH-expressing cells, though few in numbers, alters follicular development.

We further investigated the reproductive outcomes of GnRH-Cre::EP2$^{fl/+}$ and GnRH-Cre::EP2$^{fl/fl}$ mice by measuring various reproductive parameters during adulthood. Daily vaginal cytology was done on 2-month-old female mutants and littermate controls for two weeks. All females exhibited typical reproductive cyclicity over the period (Fig. 4.1E). To determine if male reproductive behavior was altered, we paired adult littermate control and GnRH-Cre::EP2$^{fl/fl}$ males with wild type sexually naive females for breeding. Time to copulatory plugs was similar in both groups, indicating male reproductive behavior being unaltered. Preliminary male testes-to-body mass ratios appeared similar between controls and GnRH-Cre::EP2$^{fl/fl}$ (Fig. 4.1F). Moreover, the number of embryonic implantation sites in the partnered females was not different (Fig. 4.1G). Indicating a lack of developmental disruption in male EP2 knockout. These findings echo the postulate discussed in light of the Ca^{2+} attenuation results that hypothalamic PGE2 signaling is developmentally regulated. Timely pre- and peripubertal sexual development in females requires PGE2 action, while both adult males and females display normal reproductive behavior and function.

Summary

The work described in this dissertation has provided a better understanding of how astrocytes from different brain regions contribute to the regulation of the central reproductive circuit. It shows that factors including sex, the time of day, and cycle stage all modulate astrocyte communication with GnRH neurons and not KNDy neurons. More specifically, activation of Gq signaling in POA and ARC astrocytes induces greater LH release in males compared to females. dmPGE2-induced GnRH neuron firing is also greater in males compared to females, suggesting a sex difference in PGE2 sensitivity. Diurnal effects were observed wherein PGE2 signaling blockade in the AM effectively reduces GnRH neuron firing following POA astrocyte activation, but blockade in the PM had no effect. Finally, this work also identified purinergic signaling as an endogenous mechanism for POA astrocyte activation, though more investigation is required to determine the necessity of POA astrocytic Ca^{2+} signaling in reproductive function *in vivo*.

Table 4.1: Statistical parameters assessing the effect of EP2 knockout in GnRH-expressing cells on puberty onset in males (Fig. 4.1A).

Property	Control	GnRH-Cre::EP2$^{fl/+}$	GnRH-Cre::EP2$^{fl/fl}$
Mice (n)	15	8	5
One-way ANOVA			
Property		Statistic	η^2
Puberty onset		$F_{(2,27)} = 0.999$, $p = 0.382$	0.074

Table 4.2: Statistical parameters assessing the effect of EP2 knockout in GnRH-expressing cells on puberty onset in females (Fig. 4.1B).

Property	Control	GnRH-Cre::EP2$^{fl/+}$	GnRH-Cre::EP2$^{fl/fl}$
Mice (n)	16	10	8
One-way ANOVA			
Property		Statistic	η^2
Puberty onset		$F_{(2,33)} = 19.163$, $\mathbf{p < 0.001}$	0.553

Table 4.3: Statistical parameters assessing the effect of EP2 knockout in GnRH-expressing cells on body mass at puberty onset in males (Fig. 4.1C).

Property	Control	GnRH-Cre::EP2$^{fl/+}$	GnRH-Cre::EP2$^{fl/fl}$
Mice (n)	15	8	5
One-way ANOVA			
Property		Statistic	η^2
Mass		$F_{(2,27)} = 0.486$, $p = 0.621$	0.037

Table 4.4: Statistical parameters assessing the effect of EP2 knockout in GnRH-expressing cells on body mass at puberty onset in females (Fig. 4.1D).

Property	Control	GnRH-Cre::EP2$^{fl/+}$	GnRH-Cre::EP2$^{fl/fl}$
Mice (n)	16	10	8
One-way ANOVA			
Property		Statistic	η^2
Mass		$F_{(2,33)} = 0.796$, $p = 0.460$	0.049

Table 4.5: Statistical parameters assessing the effect of EP2 knockout in GnRH-expressing cells on testis-to-body mass ratio (Fig. 4.1F).

Property	Control	GnRH-Cre::EP2$^{fl/fl}$
Mice (n)	4	3
Two-tailed independent samples Welch's t-test		
Property	Statistic	η^2
Testis-to-body mass ratio	t(2.25), df = 2.36, $p = 0.133$	0.682

Table 4.6: Statistical parameters assessing the effect of EP2 knockout in GnRH-expressing cells on uterine implantation sites (Fig. 4.1G).

Property	Control	GnRH-Cre::EP2$^{fl/fl}$	
Mice (n)	4	3	
Two-tailed independent samples Welch's t-test			
Property		Statistic	η^2
Testis-to-body mass ratio		t(0.71), df = 2.08, p = 0.547	0.197

Bibliography

1. Hippocrates. *Hippocrates: On the Nature of Man*. W. Heffer & Sons Ltd; 1968.

2. Jacques J. The legacy of the hippocratic treatise The Nature of Man: The theory of the four humours. In: *Greek Medicine from Hippocrates to Galen*. Koninklijke Brill NV; 2012.

3. Medvei VC. *A History of Endocrinology*. MTP Press; 1982.

4. Javier H. The four humours theory. *ESSAI*. 2014;12:21.

5. Bordeu AD, Bordeu TD, Bordeu FD. Analyse médicinale du sang. In: *Recherches Sur Les Maladies Chroniques, Leurs Rapports Avec Les Maladies Aiguës, Leurs Périodes, Leur Nature: & Fur La Manière Dont on Les Traite Aux Eaux Minérales de Bareges, & Des Autres Sources de l'Aquitaine*. Ruault; 1775.

6. Davis SR, Dinatale I, Rivera-Woll L, Davison S. Postmenopausal hormone therapy: from monkey glands to transdermal patches. *J Endocrinol*. 2005;185(2):207-222.

7. Weil A. *The Internal Secretions: For the Use of Students and Physicians*. The Macmillan Company; 1924.

8. Bernard C. *Leçons de Physiologie Expérimentale Appliqués à La Médecine*. Balliere; 1855.

9. Finger S. *Origins of Neuroscience: A History of Explorations into Brain Function*. Oxford University Press; 1994.

10. Clarke E. Aristotelian concepts of the form and function of the brain. *Bull Hist Med*. 1963;37:1-14.

11. Panegyres KP, Panegyres PK. The Ancient Greek discovery of the nervous system: Alcmaeon, Praxagoras and Herophilus. *J Clin Neurosci*. 2016;29:21-24.

12. Molnár Z. Thomas Willis (1621–1675), the founder of clinical neuroscience. *Nat Rev Neurosci*. 2004;5:329-335.

13. Berthold AA. Transplantation der hoden. *Archiv Anatomie Physiol Wiss Med*. 1849:42-46.

14. Brown-Séquard C. Note on the effects produced on man by subcutaneous injections of a liquid obtained from the testicles of animals. *Lancet*. 1889;2:105-107.

15. Bayliss WM, Starling EH. On the causation of the so-called ‘peripheral reflex secretion’ of the pancreas. (Preliminary communication.). *Proc R Soc Lond*. 1902;69(451-458):352-353.

16. Doisy EA, Veler CD, Thayer S. The preparation of the crystalline ovarian hormone from the urine of pregnant women. *J Biol Chem*. 1930;86(2):499-509.

17. Allen WM, Wintersteiner O. Crystalline progestin. *Science*. 1934;80(2069):190-191.

18. David K, Dingemanse E, Freud J, Laqueur E. Über krystallinisches männliches hormon aus hoden (testosteron), wirksamer als aus harn oder aus cholesterin bereitetes androsteron. [crystalline male hormone from the testes (testeosterone) is more effective than androsterone derived from urine or cholesterin]. 1935;233:281-283.

19. Crowe SJ, Cushing H, Homans J. *Experimental Hypophysectomy*. Vol 21. Johns Hopkins Press; 1910.

20. Fee AR, Parkes AS. Studies on ovulation I. The relation of the anterior pituitary body to ovulation in the rabbit. *J Physiol*. 1929;67(4):383-388.

21. Smith PE. The induction of precocious sexual maturity by pituitary homeotransplants. *Am J Physiol*. 1927;80(1):114-125.

22. Smith PE. The disabilities caused by hypophysectomy and their repair: The tuberal (hypothalamic) syndrome in the rat. *JAMA*. 1927;88(3):158-161.

23. Smith PE, Engle ET. Experimental evidence regarding the role of the anterior pituitary in the development and regulation of the genital system. *Am J Anat*. 1927;40(2):159-217.

24. Smith PE, Engle ET. Induction of precocious sexual maturity in the mouse by daily pituitary homeo and heterotransplants. *Proc Soc Exp Biol Med*. 1927;24(6):561-562.

25. Fevold HL, Hisaw FL, Leonard SL. The gonad stimulating and the luteinizing hormones of the anterior lobe of the hypophesis. *Am J Physiol*. 1931;97(2):291-301.

26. Aschner B. Ueber die beziehungen zwischen hypophysis und genitale. *Archiv für Gynäkologie*. 1912;97.

27. Bourgery JM. Mémoires sur l’extrémité céphalique du grand sympathique dans l’homme et les animaux mammiféres. *C R Acad Sci (Paris)*. 1845;20:1014-1020.

28. Brooks CM, Gersh J. Pericellular nerve fiber terminals in the pars nervosa and pars distalis of the rat pituitary. *Anat Rec*. 1938;70(Suppl 3):10.

29. Croll MM. Nerve fibers in the pituitary of rabbit. *J Physiol*. 1929;66:316-322.

30. Dandy WE. The nerve supply to the pituitary body. *Am J Anat*. 1913;15:333-343.

31. Hair GW. The nerve supply of the hypophysis of the cat. *Anat Rec*. 1938;71:141-160.

32. Pines IL. Über die innervation der hypophysis cerebri II. Mitteilung. *Z Gesamte Neurol Psychiatr*. 1926;100:123-138.

33. Szentágothai J, Flerkó B, Mess B, Halász B. *Hypothalamic Control of the Anterior Pituitary. An Experimental-Morphological Study*. Akadémiai Kiadó; 1962.

34. Popa G, Fielding U. The vascular link between the pituitary and the hypothalamus. *Lancet*. 1930;216(5579):238-240.

35. Wislocki GB, King LS. The permeability of the hypophysis and hypothalamus to vital dyes, with a study of the hypophyseal vascular supply. *Am J Anat*. 1936;58(2):421-472.

36. Sawyer CH. History of the neurovascular concept of hypothalamo-hypophysial control. *Biol Reprod*. 1978;18:325-328.

37. Foa C. La greffe des ovaries, en relation avec quelques questions de biologie generale. *Arch Ital Biol*. 1900;34:43-73.

38. Harris GW, Jacobsohn D. Functional grafts of the anterior pituitary gland. *Proc Biol Sci*. 1952;139(895):263-276.

39. Marshall FHA, Verney EB. The occurrence of ovulation and pseudo-pregnancy in the rabbit as a result of central nervous stimulation. *J Physiol*. 1936;86(3):327-336.

40. Harris GW. The induction of ovulation in the rabbit, by electrical stimulation of the hypothalamo-hypophysial mechanism. *Proc Biol Sci*. 1937;122(828):374-394.

41. Barry J, Cotte G. Etude preliminaire, au microscope electronique, de l'eminence mediane du cobaye. *Z Zellforch Microsk Anat*. 1961;53:714-724.

42. Green JD. Vessels and nerves of amphibian hypophyses. A study of the living circulation and of the histology of the hypophysical vessels and nerves. *Anat Rec*. 1947;99(1):21-53.

43. Harris GW. *Neural Control of the Pituitary Gland*. Edward Arnold; 1955.

44. Burgus R, Dunn TF, Desiderio DM, et al. Biological activity of synthetic polypeptide derivatives related to the structure of hypothalamic TRF. *Endocrinology*. 1970;86(3):573-582.

45. Folkers K, Enzmann F, Bøler J, Bowers CY, Schally AV. Discovery of modification of the synthetic tripeptide-sequence of the thyrotropin releasing hormone having activity. *Biochem Biophys Res Commun*. 1969;37(1):123-126.

46. Li CH, Simpson ME, Evans HM. Interstitial cell stimulating hormone. II. Method of preparation and some physico-chemical studies1. *Endocrinology*. 1940;27(5):803-808.

47. Li CH, Simpson ME, Evans HM. Purification of the pituitary interstitial cell stimulating hormone. *Science*. 1940;92(2390):355-356.

48. Li CH, Simpson ME, Evans HM. Isolation of pituitary follicle-stimulating hormone (FSH). *Science*. 1949;109(2835):445-446.

49. Bowers CY, Currie BL, Johansson KNG, Folkers K. Biological evidence that separate hypothalamic hormones release the follicle stimulating and luteinizing hormones. *Biochem Biophys Res Commun*. 1973;50(1):20-26.

50. Schally AV, Arimura A, Kastin AJ, et al. Gonadotropin-releasing hormone: one polypeptide regulates secretion of luteinizing and follicle-stimulating hormones. *Science*. 1971;173(4001):1036-1038.

51. Schally AV, Baba Y, Arimura A, Redding TW, White WF. Evidence for peptide nature of LH and FSH-releasing hormones. *Biochem Biophys Res Commun*. 1971;42(1):50-56.

52. Pelletier G, Labrie F, Puviani R, Arimura A, Schally AV. Immunohistochemical localization of luteinizing hormone-releasing hormone in the rat median eminence. *Endocrinology*. 1974;95(1):314-317.

53. Bennett GW, Edwardson JA, Holland D, Jeffcoate SL, White N. Release of imnumoreactive luteinising hormone-releasing hormone and thyrotrophin-releasing hormone from hypothalamic synaptosomes. *Nature*. 1975;257:323-325.

54. Merchenthaler I, Göres T, Sétáló G, Petrusz P, Flerkó B. Gonadotropin-releasing hormone (GnRH) neurons and pathways in the rat brain. *Cell Tissue Res*. 1984;237:15-29.

55. Conn PM, Huckle WR, Andrews WV, McArdle CA. The molecular mechanism of action of gonadotropin releasing hormone (GnRH) in the pituitary. *Recent Prog Horm Res*. 1987;43:29-68.

56. Haisenleder DJ, Dalkin AC, Ortolano GA, Marshall JC, Shupnik MA. A pulsatile gonadotropin-releasing hormone stimulus is required to increase transcription of

the gonadotropin subunit genes: evidence for differential regulation of transcription by pulse frequency in vivo. *Endocrinology*. 1991;128(1):509-517.

57. Hunzicker-Dunn M, Mayo K. Gonadotropin signaling in the ovary. In: *Knobil and Neill's Physiology of Reproduction*. 4th ed. Academic Press; 2015:895-945.

58. Smith LB, Walker WH. Hormone signaling in the testis. In: *Knobil and Neill's Physiology of Reproduction*. 4th ed. Academic Press; 2015:637-690.

59. Belchetz PE, Plant TM, Nakai Y, Keogh EJ, Knobil E. Hypophysial responses to continuous and intermittent delivery of hypothalamic gonadotropin-releasing hormone. *Science*. 1978;202(4368):631-633.

60. Wildt L, Häusler A, Marshall G, et al. Frequency and amplitude of gonadotropin-releasing hormone stimulation and gonadotropin secretion in the rhesus monkey. *Endocrinology*. 1981;109(2):376-385.

61. Midgley AR Jr, Jaffe RB. Regulation of human gonadotropins: X. Episodic fluctuation of LH during the menstrual cycle. *J Clin Endocrinol Metab*. 1971;33(6):962-969.

62. Dierschke DJ, Bhattacharya AN, Atkinson LE, Knobil E. Circhoral oscillations of plasma LH levels in the ovariectomized rhesus monkey. *Endocrinology*. 1970;87(5):850-853.

63. Baird DT, Swanston I, Scaramuzzi RJ. Pulsatile release of LH and secretion of ovarian steroidsin sheep during the luteal phase of the estrous cycle. *Endocrinology*. 1976;98(6):1490-1496.

64. Skinner DC, Evans NP, Delaleu B, Goodman RL, Bouchard P, Caraty A. The negative feedback actions of progesterone on gonadotropinreleasing hormone secretion are transduced by the classical progesterone receptor. *Proc Natl Acad Sci*. 1998;95(18):10978-10983.

65. Justyna Pielecka, Suzanne M. Moenter. Effect of steroid milieu on gonadotropin-releasing hormone-1 neuron firing pattern and luteinizing hormone levels in male mice. *Biol Reprod*. 2006;74(5):931-937.

66. Smith EP, Boyd J, Frank GR, et al. Estrogen resistance caused by a mutation in the estrogen-receptor gene in a man. *N Engl J Med*. 1994;331(16):1056-1061.

67. Kumar TR, Wang Y, Lu N, Matzuk MM. Follicle stimulating hormone is required for ovarian follicle maturation but not male fertility. *Nat Genet*. 1997;15:201-204.

68. Moon YS, Tsang BK, Simpson C, Armstrong DT. 17β-estradiol biosynthesis in cultured granulosa and thecal cells of human ovarian follicles: stimulation by follicle-stimulating hormone. *J Clin Endocrinol Metab*. 1978;47(2):263-267.

69. Evans NP, Dahl GE, Glover BH, Karsch FJ. Central regulation of pulsatile gonadotropin-releasing hormone (GnRH) secretion by estradiol during the period leading up to the preovulatory GnRH surge in the ewe. *Endocrinology*. 1994;134(4):1806-1811.

70. Moenter SM, Caraty A, Karsch FJ. The estradiol-induced surge of gonadotropin-releasing hormone in the ewe. *Endocrinology*. 1990;127(3):1375-1384.

71. Richards JS, Ascoli M. Endocrine, paracrine, and autocrine signaling pathways that regulate ovulation. *Trends Endocrinol Metab*. 2018;29(5):313-325.

72. G. D. Niswender. Molecular control of luteal secretion of progesterone. *Reproduction*. 2002;123(3):333-339.

73. Wetendorf M, DeMayo FJ. The progesterone receptor regulates implantation, decidualization, and glandular development via a complex paracrine signaling network. *Mol Cell Endocrinol*. 2012;357(1-2):108-118.

74. Roberts RM. Interferon-tau, a type 1 interferon involved in maternal recognition of pregnancy. *Cytokine Growth Factor Rev*. 2007;18(5-6):403-408.

75. Casper RF, Sheehan KL, Yen SSC. Chorionic gonadotropin prevents LRF-agonist-induced luteolysis in the human. *Contraception*. 1980;21(5):471-478.

76. Sotrel G, Helvacioglu A, Dowers S, Scommegna A, Auletta FJ. Mechanism of luteolysis: Effect of estradiol and prostaglandin F2α on corpus luteum luteinizing hormone/human chorionic gonadotropin receptors and cyclic nucleotides in the rhesus monkey. *Am J Obstet Gynecol*. 1981;139(2):134-140.

77. Kerdelhué B d, Brown S, Lenoir V, et al. Timing of initiation of the preovulatory luteinizing hormone surge and Its relationship with the circadian cortisol rhythm in the human. *Neuroendocrinology*. 2002;75(3):158-163.

78. Smith MS, Neill JD. Termination at midpregnancy of the two daily surges of plasma prolactin initiated by mating in the rat. *Endocrinology*. 1976;98(3):696-701.

79. Spies HG, Niswender GD. Levels of prolactin, LH and FSH in the serum of intact and pelvic-neurectomized rats. *Endocrinology*. 1971;88(4):937-943.

80. Nagy A. Cre recombinase: The universal reagent for genome tailoring. *genesis*. 2000;26:99-109.

81. Roth BL. DREADDs for neuroscientists. *Neuron*. 2016;89(4):683-694.

82. Lin MZ, Schnitzer MJ. Genetically encoded indicators of neuronal activity. *Nat Neurosci*. 2016;19:1142-1153.

83. Couse JF, Hewitt SC, Bunch DO, et al. Postnatal sex reversal of the ovaries in mice lacking estrogen receptors α and β. *Science*. 1999;286(5448):2328-2331.

84. Dorling AA, Todman MG, Korach KS, Herbison AE. Critical role for estrogen receptor alpha in negative feedback regulation of gonadotropin-releasing hormone mRNA expression in the female mouse. *Neuroendocrinology*. 2003;78(4):204-209.

85. Glidewell-Kenney C, Hurley LA, Pfaff L, Weiss J, Levine JE, Jameson JL. Nonclassical estrogen receptor α signaling mediates negative feedback in the female mouse reproductive axis. *Proc Natl Acad Sci*. 2007;104(19):8173-8177.

86. Glidewell-Kenney C, Weiss J, Hurley LA, Levine JE, Jameson JL. Estrogen receptor α signaling pathways differentially regulate gonadotropin subunit gene expression and serum follicle-stimulating hormone in the Female Mouse. *Endocrinology*. 2008;149(8):4168-4176.

87. Legan SJ, Tsai HW. Oestrogen receptor-α and -β immunoreactivity in gonadotropin-releasing hormone neurones after ovariectomy and chronic exposure to oestradiol. *J Neuroendocrinol*. 2003;15(12):1164-1170.

88. Ohtaki T, Shintani Y, Honda S, et al. Metastasis suppressor gene KiSS-1 encodes peptide ligand of a G-protein-coupled receptor. *Nature*. 2001;411:613-617.

89. Kotani M, Detheux M, Vandenbogaerde A, et al. The metastasis suppressor gene KiSS-1 encodes kisspeptins, the natural ligands of the orphan G protein-coupled receptor GPR54. *J Biol Chem*. 2001;276(37):34631-34646.

90. Funes S, Hedrick JA, Vassileva G, et al. The KiSS-1 receptor GPR54 is essential for the development of the murine reproductive system. *Biochem Biophys Res Commun*. 2003;312(4):1357-1363.

91. Novaira HJ, Sonko ML, Hoffman G, et al. Disrupted kisspeptin signaling in GnRH neurons leads to hypogonadotrophic hypogonadism. *Mol Endocrinol*. 2014;28(2):225-238.

92. Lehman MN, Merkley CM, Coolen LM, Goodman RL. Anatomy of the kisspeptin neural network in mammals. *Brain Res*. 2010;1364:90-102.

93. Ramaswamy S, Guerriero KA, Gibbs RB, Plant TM. Structural interactions between kisspeptin and GnRH neurons in the mediobasal hypothalamus of the male rhesus monkey (macaca mulatta) as revealed by double immunofluorescence and confocal microscopy. *Endocrinology*. 2008;149(9):4387-4395.

94. Hrabovszky E, Ciofi P, Vida B, et al. The kisspeptin system of the human hypothalamus: sexual dimorphism and relationship with gonadotropin-releasing hormone and neurokinin B neurons. *Eur J Neurosci*. 2010;31(11):1984-1998.

95. Han SK, Gottsch ML, Lee KJ, et al. Activation of gonadotropin-releasing hormone neurons by kisspeptin as a neuroendocrine switch for the onset of puberty. *J Neurosci*. 2005;25(49):11349-11356.

96. Liu X, Lee K, Herbison AE. Kisspeptin excites gonadotropin-releasing hormone neurons through a phospholipase c/calcium-dependent pathway regulating multiple ion channels. *Endocrinology*. 2008;149(9):4605-4614.

97. Liu X, Herbison AE. Small-conductance calcium-activated potassium channels control excitability and firing dynamics in gonadotropin-releasing hormone (GnRH) neurons. *Endocrinology*. 2008;149(7):3598-3604.

98. Pielecka-Fortuna J, Chu Z, Moenter SM. Kisspeptin acts directly and indirectly to increase gonadotropin-releasing hormone neuron activity and its effects are modulated by estradiol. *Endocrinology*. 2008;149(4):1979-1986.

99. Messager S, Chatzidaki EE, Ma D, et al. Kisspeptin directly stimulates gonadotropin-releasing hormone release via G protein-coupled receptor 54. *Proc Natl Acad Sci*. 2005;102(5):1761-1766.

100. Caraty A, Smith JT, Lomet D, et al. Kisspeptin synchronizes preovulatory surges in cyclical ewes and causes ovulation in seasonally acyclic ewes. *Endocrinology*. 2007;148(11):5258-5267.

101. Shahab M, Mastronardi C, Seminara SB, Crowley WF, Ojeda SR, Plant TM. Increased hypothalamic GPR54 signaling: A potential mechanism for initiation of puberty in primates. *Proc Natl Acad Sci*. 2005;102(6):2129-2134.

102. Dhillo WS, Chaudhri OB, Patterson M, et al. Kisspeptin-54 stimulates the hypothalamic-pituitary gonadal axis in human males. *J Clin Endocrinol Metab*. 2005;90(12):6609-6615.

103. Franceschini I, Lomet D, Cateau M, Delsol G, Tillet Y, Caraty A. Kisspeptin immunoreactive cells of the ovine preoptic area and arcuate nucleus co-express estrogen receptor alpha. *Neurosci Lett*. 2006;401(3):225-230.

104. Ikeda Y, Kato-Inui T, Tagami A, Maekawa M. Expression of progesterone receptor, estrogen receptors α and β, and kisspeptin in the hypothalamus during perinatal development of gonad-lacking steroidogenic factor-1 knockout mice. *Brain Res*. 2019;1712:167-179.

105. Walters KA, Edwards MC, Tesic D, et al. The role of central androgen receptor actions in regulating the hypothalamic-pituitary-ovarian axis. *Neuroendocrinology*. 2018;106(4):389-400.

106. Mayer C, Acosta-Martinez M, Dubois SL, et al. Timing and completion of puberty in female mice depend on estrogen receptor α-signaling in kisspeptin neurons. *Proc Natl Acad Sci*. 2010;107(52):22693-22698.

107. Smith JT, Cunningham MJ, Rissman EF, Clifton DK, Steiner RA. Regulation of Kiss1 gene expression in the brain of the female mouse. *Endocrinology*. 2005;146(9):3686-3692.

108. Wiegand SJ, Terasawa E. Discrete lesions reveal functional heterogeneity of suprachiasmatic structures in regulation of gonadotropin secretion in the female rat. *Neuroendocrinology*. 1982;34(6):395-404.

109. Soper BD, Weick RF. Hypothalamic and extrahypothalamic mediation of pulsatile discharges of luteinizing hormone in the ovariectomized rat. *Endocrinology*. 1980;106(1):348-355.

110. Plant TM, Krey LC, Moossy J, McCormack JT, Hess DL, Knobil E. The arcuate nucleus and the control of gonadotropin and prolactin secretion in the female rhesus monkey (macaca mulatta). *Endocrinology*. 1978;102(1):52-62.

111. Yamada K, Mano T, Hazim S, et al. Neonatal aromatase inhibition blocked defeminization of AVPV kiss1 neurons and LH surge-generating system in male rats. *Endocrinology*. 2024;165(4):bqae028.

112. Robertson JL, Clifton DK, Iglesia HO de la, Steiner RA, Kauffman AS. Circadian regulation of kiss1 neurons: Implications for timing the preovulatory gonadotropin-releasing hormone/luteinizing hormone surge. *Endocrinology*. 2009;150(8):3664-3671.

113. Clarkson J, de Tassigny X d'Anglemont, Moreno AS, Colledge WH, Herbison AE. Kisspeptin–GPR54 signaling is essential for preovulatory gonadotropin-releasing hormone neuron activation and the luteinizing hormone surge. *J Neurosci*. 2008;28(35):8691-8697.

114. Watanabe Y, Uenoyama Y, Suzuki J, et al. Oestrogen-induced activation of preoptic kisspeptin neurones may be involved in the luteinising hormone surge in male and female japanese monkeys. *J Neuroendocrinol*. 2014;26(12):909-917.

115. Smith JT, Li Q, Pereira A, Clarke IJ. Kisspeptin neurons in the ovine arcuate nucleus and preoptic area are involved in the preovulatory luteinizing hormone surge. *Endocrinology*. 2009;150(12):5530-5538.

116. Thiéry JC, Pelletier J. Multiunit activity in the anterior median eminence and adjacent areas of the hypothalamus of the ewe in relation to LH secretion. *Neuroendocrinology*. 1981;32(4):217-224.

117. Han SY, Kane G, Cheong I, Herbison AE. Characterization of GnRH pulse generator activity in male mice using GCaMP fiber photometry. *Endocrinology*. 2019;160(3):557-567.

118. Han SY, McLennan T, Czieselsky K, Herbison AE. Selective optogenetic activation of arcuate kisspeptin neurons generates pulsatile luteinizing hormone secretion. *Proc Natl Acad Sci*. 2015;112(42):13109-13114.

119. Wakabayashi Y, Nakada T, Murata K, et al. Neurokinin B and dynorphin A in kisspeptin neurons of the arcuate nucleus participate in generation of periodic oscillation of neural activity driving pulsatile gonadotropin-releasing hormone secretion in the goat. *J Neurosci*. 2010;30(8):3124-3132.

120. Krajewski SJ, Anderson MJ, Iles-Shih L, Chen KJ, Urbanski HF, Rance NE. Morphologic evidence that neurokinin B modulates gonadotropin-releasing hormone secretion via neurokinin 3 receptors in the rat median eminence. *J Comp Neurol*. 2005;489(3):372-386.

121. Navarro VM, Gottsch ML, Chavkin C, Okamura H, Clifton DK, Steiner RA. Regulation of gonadotropin-releasing hormone secretion by kisspeptin/dynorphin/neurokinin B neurons in the arcuate nucleus of the mouse. *J Neurosci*. 2009;29(38):11859-11866.

122. Greenwald-Yarnell ML, Marsh C, Allison MB, et al. ERα in Tac2 neurons regulates puberty onset in female mice. *Endocrinology*. 2016;157(4):1555-1565.

123. Dubois SL, Acosta-Martínez M, DeJoseph MR, et al. Positive, but not negative feedback actions of estradiol in adult female mice require estrogen receptor α in kisspeptin neurons. *Endocrinology*. 2015;156(3):1111-1120.

124. Wang L, Burger LL, Greenwald-Yarnell ML, Myers MG Jr, Moenter SM. Glutamatergic transmission to hypothalamic kisspeptin neurons is differentially regulated by estradiol through estrogen receptor α in adult female mice. *J Neurosci*. 2018;38(5):1061-1072.

125. Wang L, Moenter SM. Differential roles of hypothalamic AVPV and arcuate kisspeptin neurons in estradiol feedback regulation of female reproduction. *Neuroendocrinology*. 2020;110(3-4):172-184.

126. Fan X, Agid Y. At the origin of the history of glia. *Neuroscience*. 2018;385:255-271.

127. Virchow R. *Die Cellularpathologie in Ihrer Begründung Auf Physiologische Und Pathologische Gewebelehre: 20 Vorlesungen, Gehalten Während Der Monate Februar, März Und April 1858 Im Pathologischen Institute Zu Berlin*. August Hirschwald; 1858.

128. Virchow R. *Gesammelte Abhandlungen Zur Wissenschaftlichen Medicin*. Meidinger Sohn & Co.; 1856.

129. Golgi C. Sulle alterazioni dei vasi linfatici del cervello. *Riv Clin*. 1870;9:324-343.

130. Ramón y Cajal S. Estructura de los centros nerviosos de las aves. *Rev Trim Histol Norm Pat*. 1888;1:1-10.

131. Ramón y Cajal S. Contribucion al conocimiento de la neuroglia del cerebro humano. *Trab Lab Invest Biol Univ Madrid*. 1913;11:255-313.

132. Eng LF. Glial fibrillary acidic protein (GFAP): the major protein of glial intermediate filaments in differentiated astrocytes. *J Neuroimmunol*. 1985;8:203-214.

133. Foster M. *A Text Book of Physiology, Part III: The Central Nervous System*. 7th ed. MacMillan & Co., Ltd.; 1897.

134. Kölliker A. *Handbuch Der Gewebelehre Des Menschen*. Wilhelm Engelmann; 1867.

135. Andriezen WL. The neuroglia elements in the human brain. *Br Med J*. 1893;2(1700):227.

136. Lenhossék M. *Der Feinere Bau Des Nervensystems Im Lichte Neuester Forschungen: Eine Allgemeine Betrachtung Der Strukturprinzipien Des Nervensystems, Nebst Einer Darstellung Des Feineren Baues Des Rückenmarkes*. Fischer's Medicin. Buchhandlung H. Kornfeld; 1895.

137. Golgi C. Sulla fina struttura dei bulbi olfactorii. *Riv Sper Freniatr Med Leg Alien Ment*. 1875;1:405.

138. Chaslin P. Contribution à l'étude de la sclérose cerebrale. *Arch Med Exp Anat Pathol*. 1891;3:305-340.

139. Ramón y Cajal S. Algunas conjeturas sobre el mecanismo anatómico de la ideación, asociación y atención. *Rev Med Cir Pract*. 1895;36:497-508.

140. Lugaro E. Sulle funzioni della nevroglia. *Riv Patol Nerv Ment*. 1907;12:225-233.

141. Berlucchi G. The origin of the term plasticity in the neurosciences: Ernesto Lugaro and chemical synaptic transmission. *J Hist Neurosci*. 2002;11(3):305-309.

142. Peters A, Palay SL. An electron microscope study of the distribution and patterns of astroglial processes in the central nervous system. *J Anat*. 1965;99:419.

143. Ventura R, Harris KM. Three-dimensional relationships between hippocampal synapses and astrocytes. *J Neurosci*. 1999;19(16):6897-6906.

144. Araque A, Parpura V, Sanzgiri RP, Haydon PG. Tripartite synapses: glia, the unacknowledged partner. *Trends Neurosci*. 1999;22(5):208-215.

145. Hertz L, Zielke HR. Astrocytic control of glutamatergic activity: astrocytes as stars of the show. *Trends Neurosci*. 2004;27(12):735-743.

146. Bergles DE, Jahr CE. Glial contribution to glutamate uptake at schaffer collateral–commissural synapses in the hippocampus. *J Neurosci*. 1998;18(19):7709-7716.

147. Olsen ML, Khakh BS, Skatchkov SN, Zhou M, Lee CJ, Rouach N. New insights on astrocyte ion channels: Critical for homeostasis and neuron-glia signaling. *J Neurosci*. 2015;35(41):13827-13835.

148. Walz W. Role of astrocytes in the clearance of excess extracellular potassium. *Neurochem Int*. 2000;36(4-5):291-300.

149. Orkand RK, Nicholls JG, Kuffler SW. Effect of nerve impulses on the membrane potential of glial cells in the central nervous system of amphibia. *J Neurophysiol*. 1966;29(4):788-806.

150. Cornell-Bell AH, Finkbeiner SM, Cooper MS, Smith SJ. Glutamate induces calcium waves in cultured astrocytes: long-range glial signaling. *Science*. 1990;247(4941):470-473.

151. Porter JT, McCarthy KD. Hippocampal astrocytes in situ respond to glutamate released from synaptic terminals. *J Neurosci*. 1996;16(16):5073-5081.

152. Wang X, Lou N, Xu Q, et al. Astrocytic Ca2+ signaling evoked by sensory stimulation in vivo. *Nat Neurosci*. 2006;9:816-823.

153. Kofuji P, Araque A. G-protein-coupled receptors in astrocyte–neuron communication. *Neuroscience*. 2021;456:71-84.

154. Durkee CA, Covelo A, Lines J, Kofuji P, Aguilar J, Araque A. Gi/o protein-coupled receptors inhibit neurons but activate astrocytes and stimulate gliotransmission. *Glia*. 2019;67(6):1076-1093.

155. Nett WJ, Oloff SH, McCarthy KD. Hippocampal astrocytes in situ exhibit calcium oscillations that occur independent of neuronal activity. *J Neurophysiol*. 2002;87(1):528-537.

156. Agulhon C, Petravicz J, McMullen AB, et al. What is the role of astrocyte calcium in neurophysiology? *Neuron*. 2008;59(6):932-946.

157. Bindocci E, Savtchouk I, Liaudet N, Becker D, Carriero G, Volterra A. Three-dimensional Ca2+ imaging advances understanding of astrocyte biology. *Science*. 2017;356(6339):eaai8185.

158. Otsu Y, Couchman K, Lyons DG, et al. Calcium dynamics in astrocyte processes during neurovascular coupling. *Nat Neurosci*. 2015;18:210-218.

159. Agarwal A, Wu PH, Hughes EG, et al. Transient opening of the mitochondrial permeability transition pore induces microdomain calcium transients in astrocyte processes. *Neuron*. 2017;93(3):587-605.

160. Malarkey EB, Ni Y, Parpura V. Ca2+ entry through TRPC1 channels contributes to intracellular Ca2+ dynamics and consequent glutamate release from rat astrocytes. *Glia*. 2008;56(8):821-835.

161. Martin DL. Synthesis and release of neuroactive substances by glial cells. *Glia*. 1992;5:81-94.

162. Santello M, Calì C, Bezzi P. Gliotransmission and the tripartite synapse. In: *Synaptic Plasticity: Dynamics, Development and Disease*. Springer; 2012:307-331.

163. Parpura V, Basarsky TA, Liu F, Jeftinija K, Jeftinija S, Haydon PG. Glutamate-mediated astrocyte–neuron signalling. *Nature*. 1994;369:744-747.

164. Araque A, Sanzgiri RP, Parpura V, Haydon PG. Calcium elevation in astrocytes causes an NMDA receptor-dependent increase in the frequency of miniature synaptic currents in cultured hippocampal neurons. *J Neurosci*. 1998;18(17):6822-6829.

165. Araque A, Parpura V, Sanzgiri RP, Haydon PG. Glutamate-dependent astrocyte modulation of synaptic transmission between cultured hippocampal neurons. *Eur J Neurosci*. 1998;10(6):2129-2142.

166. Bezzi P, Volterra A. A neuron–glia signalling network in the active brain. *Curr Opin Neurobiol*. 2001;11(3):387-394.

167. Gundersen V, Storm-Mathisen J, Bergersen LH. Neuroglial transmission. *Physiol Rev*. 2015;95(3):695-726.

168. Kettenmann H, Zorec R. Release of gliotransmitters and transmitter receptors in astrocytes. In: *Neuroglia*. 3rd ed. Oxford University Press; 2013.

169. Hamilton NB, Attwell D. Do astrocytes really exocytose neurotransmitters? *Nat Rev Neurosci*. 2010;11:227-238.

170. Alenka Guček, Nina Vardjan, Robert Zorec. Exocytosis in astrocytes: Transmitter release and membrane signal regulation. *Neurochem Res*. 2012;37:2351-2363.

171. Rizo J. Molecular mechanisms underlying neurotransmitter release. *Annu Rev Biophys*. 2022;51:377-408.

172. Cahoy JD, Emery B, Kaushal A, et al. A transcriptome database for astrocytes, neurons, and oligodendrocytes: A new resource for understanding brain development and function. *J Neurosci*. 2008;28(1):264-278.

173. Li D, Hérault K, Silm K, et al. Lack of evidence for vesicular glutamate transporter expression in mouse astrocytes. *J Neurosci*. 2013;33(10):4434-4455.

174. Franke H, Grummich B, Härtig W, et al. Changes in purinergic signaling after cerebral injury – involvement of glutamatergic mechanisms? *Int J Dev Neurosci*. 2006;24(2-3):123-132.

175. Kreft M, Stenovec M, Rupnik M, et al. Properties of Ca2+-dependent exocytosis in cultured astrocytes. *Glia*. 2004;46(4):437-445.

176. Bowser DN, Khakh BS. Two forms of single-vesicle astrocyte exocytosis imaged with total internal reflection fluorescence microscopy. *Proc Natl Acad Sci*. 2007;104(10):4212-4217.

177. Montana V, Ni Y, Sunjara V, Hua X, Parpura V. Vesicular glutamate transporter-dependent glutamate release from astrocytes. *J Neurosci*. 2004;24(11):2633-2642.

178. Zhang Q, Pangršič T, Kreft M, et al. Fusion-related release of glutamate from astrocytes. *J Biol Chem*. 2004;279(13):12724-12733.

179. Bezzi P, Gundersen V, Galbete JL, et al. Astrocytes contain a vesicular compartment that is competent for regulated exocytosis of glutamate. *Nat Neurosci*. 2004;7:613-620.

180. Anlauf E, Derouiche A. Astrocytic exocytosis vesicles and glutamate: A high-resolution immunofluorescence study. *Glia*. 2005;49(1):96-106.

181. Jourdain P, Bergersen LH, Bhaukaurally K, et al. Glutamate exocytosis from astrocytes controls synaptic strength. *Nat Neurosci*. 2007;10:331-339.

182. Oya M, Kitaguchi T, Yanagihara Y, et al. Vesicular nucleotide transporter is involved in ATP storage of secretory lysosomes in astrocytes. *Biochem Biophys Res Commun*. 2013;438(1):145-151.

183. Martineau M, Shi T, Puyal J, et al. Storage and uptake of D-serine into astrocytic synaptic-like vesicles specify gliotransmission. *J Neurosci*. 2013;33(8):3413-3423.

184. Coco S, Calegari F, Pravettoni E, et al. Storage and release of ATP from astrocytes in culture. *J Biol Chem*. 2003;278(2):1354-1362.

185. Martineau M, Galli T, Baux G, Mothet JP. Confocal imaging and tracking of the exocytotic routes for D-serine-mediated gliotransmission. *Glia*. 2008;56(12):1271-1284.

186. Mothet JP, Pollegioni L, Ouanounou G, Martineau M, Fossier P, Baux G. Glutamate receptor activation triggers a calcium-dependent and SNARE protein-dependent release of the gliotransmitter D-serine. *Proc Natl Acad Sci*. 2005;102(15):5606-5611.

187. Echigo N, Moriyama Y. Vesicular inhibitory amino acid transporter is expressed in γ-aminobutyric acid (GABA)-containing astrocytes in rat pineal glands. *Neurosci Lett*. 2004;367(1):79-84.

188. Ye ZC, Wyeth MS, Baltan-Tekkok S, Ransom BR. Functional hemichannels in astrocytes: A novel mechanism of glutamate release. *J Neurosci*. 2003;23(9):3588-3596.

189. Contreras JE, Sáez JC, Bukauskas FF, Bennett MVL. Gating and regulation of connexin 43 (Cx43) hemichannels. *Proc Natl Acad Sci*. 2003;100(20):11388-11393.

190. Thompson RJ, MacVicar B. Connexin and pannexin hemichannels of neurons and astrocytes. *Channels*. 2008;2:81-86.

191. Ballerini P, Rathbone MP, Iorio PD, et al. Rat astroglial P2Z (P2X7) receptors regulate intracellular calcium and purine release. *Neuroreport*. 1996;7(15):2533-2538.

192. Duan S, Anderson CM, Keung EC, Chen Y, Chen Y, Swanson RA. P2X7 receptor-mediated release of excitatory amino acids from astrocytes. *J Neurosci*. 2003;23(4):1320-1328.

193. Virginio C, MacKenzie A, Rassendren FA, North RA, Surprenant A. Pore dilation of neuronal P2X receptor channels. *Nat Neurosci*. 1999;2:315-321.

194. Suadicani SO, Brosnan CF, Scemes E. P2X7 receptors mediate ATP release and amplification of astrocytic intercellular Ca2+ signaling. *J Neurosci*. 2006;26(5):1378-1385.

195. Gallo V, Suergiu R, Levi G. Kainic acid stimulates GABA release from a subpopulation of cerebellar astrocytes. *Eur J Pharmacol*. 1986;132(2-3):319-322.

196. Abdullaev IF, Rudkouskaya A, Schools GP, Kimelberg HK, Mongin AA. Pharmacological comparison of swelling-activated excitatory amino acid release and Cl− currents in cultured rat astrocytes. *J Physiol*. 2006;572(3):677-689.

197. Lee S, Yoon BE, Berglund K, et al. Channel-mediated tonic GABA release from glia. *Science*. 2010;330(6005):790-796.

198. Woo DH, Han KS, Shim JW, et al. TREK-1 and Best1 channels mediate fast and slow glutamate release in astrocytes upon GPCR activation. *Cell*. 2012;151(1):25-40.

199. Han KS, Woo J, Park H, Yoon BJ, Choi S, Lee CJ. Channel-mediated astrocytic glutamate release via Bestrophin-1 targets synaptic NMDARs. *Mol Brain*. 2013;6:4.

200. Zonta M, Angulo MC, Gobbo S, et al. Neuron-to-astrocyte signaling is central to the dynamic control of brain microcirculation. *Nat Neurosci*. 2003;6:43-50.

201. Gordon GRJ, Choi HB, Rungta RL, Ellis-Davies GCR, MacVicar BA. Brain metabolism dictates the polarity of astrocyte control over arterioles. *Nature*. 2008;456:745-749.

202. Attwell D, Buchan AM, Charpak S, Lauritzen M, MacVicar BA, Newman EA. Glial and neuronal control of brain blood flow. *Nature*. 2010;468:232-243.

203. Metea MR, Newman EA. Glial cells dilate and constrict blood vessels: A mechanism of neurovascular coupling. *J Neurosci*. 2006;26(11):2862-2870.

204. Chan BS, Satriano JA, Pucci M, Schuster VL. Mechanism of prostaglandin E2 transport across the plasma membrane of HeLa cells and Xenopus oocytes expressing the prostaglandin transporter “PGT.” *J Biol Chem*. 1998;273(12):6689-6697.

205. Takano T, Tian GF, Peng W, et al. Astrocyte-mediated control of cerebral blood flow. *Nat Neurosci*. 2006;9:260-267.

206. Davis RJ, Murdoch CE, Ali M, et al. EP4 prostanoid receptor-mediated vasodilatation of human middle cerebral arteries. *Br J Pharmacol*. 2009;141(4):580-585.

207. Serebryakov V, Zakharenko S, Snetkov V, Takeda K. Effects of prostaglandins E1 and E2 on cultured smooth muscle cells and strips of rat aorta. *Prostaglandins*. 1994;47(5):353-365.

208. Sugimoto Y, Inazumi T, Tsuchiya S. Roles of prostaglandin receptors in female reproduction. *J Biochem*. 2014;157(2):73-80.

209. Eskay RL, Eskay J, Mical RS, Porter JC. Prostaglandin E2-induced release of LHRH into hypophysial portal blood. *Endocrinology*. 1975;97(4):816-824.

210. Harms PG, Ojeda SR, McCann SM. Prostaglandin involvement in hypothalamic control of gonadotropin and prolactin release. *Science*. 1973;181(4101):760-761.

211. Ojeda SR, Jameson HE, McCann SM. Hypothalamic areas involved in prostaglandin(PG)-induced gonadotropin release. I: Effects of PGE2 and PGF2α implants on luteinizing hormone release. *Endocrinology*. 1977;100(6):1585-1594.

212. Ojeda SR, Harms PG, McCann SM. Effect of inhibitors of prostaglandin synthesis on gonadotropin release in the rat. *Endocrinology*. 1975;97(4):843-854.

213. Ojeda SR, Negro-Vilar A, McCann SM. Release of prostaglandin Es by hypothalamic tissue: Evidence for their involvement in catecholamine-induced luteinizing hormone-releasing hormone release. *Endocrinology*. 1979;104(3):617-624.

214. Armstrong DT. Prostaglandins and follicular functions. *J Reprod Fert*. 1981;62(1):283-291.

215. Armstrong DT, Grinwich DL. Blockade of spontaneous and LH-induced ovulation in rats by indomethacin, an inhibitor of prostaglandin biosynthesis. *Prostaglandins*. 1972;1(1):21-28.

216. Lau IF, Saksena SK, Chang MC. Prostaglandins F and ovulation in mice. *J Reprod Fert*. 1974;40(2):467-469.

217. Grinwich DL, Kennedy TG, Armstrong DT. Dissociation of ovulatory and steroidogenic actions of luteinizing hormone in rabbits with indomethacin, an inhibitor of prostaglandin biosynthesis. *Prostaglandins*. 1972;1(2):89-96.

218. Wallach EE, de la Cruz A, Hunt J, Wright KH, Stevens VC. The effect of indomethacin on HMG-HCG induced ovulation in the rhesus monkey. *Prostaglandins*. 1975;9(4):645-658.

219. Ainsworth L, Tsang BK, Downey BR, Baker RD, Marcus GJ, Armstrong DT. Effects of indomethacin on ovulation and luteal function in gilts. *Biol Reprod*. 1979;21(2):401-411.

220. Stacey NE, Pandey S. Effects of indomethacin and prostaglandins on ovulation of goldfish. *Prostaglandins*. 1975;9(4):597-607.

221. Espey LL. Current status of the hypothesis that mammalian ovulation is comparable to an inflammatory reaction. *Biol Reprod*. 1994;50(2):233-238.

222. Smith G, Roberts R, Hall C, Nuki G. Reversible ovulatory failure associated with the development of luteinized unruptured follicles in women with inflammatory arthritis taking non-steroidal anti-inflammatory drugs. *Br J Rheumatol*. 1996;35(5):458-462.

223. Silberstein SD, Merriam GR. Estrogens, progestins, and headache. *Neurology*. 1991;41(6):786-793.

224. Marjoribanks J, Proctor M, Farquhar C, Sangkomkamhang US, Derks RS. Nonsteroidal anti-inflammatory drugs for primary dysmenorrhoea. *Cochrane Database Syst Rev*. 2003;4:CD001751.

225. Chan WY. Prostaglandins and nonsteroidal antiinflammatory drugs in dysmenorrhea. *Annu Rev Pharmacol Toxicol*. 1983;23:131-149.

226. Ojeda SR, Campbell WB. An increase in hypothalamic capacity to synthesize prostaglandin E2 precedes the first preovulatory surge of gonadotropins. *Endocrinology*. 1982;111(4):1031-1037.

227. Ojeda SR, Urbanski HF, Katz KH, Costa ME. Activation of estradiol-positive feedback at puberty: Estradiol sensitizes the LHRH-releasing system at two different biochemical steps. *Neuroendocrinology*. 1986;43(2):259-265.

228. Smith SS, Neuringer M, Ojeda SR. Essential fatty acid deficiency delays the onset of puberty in the female rat. *Endocrinology*. 1989;125(3):1650-1659.

229. Kataoka K, Ramwell PW, Jessup S. Prostaglandins: Localization in subcellular particles of rat cerebral cortex. *Science*. 1967;157(3793):1187-1189.

230. Rettori V, Gimeno M, Lyson K, McCann SM. Nitric oxide mediates norepinephrine-induced prostaglandin E2 release from the hypothalamus. *Proc Natl Acad Sci*. 1992;89(23):11543-11546.

231. Ojeda SR, Negro-Vilar A, McCann SM. Evidence for involvement of α-adrenergic receptors in norepinephrine-induced prostaglandin E2 and luteinizing hormone-releasing hormone release from the median eminence. *Endocrinology*. 1982;110(2):409-412.

232. Katsuura G, Gottschall PE, Dahl RR, Arimura A. Interleukin-1 beta increases prostaglandin E2 in rat astrocyte cultures: Modulatory effect of neuropeptides. *Endocrinology*. 1989;124(6):3125-3127.

233. Hirst WD, Young KA, Newton R, Allport VC, Marriott DR, Wilkin GP. Expression of COX-2 by normal and reactive astrocytes in the adult rat central nervous system. *Mol Cell Neurosci*. 1999;13(1):57-68.

234. Oomagari K, Buisson B, Dumuis A, Bockaert J, Pin JP. Effect of glutamate and ionomycin on the release of arachidonic acid, prostaglandins and HETEs from cultured neurons and astrocytes. *Eur J Neurosci*. 1991;3(10):928-939.

235. Ma YJ, Emde KB von der, Rage F, Wetsel WC, Ojeda SR. Hypothalamic astrocytes respond to transforming growth factor-α with the secretion of neuroactive substances that stimulate the release of luteinizing hormone-releasing hormone. *Endocrinology*. 1997;138(1):19-25.

236. Narumiya S, Sugimoto Y, Ushikubi F. Prostanoid receptors: Structures, properties, and functions. *Physiol Rev*. 1999;79(4):1193-1226.

237. Rage F, Lee BJ, Ma YJ, Ojeda SR. Estradiol enhances prostaglandin E2 receptor gene expression in luteinizing hormone-releasing hormone (LHRH) neurons and facilitates the LHRH response to PGE2 by activating a glia-to-neuron signaling pathway. *J Neurosci*. 1997;17(23):9145-9156.

238. Leranth C, MacLusky NJ, Shanabrough M, Naftolin F. Catecholaminergic innervation of luteinizing hormone-releasing hormone and glutamic acid decarboxylase immunopositive neurons in the rat medial preoptic area: An

electron-microscopic double immunostaining and degeneration study. *Neuroendocrinology*. 1988;48(6):591-602.

239. McNeill TH, Sladek JR Jr. Fluorescence-immunocytochemistry: Simultaneous localization of catecholamines and gonadotropin-releasing hormone. *Science*. 1978;200(4337):72-74.

240. Ojeda SR, Urbanski HF, Costa ME, Hill DF, Moholt-Siebert M. Involvement of transforming growth factor alpha in the release of luteinizing hormone-releasing hormone from the developing female hypothalamus. *Proc Natl Acad Sci*. 1990;87(24):9698-9702.

241. Miyake A, Tasaka K, Otsuka S, Kohmura H, Wakimoto H, Aono T. Epidermal growth factor stimulates secretion of rat pituitary luteinizing hormone in vitro. *Acta Endocrinol*. 1985;108(2):175-178.

242. Ma YJ, Hill DF, Junier MP, Costa ME, Felder SE, Ojeda SR. Expression of epidermal growth factor receptor changes in the hypothalamus during the onset of female puberty. *Mol Cell Neurosci*. 1994;5(3):246-262.

243. Prevot V, Rio C, Cho GJ, et al. Normal female sexual development requires neuregulin–erbB receptor signaling in hypothalamic astrocytes. *J Neurosci*. 2003;23(1):230-239.

244. Dziedzic B, Prevot V, Lomniczi A, Jung H, Cornea A, Ojeda SR. Neuron-to-glia signaling mediated by excitatory amino acid receptors regulates ErbB receptor function in astroglial cells of the neuroendocrine brain. *J Neurosci*. 2003;23(3):915-926.

245. Sharif A, Duhem-Tonnelle V, Allet C, et al. Differential erbB signaling in astrocytes from the cerebral cortex and the hypothalamus of the human brain. *Glia*. 2008;57(4):362-379.

246. Prevot V, Lomniczi A, Corfas G, Ojeda SR. erbB-1 and erbB-4 receptors act in concert to facilitate female sexual development and mature reproductive function. *Endocrinology*. 2005;146(3):1465-1472.

247. Ma YJ, Junier MP, Costa ME, Ojeda SR. Transforming growth factor-α gene expression in the hypothalamus is developmentally regulated and linked to sexual maturation. *Neuron*. 1992;9(4):657-670.

248. Junier MP, Ma YJ, Costa ME, Hoffman G, Hill DF, Ojeda SR. Transforming growth factor alpha contributes to the mechanism by which hypothalamic injury induces precocious puberty. *Proc Natl Acad Sci*. 1991;88(21):9743-9747.

249. Apostolakis EM, Garai J, Lohmann JE, Clark JH, O'Malley BW. Epidermal growth factor activates reproductive behavior independent of ovarian steroids in female rodents. *Mol Endocrinol*. 2000;14(7):1086-1098.

250. Ma YJ, Hill DF, Creswick KE, et al. Neuregulins signaling via a glial erbB-2–erbB-4 receptor complex contribute to the neuroendocrine control of mammalian sexual development. *J Neurosci*. 1999;19(22):9913-9927.

251. Ma YJ, Berg-von der Emde K, Moholt-Siebert M, Hill DF, Ojeda SR. Region-specific regulation of transforming growth factor alpha (TGF alpha) gene expression in astrocytes of the neuroendocrine brain. *J Neurosci*. 1994;14(9):5644-5651.

252. Kuiri-Hänninen T, Sankilampi U, Dunkel L. Activation of the hypothalamic-pituitary-gonadal axis in infancy: Minipuberty. *Horm Res Paediatr*. 2014;82(2):73-80.

253. Devillers MM, Mhaouty-Kodja S, Guigon CJ. Female mini-puberty: Insights from mouse models. *Int J Mol Sci*. 2022;23(22):13695.

254. Olmos G, Naftolin F, Perez J, Tranque PA, Garcia-Segura LM. Synaptic remodeling in the rat arcuate nucleus during the estrous cycle. *Neuroscience*. 1989;32(3):663-667.

255. Garcia-Segura LM, Baetens D, Naftolin F. Sex differences and maturational changes in arcuate nucleus neuronal plasma membrane organization. *Dev Brain Res*. 1985;19(1):146-149.

256. Garcia-Segura LM, Perez J, Tranque PA, Olmos G, Naftolin F. Sexual differentiation of the neuronal plasma membrane: Neonatal levels of sex steroids modulate the number of exo-endocytotic images in the developing rat arcuate neurons. *Neurosci Lett*. 1988;91(1):19-23.

257. Trangue PA, Suarez I, Olmos G, Fernandez B, Garcia-Segura LM. Estradiol — induced redistribution of glial fibrillary acidic protein immunoreactivity in the rat brain. *Brain Res*. 1987;406(1-2):348-351.

258. Ullian EM, Sapperstein SK, Christopherson KS, Barres BA. Control of synapse number by glia. *Science*. 2001;291(5504):657-661.

259. Witkin JW, Ferin M, Popilskis SJ, Silverman AJ. Effects of gonadal steroids on the ultrastructure of GnRH neurons in the rhesus monkey: synaptic input and glial apposition. *Endocrinology*. 1991;129(2):1083-1092.

260. Xiong JJ, Karsch FJ, Lehman MN. Evidence for seasonal plasticity in the gonadotropin-releasing hormone (GnRH) system of the ewe: Changes in synaptic inputs onto GnRH neurons. *Endocrinology*. 1997;138(3):1240-1250.

261. Jansen HT, Cutter C, Hardy S, Lehman MN, Goodman RL. Seasonal plasticity within the gonadotropin-releasing hormone (GnRH) system of the ewe: Changes in identified GnRH inputs and glial association. *Endocrinology*. 2003;144(8):3663-3676.

262. Parry DM, Goldsmith AR. Ultrastructural evidence for changes in synaptic input to the hypothalamic luteinizing hormone-releasing hormone neurons in photosensitive and photorefractory starlings. *J Neuroendocrinol*. 1993;5(4):387-395.

263. Amateau SK, McCarthy MM. A novel mechanism of dendritic spine plasticity involving estradiol induction of prostaglandin-E2. *J Neurosci*. 2002;22(19):8586-8596.

264. Mong JA, McCarthy MM. Steroid-induced developmental plasticity in hypothalamic astrocytes: Implications for synaptic patterning. *J Neurobiol*. 1999;40(4):602-619.

265. Hösli E, Jurasin K, Rühl W, Lüthy R, Hösli L. Colocalization of androgen, estrogen and cholinergic receptors on cultured astrocytes of rat central nervous system. *Int J Dev Neurosci*. 2001;19(1):11-19.

266. Hösli E, Rühl W, Hösli L. Histochemical and electrophysiological evidence for estrogen receptors on cultured astrocytes: colocalization with cholinergic receptors. *Int J Dev Neurosci*. 2000;18(1):101-111.

267. Santagati S, Melcangi RC, Celotti F, Martini L, Maggi A. Estrogen receptor is expressed in different types of glial cells in culture. *J Neurochem*. 1994;63(6):2058-2064.

268. Kuo J, Hamid N, Bondar G, Prossnitz ER, Micevych P. Membrane estrogen receptors stimulate intracellular calcium release and progesterone synthesis in hypothalamic astrocytes. *J Neurosci*. 2010;30(39):12950-12957.

269. Micevych P, Sinchak K, Mills RH, Tao L, LaPolt P, Lu JKH. The luteinizing hormone surge Is preceded by an estrogen-induced increase of hypothalamic progesterone in ovariectomized and adrenalectomized rats. *Neuroendocrinology*. 2003;78(1):29-35.

270. McCarthy MM, Todd BJ, Amateau SK. Estradiol modulation of astrocytes and the establishment of sex differences in the brain. *Ann N Y Acad Sci*. 2006;1007(1):283-297.

271. Gu GB, Simerly RB. Projections of the sexually dimorphic anteroventral periventricular nucleus in the female rat. *J Comp Neurol*. 1998;384(1):142-164.

272. Simerly RB. Wired for reproduction: Organization and development of sexually dimorphic circuits in the mammalian forebrain. *Annu Rev Neurosci*. 2002;25:507-536.

273. Raisman G, Field PM. Sexual dimorphism in the neurophil of the preoptic area of the rat and its dependence on neonatal androgen. *Brain Res*. 1973;54:1-29.

274. Bakker J, De Mees C, Douhard Q, et al. Alpha-fetoprotein protects the developing female mouse brain from masculinization and defeminization by estrogens. *Nat Neurosci*. 2006;9:220-226.

275. Barraclough CA. Production of anovulatory, sterile rats by single injections of testosterone propionate. *Endocrinology*. 1961;68(1):62-67.

276. Amateau SK, McCarthy MM. Sexual differentiation of astrocyte morphology in the developing rat preoptic area. *J Neuroendocrinol*. 2002;14(11):904-910.

277. Amateau SK, McCarthy MM. Induction of PGE2 by estradiol mediates developmental masculinization of sex behavior. *Nat Neurosci*. 2004;7:643-650.

278. Prevot V, Croix D, Bouret S, et al. Definitive evidence for the existence of morphological plasticity in the external zone of the median eminence during the rat estrous cycle: implication of neuro-glio-endothelial interactions in gonadotropin-releasing hormone release. *Neuroscience*. 1999;94(3):809-819.

279. Mullier A, Bouret SG, Prevot V, Dehouck B. Differential distribution of tight junction proteins suggests a role for tanycytes in blood-hypothalamus barrier regulation in the adult mouse brain. *J Comp Neurol*. 2009;518(7):943-962.

280. Kozlowski GP, Coates PW. Ependymoneuronal specializations between LHRH fibers and cells of the cerebroventricular system. *Cell Tissue Res*. 1985;242:301-311.

281. King JC, Letourneau RJ. Luteinizing hormone-releasing hormone terminals in the median eminence of rats undergo dramatic changes after gonadectomy, as revealed by electron microscopic image analysis. *Endocrinology*. 1994;134(3):1340-1351.

282. De Seranno S, Estrella C, Loyens A, et al. Vascular endothelial cells promote acute plasticity in ependymoglial cells of the neuroendocrine brain. *J Neurosci*. 2004;24(46):10353-10363.

283. Giacobini P. Shaping the reproductive system: Role of semaphorins in gonadotropin-releasing hormone development and function. *Neuroendocrinology*. 2015;102(3):200-215.

284. Hanchate NK, Giacobini P, Lhuillier P, et al. SEMA3A, a gene involved in axonal pathfinding, is mutated in patients with Kallmann Syndrome. *PLoS Genet*. 2012;8:e1002896.

285. Cashion AB, Smith MJ, Wise PM. The morphometry of astrocytes in the rostral preoptic area exhibits a diurnal rhythm on proestrus: relationship to the luteinizing hormone surge and effects of age. *Endocrinology*. 2003;144(1):274-280.

286. Cooper RL, Conn PM, Walker RF. Characterization of the LH surge in middle-aged female rats. *Biol Reprod*. 1980;23(3):611-615.

287. Clasadonte J, Poulain P, Hanchate NK, Corfas G, Ojeda SR, Prevot V. Prostaglandin E2 release from astrocytes triggers gonadotropin-releasing hormone (GnRH) neuron firing via EP2 receptor activation. *Proc Natl Acad Sci*. 2011;108(38):16104-16109.

288. Vanacker C, DeFazio RA, Sykes CM, Moenter SM. A role for glial fibrillary acidic protein (GFAP)-expressing cells in the regulation of gonadotropin-releasing hormone (GnRH) but not arcuate kisspeptin neuron output in male mice. *Elife*. 2021;10:e68205.

289. Karsch FJ, Cummins JT, Thomas GB, Clarke IJ. Steroid feedback inhibition of pulsatile secretion of gonadotropin-releasing hormone in the ewe. *Biol Reprod*. 1987;36(5):1207-1218.

290. Moenter SM, Brand RM, Midgley AR, Karsch FJ. Dynamics of gonadotropin-releasing hormone release during a pulse. *Endocrinology*. 1992;130(1):503-510.

291. Dalkin AC, Haisenleder DJ, Ortolano GA, Ellis TR, Marshall JC. The frequency of gonadotropin-releasing-hormone stimulation differentially regulates gonadotropin subunit messenger ribonucleic acid expression. *Endocrinology*. 1989;125(2):917-923.

292. Karsch FJ, Moenter SM, Caraty A. The preovulatory surge of gonadotropin releasing hormone. In: *Modes of Action of GnRH and GnRH Analogs*. Springer; 1992:241-255.

293. Gore AC. Factors regulating GnRH neurons. In: *GnRH: The Master Molecule of Reproduction*. 1st ed. Kluwer Academic Publishers; 2002:93-123.

294. Smith JT, Dungan HM, Stoll EA, et al. Differential regulation of KiSS-1 mRNA expression by sex steroids in the brain of the male mouse. *Endocrinology*. 2005;146(7):2976-2984.

295. Moore AM, Coolen LM, Porter DT, Goodman RL, Lehman MN. KNDy cells revisited. *Endocrinology*. 2018;159(9):3219-3234.

296. Oakley AE, Clifton DK, Steiner RA. Kisspeptin signaling in the brain. *Endocr Rev*. 2009;30(6):713-743.

297. Lehman MN, Coolen LM, Goodman RL. Minireview: kisspeptin/neurokinin B/dynorphin (KNDy) cells of the arcuate nucleus: a central node in the control of gonadotropin-releasing hormone secretion. *Endocrinology*. 2010;151(8):3479-3489.

298. Vanacker C, Moya MR, DeFazio RA, Johnson ML, Moenter SM. Long-term recordings of arcuate nucleus kisspeptin neurons reveal patterned activity that is modulated by gonadal steroids in male mice. *Endocrinology*. 2017;158(10):3553-3564.

299. Ruka KA, Burger LL, Moenter SM. Both estrogen and androgen modify the response to activation of neurokinin-3 and κ-opioid receptors in arcuate kisspeptin neurons from male mice. *Endocrinology*. 2016;157(2):752-763.

300. Vas S, Wall E, Zhou Z, Kalmar L, Han SY, Herbison AE. Long-term recordings of arcuate nucleus kisspeptin neurons across the mouse estrous cycle. *Endocrinology*. 2024;165(3):bqae009.

301. Clasadonte J, Prevot V. The special relationship: glia–neuron interactions in the neuroendocrine hypothalamus. *Nat Rev Endocrinol*. 2018;14:25-44.

302. Bazargani N, Attwell D. Astrocyte calcium signaling: the third wave. *Nat Neurosci*. 2016;19:182-189.

303. Ojeda SR, Lomniczi A, Sandau US. Glial–gonadotrophin hormone (GnRH) neurone interactions in the median eminence and the control of GnRH secretion. *J Neuroendocrinol*. 2008;20(6):732-742.

304. Bonder DE, McCarthy KD. Astrocytic Gq-GPCR-linked IP3R-dependent Ca2+ signaling does not mediate neurovascular coupling in mouse visual cortex in vivo. *J Neurosci*. 2014;34(39):13139-13150.

305. Chen N, Sugihara H, Kim J, et al. Direct modulation of GFAP-expressing glia in the arcuate nucleus bi-directionally regulates feeding. *Elife*. 2016;5:e18716.

306. Suter KJ, Song WJ, Sampson TL, et al. Genetic targeting of green fluorescent protein to gonadotropin-releasing hormone neurons: characterization of whole-cell electrophysiological properties and morphology. *Endocrinology*. 2000;141(1):412-419.

307. Ruka KA, Burger LL, Moenter SM. Regulation of arcuate neurons coexpressing kisspeptin, neurokinin B, and dynorphin by modulators of neurokinin 3 and κ-opioid receptors in adult male mice. *Endocrinology*. 2013;154(8):2761-2771.

308. Wagenmaker ER, Moenter SM. Exposure to acute psychosocial stress disrupts the luteinizing hormone surge independent of estrous cycle alterations in female mice. *Endocrinology*. 2017;158(8):2593-2602.

309. Simon MM, Greenaway S, White JK, et al. A comparative phenotypic and genomic analysis of C57BL/6J and C57BL/6N mouse strains. *Genome Biol*. 2013;14:R82.

310. Haustein MD, Kracun S, Lu XH, et al. Conditions and constraints for astrocyte calcium signaling in the hippocampal mossy fiber pathway. *Neuron*. 2014;82(2):413-429.

311. Perea G, Yang A, Boyden ES, Sur M. Optogenetic astrocyte activation modulates response selectivity of visual cortex neurons in vivo. *Nat Commun*. 2014;5:3262.

312. Yang CF, Chiang MC, Gray DC, et al. Sexually dimorphic neurons in the ventromedial hypothalamus govern mating in both sexes and aggression in males. *Cell*. 2013;153(4):896-909.

313. Ogawa Y, Sano T, Irisa M, et al. FcRγ-dependent immune activation initiates astrogliosis during the asymptomatic phase of Sandhoff disease model mice. *Sci Rep*. 2017;7:40518.

314. Zhang S, Xu M, Chang WC, et al. Organization of long-range inputs and outputs of frontal cortex for top-down control. *Nat Neurosci*. 2016;19:1733-1742.

315. Li B, Qi S, Sun G, et al. Leptin suppresses adenosine triphosphate-induced impairment of spinal cord astrocytes. *J Neurosci Res*. 2016;94(10):924-935.

316. Kerman IA, Shabrang C, Taylor L, Akil H, Watson SJ. Relationship of presympathetic-premotor neurons to the serotonergic transmitter system in the rat brainstem. *J Comp Neurol*. 2006;499(6):882-896.

317. Steyn FJ, Wan Y, Clarkson J, Veldhuis JD, Herbison AE, Chen C. Development of a methodology for and assessment of pulsatile luteinizing hormone secretion in juvenile and adult male mice. *Endocrinology*. 2013;154(12):4939-4945.

318. Nunemaker CS, DeFazio RA, Moenter SM. A targeted extracellular approach for recording long-term firing patterns of excitable cells: a practical guide. *Biol Proced Online*. 2003;5:53-62.

319. Alcami P, Franconville R, Llano I, Marty A. Measuring the firing rate of high-resistance neurons with cell-attached recording. *J Neurosci*. 2012;32(9):3118-3130.

320. Jia H, Rochefort NL, Chen X, Konnerth A. In vivo two-photon imaging of sensory-evoked dendritic calcium signals in cortical neurons. *Nat Protoc*. 2011;6:28-35.

321. Underwood AJ. *Experiments in Ecology: Their Logical Design and Interpretation Using Analysis of Variance*. 1st ed. Cambridge University Press; 1997.

322. Hainfellner JA, Voigtländer T, Ströbel T, et al. Fibroblasts can express glial fibrillary acidic protein (GFAP) in vivo. *J Neuropathol Exp Neurol*. 2001;60(5):449-461.

323. Wang L, DeFazio RA, Moenter SM. Excitability and burst generation of AVPV kisspeptin neurons are regulated by the estrous cycle via multiple conductances modulated by estradiol action. *eNeuro*. 2016;3(3):eneuro.0094-16.2016.

324. Phumsatitpong C, Guzman RM de, Zuloaga DG, Moenter SM. A CRH receptor type 1 agonist increases GABA transmission to GnRH neurons in a circulating-estradiol-dependent manner. *Endocrinology*. 2020;161(11):bqaa140.

325. Cecyn MN, Abrahao KP. Where do you measure the Bregma for rodent stereotaxic surgery? *IBRO Neurosci Rep*. 2023;15:143-148.

326. Phillips CD, DeFazio RA, Moenter SM. Sex and time of day alter the interactions between hypothalamic glia and the neural circuits controlling reproduction. *Endocrinology*. 2025;166:bqaf057.

327. Requie LM, Gómez-Gonzalo M, Speggiorin M, et al. Astrocytes mediate long-lasting synaptic regulation of ventral tegmental area dopamine neurons. *Nat Neurosci*. 2022;25:1639-1650.

328. D'Ascenzo M, Fellin T, Terunuma M, et al. mGluR5 stimulates gliotransmission in the nucleus accumbens. *Proc Natl Acad Sci*. 2007;104(6):1995-2000.

329. Kang S, Hong SI, Lee J, et al. Activation of astrocytes in the dorsomedial striatum facilitates transition from habitual to goal-directed reward-seeking behavior. *Biol Psychiatry*. 2020;88(10):797-808.

330. Tang W, Szokol K, Jensen V, et al. Stimulation-evoked Ca2+ signals in astrocytic processes at hippocampal CA3–CA1 synapses of adult mice are modulated by glutamate and ATP. *J Neurosci*. 2015;35(7):3016-3021.

331. Moore AM, Coolen LM, Lehman MN. In vivo imaging of the GnRH pulse generator reveals a temporal order of neuronal activation and synchronization during each pulse. *Proc Natl Acad Sci*. 2022;119(6):e2117767119.

332. McQuillan HJ, Han SY, Cheong I, Herbison AE. GnRH pulse generator activity across the estrous cycle of female mice. *Endocrinology*. 2019;160(6):1480-1491.

333. Clarkson J, Han SY, Piet R, et al. Definition of the hypothalamic GnRH pulse generator in mice. *Proc Natl Acad Sci*. 2017;114(47):E10216-E10223.

334. Kauffman AS. Coming of age in the Kisspeptin Era: Sex differences, development, and puberty. *Mol Cell Endocrinol*. 2010;324(1-2):51-63.

335. Mong JA, Glaser E, McCarthy MM. Gonadal steroids promote glial differentiation and alter neuronal morphology in the developing hypothalamus in a regionally specific manner. *J Neurosci*. 1999;19(4):1464-1472.

336. Lenz KM, McCarthy MM. Organized for sex – steroid hormones and the developing hypothalamus. *Eur J Neurosci*. 2010;32(12):2096-2104.

337. Mong JA, McCarthy MM. Ontogeny of sexually dimorphic astrocytes in the neonatal rat arcuate. *Brain Res Dev Brain Res*. 2002;139(2):151-158.

338. Spitzbarth TL, Horton TH, Lifka J, Schwartz NB. Pituitary gonadotropin content in gonadectomized rats: immunoassay measurements influenced by extraction solvent and testosterone replacement. *J Androl*. 1988;9(4):294-304.

339. Gay VL, Midgley ARJr. Response of the adult rat to orchidectomy and ovariectomy as determined by LH radioimmunoassay. *Endocrinology*. 1969;84(6):1359-1364.

340. Elskus AA, Phelps AF, Schwartz NB. Acute sex differences in serum LH levels in gonadectomized rats: investigation of pituitary response to GnRH pulse frequency and prolactin secretion as etiological agents. *Neuroendocrinology*. 1995;61(3):301-309.

341. Fallest PC, Hiatt ES, Schwartz NB. Effects of gonadectomy on the in vitro and in vivo gonadotropin responses to gonadotropin-releasing hormone in male and female rats. *Endocrinology*. 1989;124(3):1370-1379.

342. Baroncini M, Allet C, Leroy D, Beauvillain JC, Francke JP, Prevot V. Morphological evidence for direct interaction between gonadotrophin-releasing hormone neurones and astroglial cells in the human hypothalamus. *J Neuroendocrinol*. 2007;19(9):691-702.

343. Prevot V, Dutoit S, Croix D, Tramu G, Beauvillain JC. Semi-quantitative ultrastructural analysis of the localization and neuropeptide content of gonadotropin releasing hormone nerve terminals in the median eminence throughout the estrous cycle of the rat. *Neuroscience*. 1998;84(1):177-191.

344. Giacobini P, Parkash J, Campagne C, et al. Brain endothelial cells control fertility through ovarian-steroid–dependent release of semaphorin 3A. *PLoS Biol*. 2014;12(3):e1001808.

345. Parkash J, Messina A, Langlet F, et al. Semaphorin7A regulates neuroglial plasticity in the adult hypothalamic median eminence. *Nat Commun*. 2015;6:6385.

346. Chen X, Moenter SM. Gonadal feedback alters the relationship between action potentials and hormone release in gonadotropin-releasing hormone neurons in male mice. *J Neurosci*. 2023;43(40):6717-6730.

347. Glanowska KM, Moenter SM. Endocannabinoids and prostaglandins both contribute to GnRH neuron-GABAergic afferent local feedback circuits. *J Neurophysiol*. 2011;106(6):3073-3081.

348. Rurak GM, Simard S, Freitas-Andrade M, et al. Sex differences in developmental patterns of neocortical astroglia: A mouse translatome database. *Cell Rep*. 2022;38(5):110310.

349. Ludwig M, Sabatier N, Dayanithi G, Russell JA, Leng G. The active role of dendrites in the regulation of magnocellular neurosecretory cell behavior. *Prog Brain Res*. 2002;139:247-255.

350. Glanowska KM, Moenter SM. Differential regulation of GnRH secretion in the preoptic area (POA) and the median eminence (ME) in male mice. *Endocrinology*. 2015;156(1):231-241.

351. Ojeda SR, Urbanski HF, Katz KH, Costa ME. Prostaglandin E2 releases luteinizing hormone-releasing hormone from the female juvenile hypothalamus through a Ca2+-dependent, calmodulin-independent mechanism. *Brain Res*. 1988;441(1-2):339-351.

352. Müller-Fielitz H, Stahr M, Bernau M, et al. Tanycytes control the hormonal output of the hypothalamic-pituitary-thyroid axis. *Nat Commun*. 2017;8:484.

353. Larramona-Arcas R, González-Arias C, Perea G, et al. Sex-dependent calcium hyperactivity due to lysosomal-related dysfunction in astrocytes from APOE4 versus APOE3 gene targeted replacement mice. *Mol Neurodegener*. 2020;15:35.

354. Kuo J, Hamid N, Bondar G, Dewing P, Clarkson J, Micevych P. Sex differences in hypothalamic astrocyte response to estradiol stimulation. *Biol Sex Differ*. 2010;1:7.

355. Micevych PE, Chaban V, Ogi J, Dewing P, Lu JKH, Sinchak K. Estradiol stimulates progesterone synthesis in hypothalamic astrocyte cultures. *Endocrinology*. 2007;148(2):782-789.

356. Panatier A, Theodosis DT, Mothet JP, et al. Glia-derived D-serine controls NMDA receptor activity and synaptic memory. *Cell*. 2006;125(4):775-784.

357. Burger LL, Vanacker C, Phumsatitpong C, et al. Identification of genes enriched in GnRH neurons by translating ribosome affinity purification and RNAseq in mice. *Endocrinology*. 2018;159(4):1922-1940.

358. Claes M, De Groef L, Moons L. The DREADDful hurdles and opportunities of the chronic chemogenetic toolbox. *Cells*. 2022;11(7):1110.

359. Shivachar AC. Cannabinoids inhibit sodium-dependent, high-affinity excitatory amino acid transport in cultured rat cortical astrocytes. *Biochem Pharmacol*. 2007;73(12):2004-2011.

360. Moldrich G, Wenger T. Localization of the CB1 cannabinoid receptor in the rat brain. An immunohistochemical study. *Peptides*. 2000;21(11):1735-1742.

361. Lauckner JE, Hille B, Mackie K. The cannabinoid agonist WIN55,212-2 increases intracellular calcium via CB1 receptor coupling to Gq/11 G proteins. *Proc Natl Acad Sci*. 2005;102(52):19144-19149.

362. Fellin T, Sul JY, D'ascenzo M, Takano H, Pascual O, Haydon PG. Bidirectional astrocyte–neuron communication: The many roles of glutamate and ATP. In: *Purinergic Signalling in Neuron–Glia Interactions*. Vol 276. Novartis Foundation. 2006.

363. Oberheim NA, Goldman SA, Nedergaard M. Heterogeneity of astrocytic form and function. In: *Astrocytes*. Methods in Molecular Biology. Humana Press; 2011.

364. Yu X, Taylor AMW, Nagai J, et al. Reducing astrocyte calcium signaling in vivo alters striatal microcircuits and causes repetitive behavior. *Neuron*. 2018;99(6):1170-1187.

365. Haeussler M, Schönig K, Eckert H, et al. Evaluation of off-target and on-target scoring algorithms and integration into the guide RNA selection tool CRISPOR. *Genome Biol*. 2016;17:148.

366. Concordet JP, Haeussler M. CRISPOR: intuitive guide selection for CRISPR/Cas9 genome editing experiments and screens. *Nucleic Acids Res*. 2018;46(W1):W242-W245.

367. Bustin SA. Quantification of mRNA using real-time reverse transcription PCR (RT-PCR): trends and problems. *J Mol Endocrinol*. 2002;29:23-39.

368. Sun W, McConnell E, Pare JF, et al. Glutamate-dependent neuroglial calcium signaling differs between young and adult brain. *Science*. 2013;339(6116):197-200.

369. Abbracchio MP, Boeynaems JM, Barnard EA, et al. Characterization of the UDP-glucose receptor (re-named here the P2Y14 receptor) adds diversity to the P2Y receptor family. *Trends Pharmacol Sci*. 2003;24(2):52-55.

370. Nicholas RA, Watt WC, Lazarowski ER, Li Q, Harden K. Uridine nucleotide selectivity of three phospholipase C-activating P2 receptors: identification of a UDP-selective, a UTP-selective, and an ATP- and UTP-specific receptor. *Mol Pharmacol*. 1996;50(2):224-229.

371. Hechler B, Eckly A, Ohlmann P, Cazenave JP, Gachet C. The P2Y1 receptor, necessary but not sufficient to support full ADP-induced platelet aggregation, is not the target of the drug clopidogrel. *Br J Haematol*. 1998;103(3):858-866.

372. Lenz G, Gottfried C, Luo Z, et al. P2Y purinoceptor subtypes recruit different Mek activators in astrocytes. *Br J Pharmacol*. 2000;129(5):927-936.

373. Shigetomi E, Hirayama YJ, Ikenaka K, Tanaka KF, Koizumi S. Role of purinergic receptor P2Y1 in spatiotemporal Ca2+ dynamics in astrocytes. *J Neurosci*. 2018;38(6):1383-1395.

374. Shinozaki Y, Shibata K, Yoshida K, et al. Transformation of astrocytes to a neuroprotective phenotype by microglia via P2Y1 receptor downregulation. *Cell Rep*. 2017;19(6):1151-1164.

375. Shen W, Chen F, Tang Y, et al. Astrocytic GAT-3 regulates synaptic transmission and memory formation in the dentate gyrus. *Glia*. 2024;73(4):788-804.

376. Porter JT, McCarthy KD. GFAP-positive hippocampal astrocytes in situ respond to glutamatergic neuroligands with increases in [Ca2+]i. *Glia*. 1995;13(2):101-112.

377. Pasti L, Volterra A, Pozzan T, Carmignoto G. Intracellular calcium oscillations in astrocytes: A highly plastic, bidirectional form of communication between neurons and astrocytes in situ. *J Neurosci*. 1997;17(20):7817-7830.

378. Latour I, Gee CE, Robitaille R, Lacaille JC. Differential mechanisms of Ca2+ responses in glial cells evoked by exogenous and endogenous glutamate in rat hippocampus. *Hippocampus*. 2001;11(2):132-145.

379. Sun MY, Devaraju P, Xie AX, et al. Astrocyte calcium microdomains are inhibited by Bafilomycin A1 and cannot be replicated by low-level Schaffer collateral stimulation in situ. *Cell Calcium*. 2014;55(1):1-16.

380. Panatier A, Robitaille R. Astrocytic mGluR5 and the tripartite synapse. *Neuroscience*. 2016;323:29-34.

381. Iino M, Goto K, Kakegawa W, et al. Glia-synapse interaction through Ca2+-permeable AMPA receptors in Bergmann glia. *Science*. 2001;292(5518):926-929.

382. Rusakov DA. The role of perisynaptic glial sheaths in glutamate spillover and extracellular Ca2+ depletion. *Biophys J*. 2001;81(4):1947-1959.

383. Clarkson J, Herbison AE. Development of GABA and glutamate signaling at the GnRH neuron in relation to puberty. *Mol Cell Endocrinol*. 2006;254-255:32-38.

384. Wray S, Hoffman G. Postnatal morphological changes in rat LHRH neurons correlated with sexual maturation. *Neuroendocrinology*. 1986;43(2):93-97.

385. Finkbeiner S, Stevens CF. Applications of quantitative measurements for assessing glutamate neurotoxicity. *Proc Natl Acad Sci*. 1988;85(11):4071-4074.

386. Kano M, Ohno-Shosaku T, Hashimotodani Y, Uchigashima M, Watanabe M. Endocannabinoid-mediated control of synaptic transmission. *Physiol Rev*. 2009;89(1):309-380.

387. Navarrete M, Araque A. Endocannabinoids potentiate synaptic transmission through stimulation of astrocytes. *Neuron*. 2010;68(1):113-126.

388. Torres E, Pellegrino G, Granados-Rodríguez M, et al. Kisspeptin signaling in astrocytes modulates the reproductive axis. *J Clin Invest*. 2024;134(15):e172908.

389. Lomniczi A, Ojeda SR. A role for glial cells of the neuroendocrine brain in the central control of female sexual development. In: *Astrocytes in (Patho)Physiology of the Nervous System*. Springer; 2009.

390. Sandau US, Mungenast AE, Alderman Z, et al. SynCAM1, a synaptic adhesion molecule, is expressed in astrocytes and contributes to erbB4 receptor-mediated control of female sexual development. *Endocrinology*. 2011;152(6):2364-2376.

391. Burnstock G, Verkhratsky A. Evolutionary origins of the purinergic signalling system. *Acta Physiol*. 2009;195(4):415-447.

392. Burnstock G. Purinergic receptors. *J Theor Biol*. 1976;62(2):491-503.

393. Franke H, Sauer C, Rudolph C, Krügel U, Hengstler JG, Illes P. P2 receptor-mediated stimulation of the PI3-K/Akt-pathway in vivo. *Glia*. 2009;57(10):1031-1045.

394. Tavakoli NS, Malone SG, Anderson TL, et al. Astrocyte Ca2+ in the dorsal striatum suppresses neuronal activity to oppose cue-induced reinstatement of cocaine seeking. *Front Cell Neurosci*. 2024;18:1347491.

395. Stoica L, Ahmed SS, Gao G, Sena-Esteves M. Gene transfer to the CNS using recombinant adeno-associated virus. *Curr Protoc Microbiol*. 2013;29:14D.5.1-14D.5.18.

396. Gruntman AM, Su L, Su Q, Gao G, Mueller C, Flotte TR. Stability and compatibility of recombinant adeno-associated virus under conditions commonly encountered in human gene therapy trials. *Hum Gene Ther Methods*. 2015;26(2):71-76.

397. Clayton RN, Catt KJ. Regulation of pituitary gonadotropin-releasing hormone receptors by gonadal hormones. *Endocrinology*. 1981;108(3):887-895.

398. Debeljuk L, Rozados R, Daskal H, Vélez CV. Variation of the pituitary response to LH-releasing hormone (LH-RH) during a 24-hour period in male, diestrous female and androgenized female rats. *Neuroendocrinology*. 1975;17(1):48-53.

399. Ho Y, Hu P, Peel MT, et al. Single-cell transcriptomic analysis of adult mouse pituitary reveals sexual dimorphism and physiologic demand-induced cellular plasticity. *Protein Cell*. 2020;11(8):565-583.

400. Hou H, Chan C, Yuki KE, et al. Postnatal developmental trajectory of sex-biased gene expression in the mouse pituitary gland. *Biol Sex Differ*. 2022;13:57.

401. Kit OI, Frantsiyants EM, Bandovkina VA, et al. Features of changes in the content of hormones of the hypothalamic-pituitary tract depending on the independent or combined variant of B16/F10 melanoma growth in mice of both sexes. *Cardiometry*. 2023;(27):33-39.

402. de Tassigny X d'Anglemont, Fagg LA, Carlton MBL, Colledge WH. Kisspeptin can stimulate gonadotropin-releasing hormone (GnRH) release by a direct action at GnRH nerve terminals. *Endocrinology*. 2008;149(8):3926-3932.

403. Herde MK, Iremonger KJ, Constantin S, Herbison AE. GnRH neurons elaborate a long-range projection with shared axonal and dendritic functions. *J Neurosci*. 2013;33(31):12689-12697.

404. Prevot V, Cornea A, Mungenast A, Smiley G, Ojeda SR. Activation of erbB-1 signaling in tanycytes of the median eminence stimulates transforming growth factor β1 release via prostaglandin E2 production and induces cell plasticity. *J Neurosci*. 2003;23(33):10622-10632.

405. Cahill PS, Walker QD, Finnegan JM, Mickelson GE, Travis ER, Wightman RM. Microelectrodes for the measurement of catecholamines in biological systems. *Anal Chem*. 1996;68(18):3180-3186.

406. Glanowska KM, Venton BJ, Moenter SM. Fast scan cyclic voltammetry as a novel method for detection of real-time gonadotropin-releasing hormone release in mouse brain slices. *J Neurosci*. 2012;32(42):14664-14669.

407. Garcia-Segura LM, Lorenz B, DonCarlos LL. The role of glia in the hypothalamus: implications for gonadal steroid feedback and reproductive neuroendocrine output. *Reproduction*. 2008;135(4):419-429.

408. Cottrell EC, Campbell RE, Han SK, Herbison AE. Postnatal remodeling of dendritic structure and spine density in gonadotropin-releasing hormone neurons. *Endocrinology*. 2006;147(8):3652-3661.

409. Perera AD, Plant TM. Ultrastructural studies of neuronal correlates of the pubertal reaugmentation of hypothalamic gonadotropin-releasing hormone (GnRH) release in the rhesus monkey (Macaca mulatta). *J Comp Neurol*. 1997;385(1):71-82.

410. Garcia-Segura LM, Melcangi RC. Steroids and glial cell function. *Glia*. 2006;54(6):485-498.

411. Mong JA, Blutstein T. Estradiol modulation of astrocytic form and function: Implications for hormonal control of synaptic communication. *Neuroscience*. 2006;138(3):967-975.

412. Zimmermann P. Estrogen-dependent changes in the functional interrelationships among neurons, ependymal cells and glial cells of the arcuate nucleus. *Cell Tissue Res*. 1982;227:113-128.

413. Czieselsky K, Prescott M, Porteous R, et al. Pulse and surge profiles of luteinizing hormone secretion in the mouse. *Endocrinology*. 2016;157(12):4794-4802.

414. Reynoso MA, Juntawong P, Lancia M, Blanco FA, Bailey-Serres J, Zanetti ME. Translating ribosome affinity purification (TRAP) followed by RNA sequencing technology (TRAP-SEQ) for quantitative assessment of plant translatomes. In: *Plant Functional Genomics*. Humana Press; 2015.

415. Dungan HM, Clifton DK, Steiner RA. Minireview: Kisspeptin neurons as central processors in the regulation of gonadotropin-releasing hormone secretion. *Endocrinology*. 2006;147(3):1154-1158.

416. Mohr MA, Esparza LA, Steffen P, Micevych PE, Kauffman AS. Progesterone receptors in AVPV kisspeptin neurons are sufficient for positive feedback induction of the LH surge. *Endocrinology*. 2021;162(11):bqab161.

417. Micevych P, Sinchak K. Estradiol regulation of progesterone synthesis in the brain. *Mol Cell Endocrinol*. 2008;290(1-2):44-50.

418. Stephens SBZ, Tolson KP, Rouse ML Jr, et al. Absent progesterone signaling in kisspeptin neurons disrupts the LH surge and impairs fertility in female mice. *Endocrinology*. 2015;156(9):3091-3097.

419. Fernandez-Galaz MC, Muñoz RM, Villanua MA, Garcia-Segura LM. Diurnal oscillation in glial fibrillary acidic protein in a perisuprachiasmatic area and Its relationship to the luteinizing hormone surge in the female rat. *Neuroendocrinology*. 1999;70(5):368-376.

420. Watts AG, Swanson LW, Sanchez-Watts G. Efferent projections of the suprachiasmatic nucleus: I. Studies using anterograde transport of Phaseolus vulgaris leucoagglutinin in the rat. *J Comp Neurol*. 1987;258(2):204-229.

421. Brancaccio M, Patton AP, Chesham JE, Maywood ES, Hastings MH. Astrocytes control circadian timekeeping in the suprachiasmatic nucleus via glutamatergic signaling. *Neuron*. 2017;93(6):1420-1435.e5.

422. Sharif A, Prevot V. Astrogenesis in the hypothalamus: A life-long process contributing to the development and plasticity of neuroendocrine networks. *Front Neuroendocrinol*. 2024;75:101154.

423. Goodman T, Nayar SG, Clare S, et al. Fibroblast growth factor 10 is a negative regulator of postnatal neurogenesis in the mouse hypothalamus. *Development*. 2020;147(13):dev180950.

424. Yoo S, Kim J, Lyu P, et al. Control of neurogenic competence in mammalian hypothalamic tanycytes. *Sci Adv*. 2021;7(22):eabg3777.

425. Pellegrino G, Martin M, Allet C, et al. GnRH neurons recruit astrocytes in infancy to facilitate network integration and sexual maturation. *Nat Neurosci*. 2021;24:1660-1672.

426. Bezzi P, Carmignoto G, Pasti L, et al. Prostaglandins stimulate calcium-dependent glutamate release in astrocytes. *Nature*. 1998;391:281-285.

427. Buell G, Collo G, Rassendren F. P2X receptors: An emerging channel family. *Eur J Neurosci*. 1996;8(10):2221-2228.

428. Yu S, François M, Huesing C, Münzberg H. The hypothalamic preoptic area and body weight control. *Neuroendocrinology*. 2018;106(2):187-194.

429. Xu Y, Nedungadi TP, Zhu L, et al. Distinct hypothalamic neurons mediate estrogenic effects on energy homeostasis and reproduction. *Cell Metab*. 2011;14(4):453-465.

430. Castellano JM, Bentsen AH, Mikkelsen JD, Tena-Sempere M. Kisspeptins: Bridging energy homeostasis and reproduction. *Brain Res*. 2010;1364:129-138.

431. de Tassigny X d'Anglemont, Fagg LA, Dixon JPC, et al. Hypogonadotropic hypogonadism in mice lacking a functional Kiss1 gene. *Proc Natl Acad Sci*. 2007;104(25):10714-10719.

432. Nandankar N, Negrón AL, Wolfe A, Levine JE, Radovick S. Deficiency of arcuate nucleus kisspeptin results in postpubertal central hypogonadism. *Am J Physiol Endocrinol Metab*. 2021;321(2):E264-E280.

433. de Seranno S, de Tassigny X d'Anglemont, Estrella C, et al. Role of estradiol in the dynamic control of tanycyte plasticity mediated by vascular endothelial cells in the median eminence. *Endocrinology*. 2010;151(4):1760-1772.

434. Kennedy GC, Mitra J. Body weight and food intake as initiating factors for puberty in the rat. *J Physiol*. 1963;166(2):408-418.

435. Nestor CC, Kelly MJ, Rønnekleiv OK. Cross-talk between reproduction and energy homeostasis: central impact of estrogens, leptin and kisspeptin signaling. *Horm Mol Biol Clin Investig*. 2014;17(3):109-128.

436. Wickramasuriya N, Hawkins R, Atwood C, Butler T. The roles of GnRH in the human central nervous system. *Horm Behav*. 2022;145:105230.

437. Dubois EA, Zandbergen MA, Peute J, Th HJG. Evolutionary development of three gonadotropin-releasing hormone (GnRH) systems in vertebrates. *Brain Res Bull*. 2002;57(3-4):413-418.

438. Skrapits K, Sárvári M, Farkas I, et al. The cryptic gonadotropin-releasing hormone neuronal system of human basal ganglia. *Elife*. 2021;10:e67714.

439. Martínez-Moreno CG, Calderón-Vallejo D, Harvey S, Arámburo C, Quintanar JL. Growth hormone (GH) and gonadotropinrReleasing hormone (GnRH) in the central nervous system: A potential neurological combinatory therapy? *Int J Mol Sci*. 2018;19(2):375.

440. Berger H, Heinrich N, Albrecht E, et al. Gonadotropin-releasing hormone (GnRH) analogs: relationship between their structure, proteolytic inactivation and pharmacokinetics in rats. *Regul Pept*. 1991;33(3):299-311.

441. Ciaramella V, Chianese R, Pariante P, Fasano S, Pierantoni R, Meccariello R. Expression analysis of Gnrh1 and Gnrhr1 in spermatogenic cells of rat. *Int J Endocrinol*. 2015;982726.

442. Hapgood JP, Sadie H, Biljon WV, Ronacher K. Regulation of expression of mammalian gonadotrophin-releasing hormone receptor genes. *J Neuroendocrinol*. 2005;17(10):619-638.

443. Choi JH, Gilks CB, Auersperg N, Leung PCK. Immunolocalization of gonadotropin-releasing hormone (GnRH)-I, GnRH-II, and type I GnRH receptor during follicular development in the human ovary. *J Clin Endocrinol Metab*. 2006;91(11):4562-4570.

444. Kakar SS, Grantham K, Musgrove LC, Devor D, Sellers JC, Neill JD. Rat gonadotropin-releasing hormone (GnRH) receptor: tissue expression and hormonal regulation of its mRNA. *Mol Cell Endocrinol*. 1994;101(1-2):151-157.

445. Kim SO, Harris SM, Duffy DM. Prostaglandin E2 (EP) receptors mediate PGE2-specific events in ovulation and luteinization within primate ovarian follicles. *Endocrinology*. 2014;155(4):1466-1475.

446. Hayashi S, Noda Y, Mori T. Analysis of the role of prostaglandins in the fertilization process. *Eur J Obstet Gynecol Reprod Biol*. 1988;29(4):287-297.

447. Hizaki H, Segi E, Sugimoto Y, et al. Abortive expansion of the cumulus and impaired fertility in mice lacking the prostaglandin E receptor subtype EP2. *Proc Natl Acad Sci*. 1999;96(18):10501-10506.

448. Segi E, Haraguchi K, Sugimoto Y, et al. Expression of messenger RNA for prostaglandin E receptor subtypes EP4/EP2 and cyclooxygenase isozymes in mouse periovulatory follicles and oviducts during superovulation. *Biol Reprod*. 2003;68(3):804-811.

449. Ronnekleiv OK, Kelly MJ. Luteinizing hormone-releasing hormone neuronal system during the estrous cycle of the female rat: Effects of surgically induced persistent estrus. *Neuroendocrinology*. 1986;43(5):564-576.

450. Kinnear HM, Tomaszewski CE, Chang AL, et al. The ovarian stroma as a new frontier. *Reproduction*. 2020;160(3):R25-R39.